NAVAL POSTGRADUATE SCHOOL

MONTEREY, CALIFORNIA

THESIS

REDUCTION EXPANSION SYNTHESIS OF NICKEL-BASED CERMETS AND POTENTIAL MILITARY AND AEROSPACE APPLICATIONS

by

Andrew Bishop

June 2020

Thesis Advisor: Jonathan Phillips
Co-Advisor: Claudia C. Luhrs

THIS PAGE INTENTIONALLY LEFT BLANK

REPORT DOCUMENTATION PAGE			*Form Approved OMB No. 0704-0188*

1. AGENCY USE ONLY *(Leave blank)*	**2. REPORT DATE** June 2020	**3. REPORT TYPE AND DATES COVERED** Master's thesis

4. TITLE AND SUBTITLE
REDUCTION EXPANSION SYNTHESIS OF NICKEL-BASED CERMETS AND POTENTIAL MILITARY AND AEROSPACE APPLICATIONS

5. FUNDING NUMBERS

6. AUTHOR(S) Andrew Bishop

7. PERFORMING ORGANIZATION NAME(S) AND ADDRESS(ES)
Naval Postgraduate School
Monterey, CA 93943-5000

8. PERFORMING ORGANIZATION REPORT NUMBER

9. SPONSORING / MONITORING AGENCY NAME(S) AND ADDRESS(ES)
N/A

10. SPONSORING / MONITORING AGENCY REPORT NUMBER

11. SUPPLEMENTARY NOTES The views expressed in this thesis are those of the author and do not reflect the official policy or position of the Department of Defense or the U.S. Government.

12a. DISTRIBUTION / AVAILABILITY STATEMENT
Approved for public release. Distribution is unlimited.

12b. DISTRIBUTION CODE
A

13. ABSTRACT (maximum 200 words)

This thesis demonstrated that the use of the Reduction Expansion Synthesis manufacturing process can be applied to cermet or metal matrix composite materials. This could potentially have a significant impact in the aerospace field because cermets and metal matrix composites have several desirable thermal resistance qualities. The Reduction Expansion Synthesis process was utilized on several different mixture ratios of nickel, nickel oxide, and ceramic powder. The various products created consisted of solid parts and films. These products were analyzed and compared utilizing methods such as scanning electron microscopy, Vickers hardness testing, energy dispersive spectroscopy, and light reflection analysis. It was found that 1% silica mixtures would produce the most effective cermet parts and that these mixtures can be applied to films on several metal substrates. These products have the potential to be useful for cermet coatings, which can be used to absorb high amounts of solar radiation and retain infrared radiation for use in a heat engine or for heat-resistant, ductile aerospace structural and electrical components.

14. SUBJECT TERMS
Reduction Expansion Synthesis, cermets, nickel-alumina, characterization, nanoparticles, aerospace materials, novel manufacturing

15. NUMBER OF PAGES
135

16. PRICE CODE

17. SECURITY CLASSIFICATION OF REPORT	**18. SECURITY CLASSIFICATION OF THIS PAGE**	**19. SECURITY CLASSIFICATION OF ABSTRACT**	**20. LIMITATION OF ABSTRACT**
Unclassified	Unclassified	Unclassified	UU

NSN 7540-01-280-5500

Standard Form 298 (Rev. 2-89)
Prescribed by ANSI Std. 239-18

THIS PAGE INTENTIONALLY LEFT BLANK

Approved for public release. Distribution is unlimited.

REDUCTION EXPANSION SYNTHESIS OF NICKEL-BASED CERMETS AND POTENTIAL MILITARY AND AEROSPACE APPLICATIONS

Andrew Bishop
Ensign, United States Navy
BS, United States Naval Academy, 2019

Submitted in partial fulfillment of the
requirements for the degree of

MASTER OF SCIENCE IN ASTRONAUTICAL ENGINEERING

from the

NAVAL POSTGRADUATE SCHOOL
June 2020

Approved by: Jonathan Phillips
Advisor

Claudia C. Luhrs
Co-Advisor

Garth V. Hobson
Chair, Department of Mechanical and Aerospace Engineering

THIS PAGE INTENTIONALLY LEFT BLANK

ABSTRACT

This thesis demonstrated that the use of the Reduction Expansion Synthesis manufacturing process can be applied to cermet or metal matrix composite materials. This could potentially have a significant impact in the aerospace field because cermets and metal matrix composites have several desirable thermal resistance qualities. The Reduction Expansion Synthesis process was utilized on several different mixture ratios of nickel, nickel oxide, and ceramic powder. The various products created consisted of solid parts and films. These products were analyzed and compared utilizing methods such as scanning electron microscopy, Vickers hardness testing, energy dispersive spectroscopy, and light reflection analysis. It was found that 1% silica mixtures would produce the most effective cermet parts and that these mixtures can be applied to films on several metal substrates. These products have the potential to be useful for cermet coatings, which can be used to absorb high amounts of solar radiation and retain infrared radiation for use in a heat engine or for heat-resistant, ductile aerospace structural and electrical components.

THIS PAGE INTENTIONALLY LEFT BLANK

TABLE OF CONTENTS

THIS PAGE INTENTIONALLY LEFT BLANK

LIST OF FIGURES

THIS PAGE INTENTIONALLY LEFT BLANK

LIST OF TABLES

THIS PAGE INTENTIONALLY LEFT BLANK

LIST OF ACRONYMS AND ABBREVIATIONS

3D	three-dimensional
AM	additive manufacturing
AMF	Advanced Manufacturing Facility
DOD	Department of Defense
EDS	energy dispersive spectroscopy
HIP	hot isostatic pressing
IR	infrared
ISS	International Space Station
MIM	metal injection molding
MISSE	Materials International Space Station Experiment
MMC	metal matrix composite
NASA	National Aeronautics and Space Administration
NPS	Naval Postgraduate School
PIM	powder injection molding
RES	reduction expansion synthesis
RES-C	reduction expansion synthesis cermet
RES-SM	reduction expansion synthesis sintered metal
SEM	scanning electron microscope
U.K.	United Kingdom
UV	ultraviolet

THIS PAGE INTENTIONALLY LEFT BLANK

ACKNOWLEDGMENTS

I would like to thank my advisor, Professor Jonathan Phillips, for always encouraging me to explore and for helping to keep my scientific curiosity alive. He always wanted me to be rich and famous. In addition, I want to thank my co-advisor, Professor Claudia Luhrs, for keeping me on track and making me feel welcome on the materials team. I would also like to thank my program officer, CDR Crane, and the air warfare liaison, CAPT McCabe, for making sure I was still focused on the future.

Finally, I would like to thank my family and my fiancée, Emily, for always supporting me and encouraging me through many long days of writing. I am thankful for all of you!

THIS PAGE INTENTIONALLY LEFT BLANK

I. INTRODUCTION

New methods of manufacturing are always being explored, from casting to additive manufacturing. The ability to cut down the cost of manufacturing and time to produce various components is of huge interest to both industry and defense. In this research, a new process will be explored for the development of cermets, or metal matrix composites. These materials have significant potential in both industry and defense sectors because of their unique and tailorable properties. However, many of the processing techniques for these types of materials often involve expensive or time-consuming techniques such as spray forming, which atomizes molten metal, or diffusion bonding, which uses high temperatures and pressures [1]. The process in this report utilized relatively low temperatures and short processing times, using only easy to obtain and handle powders as precursors.

A. RESEARCH OBJECTIVES

This primary goal of the work herein was to explore a novel, potentially simpler, faster, and less expensive method for creating cermets. This program is of value because there are a host of applications of military and commercial value for a simpler, faster, field/space deployable method for manufacturing cermets. Specifically, this thesis was designed to test the hypothesis that a variant of Reduction Expansion Synthesis (RES), a manufacturing process developed at the Naval Postgraduate School, known as RES-Cermet (RES-C), is a viable process for making various compositions of cermet solid parts and cermet surface films on metal substrates. The RES-C process was theorized to be a simple extrapolation of the basic techniques in the RES process. Testing the hypothesis required both developing the RES-C process and testing the parts/films made to determine composition, morphology, strength, and, for films specifically, the optical properties. Naturally, feedback from materials characterization was employed to improve the RES-C process.

The initial cermet fabrication work was designed to study the effect of production parameters on properties. Specifically, in the first stage of the work, the gross scale mechanical and electromagnetic properties of cermets formed as a function of the mixture

ratios and compositions of ceramics and metal powder precursors were studied to determine methods that would produce cermets with desired properties. The second part of the study, microanalysis of the various components created, was done to help characterize the effectiveness of the RES process and to determine if this method can be utilized in military or aerospace applications. These objectives were reached and this research demonstrated that, with additional development, there is the potential for this novel manufacturing technique to be applied to a set of materials with extremely desirable qualities and vast applications within the military and aerospace fields.

B. MOTIVATION

The U.S. military and Department of Defense (DOD) have a vested interest in producing new parts quickly and cheaply for use in the combat environment. Resupply in the operational theatre can be slow and uncertain. Manufacturing on station would provide a quick and effective solution. One possible solution: additive manufacturing (AM) or 3D printing. There has been significant investment in recent years in this area by the Department of Defense, and progress is generally defined in three areas, specifically related to additive manufacturing. According to Dr. Schrand in her article on "Additive Manufacturing in the DOD" the three areas are "(1) dedicated DOD Service AM implementation plans, (2) a Federally-funded national network of manufacturing institutes with an increasing number of research programs, and (3) successful AM efforts, including repairs and parts production for noncritical and flight/submarine-critical parts" [2].

The repair or manufacturing of high-performance components is a priority. For example, the Air Force has researched polymer composites made with carbon fiber that can be used in difficult environments, such as engine components and leading edges of fighter aircraft [2]. Sample components are shown in Figure 1.

Figure 1. High-temperature carbon fiber composite. Source: [2].

Cermets, created by some mixture of both metal and ceramic, generally have the capability to resist high temperatures, have high thermal conductivity, have a low coefficient of thermal expansion, and have high specific stiffness and strength [3]. These properties make them especially desirable for military use, and military use in the space environment in particular. Indeed, the space environment is extremely harsh and unforgiving, with extremes such as vacuum, thermal radiation, atomic oxygen, and plasma. Re-entry vehicles routinely reach temperatures more than 1500 °C, for example [3].

The current methods for manufacturing these metal matrix composites or cermets are complex, slow, expensive, and involve extremely high heats or pressures. Therefore, a new, simpler, and cheaper method for creating these materials is required for on-site production in military deployments and fabrication in the space environment. In fact, a simpler and more energy-efficient method could replace all current cermet technology. It could lend itself to use as an on-orbit manufacturing technique, or large- scale production. To fill this need, a novel AM method for cermets is introduced and evaluated herein. The RES method could be considered AM in the sense that multiple treatments can be applied in succession to modify/improve the part being created. This is especially relevant for films, in which a layer can be applied to the substrate, treated, and then another layer added in succession. The conclusion reached is that this new method of cermet manufacture could enable production in mobile environments, such as Marines on deployment, shipboard, or even in space using simple, standard equipment (rather than equipment customized for the process).

C. SPACE APPLICATIONS

One unique application of cermets: conversion of solar energy to heat energy for space vehicles. Different types of cermets present a high absorbance in the solar spectrum and low emittance in the infrared (IR) spectrum. Thus, incident visible spectrum energy can be converted to the "heat energy" spectrum (IR). A multilayer material consisting of an anti-reflection coating, the cermet, and an IR reflector all layered on a substrate is the typical design [4]. The basic schematic is shown in Figure 2. The idea is that the anti-reflection coating (ARC) will minimize solar energy being reflected from the surface, the cermet provides selective absorption properties, and the IR reflector helps to reduce losses due to radiation. The ideal cermet material will behave closer to metal in the IR spectrum and ceramic in the visible [4].

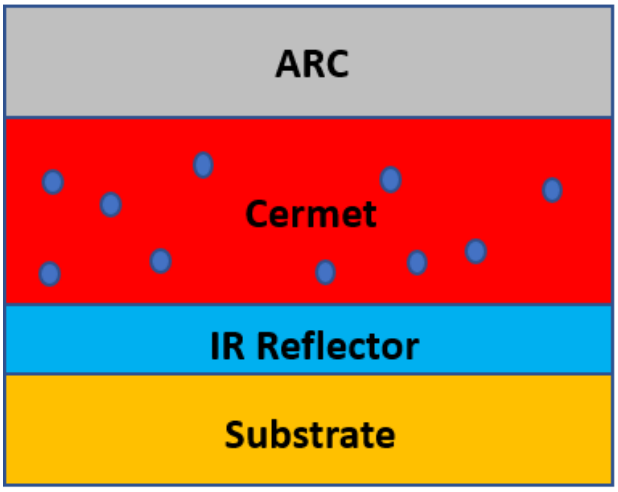

Figure 2. Representation of a cermet-based multilayer material. Adapted from [4].

There are several options for creating these multi-layer materials such as electroplating, anodizing, evaporation, and chemical vapor deposition. Sputtering and solution-based methods are also common [4]. A specific type of cermet that has been proposed for space applications is a film of gold and aluminum oxide (alumina) sputter deposited on silicon substrates. The idea would be to optimize photo-thermal energy conversion and provide energy for a Stirling-type space engine, which converts heat to

mechanical energy. The films that provided the best power were typically 80–100 nm with 20–30% gold present [5]. These films can have multiple layers or be graded throughout. Furthermore, a titanium and alumina cermet was also tested on the Materials International Space Station Experiment (MISSE), as shown in Figure 3. The mixture of these two materials was identified as the most durable against atomic oxygen, vacuum, and UV radiation and it was determined that it could provide a robust thermal concentrator for at least 1.45 years [6].

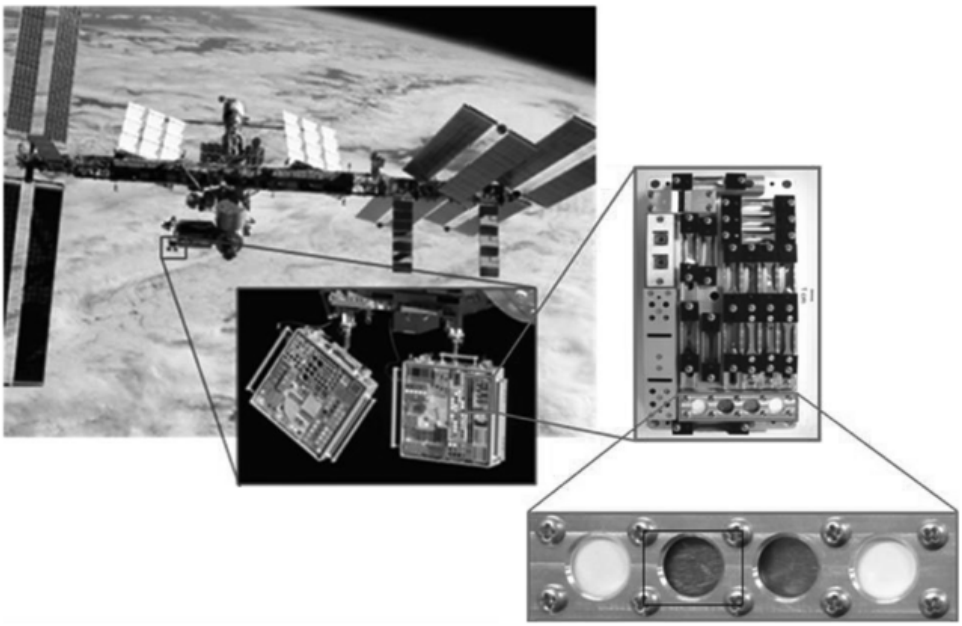

Figure 3. The cermet film experiment on MISSE 6. Source: [6].

D. MANUFACTURING METHODS IN SPACE

To fully understand the scope of manufacturing in space, it is useful to define two separate areas. The first area is on-orbit manufacturing, which at this point is relatively unexplored with the only examples being polymer manufacture on the International Space Station (ISS). The second area is on-orbit assembly, which is much more advanced than manufacturing and has to do with building larger components from already manufactured parts. This has already been done on a very large scale. Indeed, the space station was assembled from very large parts individually launched and placed in orbit [7].

1. Difficulties

The most common area being explored in on-orbit manufacturing is additive manufacturing, but conventional manufacturing is being explored as well. One frequent objection to AM on-orbit is that specialized metals or composites are needed for spacecraft parts. Yet, feasible processes to AM specialized materials have not been demonstrated. Moreover, there are time, size, and power concerns with this type of manufacturing [7]. For example, a small hand tool took almost four hours to make on the first 3D printer on the ISS. Additionally, printers on the ISS consume around 600 W of power, and if metals were to be introduced in the form of sintering printers, that number can be expected to be increased by a factor of 10. The time and power concerns would, of course, be even greater the larger and more complex the parts [7].

2. Finding a Solution

Only a small number of programs, mostly government supported, are exploring on-orbit AM due to its relative infancy and high risk. The company Made In Space, launched a 3D Printer to the ISS in 2014 and utilized plastic as the basis for manufacturing. The same company eventually provided the Additive Manufacturing Facility (AMF) to the ISS in 2016 that can manufacture components utilizing several different polymers [7]. Currently, the primary push is to develop toward additive manufacturing of metals in space, and a U.K. firm has developed a printer that utilizes metal powder and has been tested in the weightless environment of a diving airplane. The ultimate goal, however, would be to eventually utilize *in-situ* resources to create parts in space [7]. A good example was produced by the company Planetary Resources in the form of a propulsion system created from materials found in asteroids, as indicated in Figure 4.

Figure 4. A propulsion system 3D manufactured from asteroid material. Source: [7].

However, these methods all involve additive manufacturing and are fraught with the same issues as described previously. This thesis will attempt to present data for a potential new method to combat some of these issues and allow for a more efficient and stable method of manufacturing while on-orbit.

E. ADDITIONAL APPLICATIONS

A unique application of metal matrix composites to the aerospace field is the ventral fins and fuel access cover on the F-16, which were made from discontinuously reinforced aluminum. The fin is shown in Figure 5. This was done because aerodynamic buffeting was causing issues with the original structure that caused it to fail [8]. Another example: aluminum "reinforced with 50% B monofilaments is used in 243 MMC tubes for construction of each Space Shuttle Orbiter mid-fuselage main frame and rib truss members, frame stabilizing struts and nose landing gear and drag brace supports" [8]. This ultimately saved 143 kg over alternative methods. Aluminum alloy reinforced with graphite fibers was also used on the Hubble Space Telescope for antenna masts. In addition, more cost-effective discontinuously reinforced aluminum with silicon carbide has been tested and flight qualified [8]. Techniques for creating cermets simpler, faster and with lower cost will likely lead to more extensive applications.

Figure 5. F-16 showing the ventral fin at the back of the aircraft. Source: [8].

II. OVERVIEW OF CURRENT CERMET MANUFACTURING PROCESSES

Metal matrix composites are a class of materials in which two or more phases are combined but are physically or chemically separate within the material. As the name implies, the metal is the phase in which the other substance is distributed (the matrix) and is continuous throughout. There are three types of metal matrix composites: particle reinforced, fiber-reinforced, and continuously reinforced. This study will mainly focus on the particle reinforced metal composites. Presently, these types of composites are made through a variety of methods such as spray techniques or through some sort of powder mixing with hot isostatic pressing (HIP) [1].

A. HISTORY OF CERMETS/METAL MATRIX COMPOSITES

This category of materials was initially explored around 1960, with the development of steel-reinforced copper [3]. This timeframe saw a strong motivation to develop new materials for military use to drive up performance, with cost being a secondary concern. This development by the military eventually led to a more widespread use within the commercial sector. However, by 1970, development stagnated and was no longer prioritized as the focus for military systems shifted to cost effectiveness and affordability. Around 1980, new technology, discontinuously reinforced composites, drove down the cost of cermets significantly, demonstrating these materials could be employed in a cost-competitive manner [8]. Since that time, government-funded research/development programs improved understanding of the advantages of these materials. This, in turn, led to a significant increase in study/development, and actual deployment [8].

B. COMMON MANUFACTURING TECHNIQUES

The preferred methods for manufacturing metal matrix composites are different for solids and films. These methods, as they relate to discontinuously reinforced composites, always include a method for mixing the “reinforcement” phase into the primary phase during creation. For example, stir casting is a common large-scale method that involves

high energy mixing of ceramic particles into molten metal. These melts can then be cast as ingots or rolling bloom [8]. In addition, powder metallurgy processes start with high shear powder mixing followed by sintering and hot pressing and finished by forging or rolling. Powder metallurgy processes for manufacturing solid parts are extremely popular in industry due to low cost and a vast range of finishing and tailor-ability available [8].

Typical film processes are electroplating and sputtering, although deposition from solution is also occasionally employed. Electroplating has been used to create chrome solar absorbing film utilizing 75% chromium and 25% chromium oxide. The process involves a metal anode being placed into an electrolyte solution and a current being applied to drive the ions from this metal to coat another metal also in the solution. In sputtering, a target material surface is eroded by a particle beam, and the vapor that is produced condenses on another surface, known as the substrate [4]. Usually, ceramic material and metal are sputtered at the same time as the vapor from each is directed toward a substrate, and the two phases mix as they adhere, creating a discontinuously reinforced composite. Finally, nickel-alumina cermets have also been created from solutions containing solvated metal. For example, nickel chains were embedded in an alumina matrix utilizing an aqueous solution and a chelating agent. Solution processes do have some issues such as non-uniform film thickness and negative environmental impacts [4].

A novel method that has been utilized for creating solid cermet parts incorporates a reduction and hot-pressing process. Nickel and nickel oxide particles were dispersed within alumina and this was reduced under 700 °C then hot pressed at 1450 °C under a pressure of 30 MPa for 1 hour [9]. It was shown that the nickel particles were often present at the grain boundaries of the alumina. The research proved that both the magnetic and mechanic properties could be controlled by the amount of nickel added to the mixture during processing and, generally, toughness was increased by the nickel inclusion [9].

III. BACKGROUND FOR REDUCTION EXPANSION SYNTHESIS TECHNOLOGIES

Reduction Expansion Synthesis (RES) [10–15], is a set of technologies based on a novel "reduction" chemistry invented and developed at the Naval Postgraduate School. There are key similarities to all RES chemistry. First, in all cases, the process starts with a primary step: thermal decomposition of solids, such as urea, under inert gas. This primary step chemistry creates volatile "reducing" radicals that can be harnessed to create a wide range of products based on designed secondary reactions. Novel processes developed on the basis of the RES concept include the batch generation of sub-micron metal and metal alloy particles [11,13], metal thin film formation [14,15], metal part formation from mixtures of metal and metal oxide particles [10], and graphene from graphite oxide [12].

In all "metal" variants of RES, the key secondary step is the reaction of reducing radicals with metal oxide, metal salts, or metal hydroxides. It is postulated the radicals interact with oxygen atoms in metal oxides to create products such as CO_2 and H_2O that subsequently leave the process reactor as gas. The heavy metal atoms/metallic clusters produced via the removal of oxygen are not volatile, and do not leave the reactor. Instead, based on proper arrangement of materials within the bed, these species migrate, as per the Ostwald Ripening mechanism, leading to metal particle growth and sintering [10,11,13–15].

A. SPECIFIC RES PROCESSES

The first Reduction Expansion Synthesis, or RES, technology, a method to synthesize submicron and nano-metal particles from metal oxide precursors, is exemplary of the simplicity and low cost of all RES processes. Simply pour a mixture of metal oxide powder and fertilizer (urea) into a high temperature "baking dish," flush with an inert gas (e.g., nitrogen) and heat to 850 °C for 10 minutes. The only limit to batch size is the furnace dimension. This idea was first implemented utilizing iron and nickel but was later expanded to other metals, such as magnetic alloy powders [13]. It was eventually shown that ferromagnetic and magnetic rare-earth alloys could be produced such as cobalt nickel and samarium-cobalt, and these powders could be useful for either metal injection molding (MIM) or 3D Printing.

This supported the idea that RES could be considered a general manufacturing technique and applied to several different substances or mixtures [11]. In addition, this process has also been utilized to dope graphene sheets with nitrogen, utilizing graphite oxide and urea as precursors. This method was shown to be useful in controlling the amount of nitrogen that was present in the graphene and these samples were used as electrodes in various batteries, with improved performance compared to standard methods [12].

The "variation" of RES employed to make solid parts (RES-SM) and metal films on existing metal (Cr-RES) are the methods most related to the current study of creating solids and film cermets. Examples of both are shown in Figures 6 and 7. In Figure 6, an iron wire was coated with chrome using a variant on the original particle creating RES process. The process in brief: A paste consisting primarily of well-mixed chrome oxide, urea, and water is spread on the surface of the target metal. The part is then dried. Finally, the coated piece is heated to about 800 °C under flow of an inert gas for about 10 minutes [14].

For thicker pieces, such as the tensile specimen shape shown in Figure 7, the Cr-RES process does not work. Modifications are required to keep the pressure burst associated with the sudden decomposition of urea from destroying the designed shape. Specifically: i) the metal precursor used was a mixture of metal and metal oxide particles and ii) the urea is not mixed with the metal precursors, but rather is placed "upstream" such that the radicals created by the thermal decomposition of urea pass through the metal/metal oxide bed. These radicals reduce the metal oxide, leaving metal atoms that migrate to form bridges between existing metal particles. All of this occurring in less than twenty minutes in a conventional furnace at about 900 °C [10].

The "brown bodies" created in the RES-SM process are similar, actually significantly denser, to those generated over many days using the PIM process. The time advantage of the RES-SM process arises from the fact that no "de-bonding" step is required [10]. Also, there is no need for the additional steps associated with PIM: i) there is no mixing in RES-SM; ii) there is no need for a high pressure (ca. 300 atm) apparatus to inject the precursor "gel" into the molds. Dispensing with all these steps saves significantly on capital investment and time and shows that RES-SM could prove to be a commercial success [10].

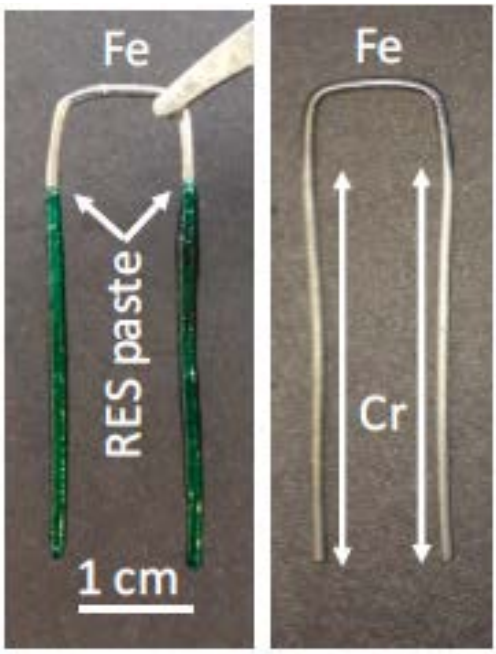

Chrome coating on an iron wire from the RES process.

Figure 6. Examples of the RES process on films. Source: [14].

A rectangular nickel body created through RES showing faithfulness to mold shape and indicating significant sintering.

Figure 7. RES process applied to sintered metal parts. Source: [10].

Pursuing a variant of RES for cermet production is justified on the basis of cost, simplicity, and portability. Cost reduction occurs because the only “major” hardware is

"off the shelf" furnaces [13]. Simplicity includes the fact that the process is basically "shake, put into a mold, and bake," requiring little training. Portability is a function of the first two: all that is required is a simple electric furnace, simple glassware, molds, powder, and inert gas.

B. RES THEORY

RES processes all employ solid reactants capable of producing reducing species upon thermal decomposition in a unique manner. Specifically, before RES, there was no process employing solid reductants to make metal particles, metal films, catalysts, graphene, or for any use in additive manufacturing. Surprisingly, there was only one major technology that employed solid reducing agents: steel making using coal. In fact, fully understanding the mechanism of steel-making was the inspiration for the genesis of the RES technique [16,17].

In brief, the chemistry of steelmaking, the "original" RES-like process, is as follows: i) In a hearth, alternating beads of coal mixed with "flux," where a flux is generally potassium or sodium carbonate, and iron oxide are organized. ii) The bed is heated, causing the "flux" to spread as a near mono-layer on the coal. iii) Oxygen atoms from the flux react with the coal to make carbon monoxide/CO. The flux is now in an oxygen-deficient state. iv) CO diffuses to the iron oxide. v) CO reacts with the oxygen in the iron oxide, creating metallic iron and CO_2. vi) Oxygen is admitted to the reactor. It returns the flux to the fully oxidized state. vii) Return to Step iii and repeat until all of the iron oxide is reduced. The resulting liquid metal runs out of the reactor and is now ready to be shaped and hardened [16,17].

RES is inspired by the success of coal-based steel making. The "general" model of coal-based steel making involves some unique steps which parallel processes found in RES. First, "reducing" radicals are created from solids. Second, the radicals thus formed can act locally to reduce metal. Third, this type of chemistry can be manipulated to create convenient, low-cost approaches to the production of valuable materials [16,17].

The first example of RES, one using reducing radicals produced from solids, was the reduction of metal oxide particles from the byproduct of urea decomposition. Unlike

steel making, no oxygen admission is required. Unlike coal, urea decomposes upon heating directly, no catalyst required, to create volatile reducing radicals. But, as in coal-based steel making, the reducing species are released from solids placed near the target oxide. Thus, in this earliest form of RES, all that is required is the presence of urea, or a similar solid that releases reducing gases upon thermal decomposition, near metal oxide to be heated in an inert gas (e.g., nitrogen or argon) environment [13].

A relevant variation on the above is the production of solid metals of designed shape. The process involves essentially the same chemistry. First, metal and metal oxide particles are mixed. A solid that thermally decomposes to generate reducing radicals, such as urea, is placed nearby/upstream. The metal/metal oxide mix and nearby urea are placed in a furnace, through which inert gas is flowing, and heated to around 950 °C (well above the decomposition temperature of urea) [10]. When the urea decomposes it creates radicals, these strip the oxygen atoms off of the metal oxide creating volatile gases such as carbon dioxide. The metal (e.g., nickel) oxide is reduced at this point, which causes the nickel ions to become mobile and they bond to the nearest metal atom. The process forms bridges or necks between the metal atom and the mobile nickel ion, and this process is repeated throughout an entire mixture until all the nickel oxide is reduced. Essentially, this causes the nickel to sinter together at temperatures much lower than the typical melting temperature [10]. Overall, the sintering process is anticipated based on known sintering behavior of metals at elevated temperature and the mechanism is extremely similar to Ostwald Ripening, and has been explored in-depth in previous work [10,11,13].

C. THEORY OF RES APPLICATION TO CERMETS

The key assumption for the proposed application of RES to cermet formation is that the simple addition of ceramic particles to a mixture of metal and metal oxide will not negatively impact the RES-SM process. That is, the cermet RES process is intended to be nearly identical to the RES-SM process, the sole change being the addition of ceramic particles to the physical mixture of metal and metal oxide particles. The primary formation hypothesis is that the ceramic particles will be “squeezed” together by the surrounding metal particles as they bond to each either during the sintering phase. That is, the ceramic

particles will be held in place by physical, not chemical, forces. It is anticipated that the addition of the ceramics will not impact that actual chemical reaction that takes place between the reducing agent and the metal oxide; however, some potential difficulties do exist. For example, the ceramics may act as a type of “heat sink” and reduce the amount of heat energy that drives the mobile metal atoms to bond to each other and the nickel particles. It may also prevent full sintering by “blocking” places that mobile atoms can attach. Given the “qualitative” nature of RES theory, only an experimental trial can be employed to test RES applicability to the manufacture of cermets.

IV. CONTROL STUDIES ON PURE NICKEL

To obtain an accurate idea of how well the cermets performed in a general sense, two pure nickel pieces were created utilizing the RES process, which provided some interesting results as control studies. The control components were theoretical “best case” scenarios for creating a pure nickel part utilizing RES, and a nickel part that had been “activated” in hydrogen peroxide following a procedure explained in previous work [10].

A. INTRODUCTION

The focus of this chapter is on the use of the RES process to make solid pieces of pure nickel of a designated shape to compare to future experiments involving cermets. The primary parameter that was varied in this case was whether the nickel particles were “activated” before experimentation, allowing for cleaning of the surface to occur. The results for the solid nickel bodies were interesting and provided valuable data for comparison, especially in relation to hardness testing and overall structure of the bodies. This control study also produced the largest self-supporting nickel body formed from the RES-SM process to date.

B. EXPERIMENTAL

Overall, there were several distinct phases or variables in the creation of these metal pieces. The variables can be divided into chemical preparation, mixture preparation, gas flow optimization and timing into the furnace to create a neutral atmosphere, furnace heat, and the specific techniques used to analyze the results.

1. Chemical Preparation

The first piece was created by physically mixing 5 μm nickel powder (Sigma-Aldrich, 99.7%) and 45 μm nickel powder (Goodfellow, 99.5%) with an equal amount of nickel oxide powder (Sigma-Aldrich, 99%) for a 1:1 total nickel powder to nickel oxide ratio by mass. The primary reason for utilizing two different sizes of nickel powder was the theory that this variation would allow for better packing of the particles and, therefore, stronger sintering.

The second part mixture that was created with pure nickel had the additional step of activation applied to it. This involved placing 5-µm and 45-µm nickel powder into a beaker and covering it with 30% hydrogen peroxide under a fume hood. This was then put on a hot plate at 250 °C until boiling occurred, and then removed until boiling stopped. Finally, this was placed back on the hot plate at a lower heat until all remaining liquid had evaporated. This was done to change the surface of the particles by cleaning to provide an ideal surface for the RES process to occur [10].

2. Mixture Preparation

The nickel and nickel oxide powders were mixed with a pedestal for roughly 2 minutes. The mixture was then formed into a mold and it was shown that the powder mixture would retain its shape if packed down slightly by hand. The mold was made from two pieces of acrylic that had been shaped utilizing a laser cutter and is shown in Figure 8. When full, this mold ("bar" mold) could hold approximately 6.6 g of metal precursor powder.

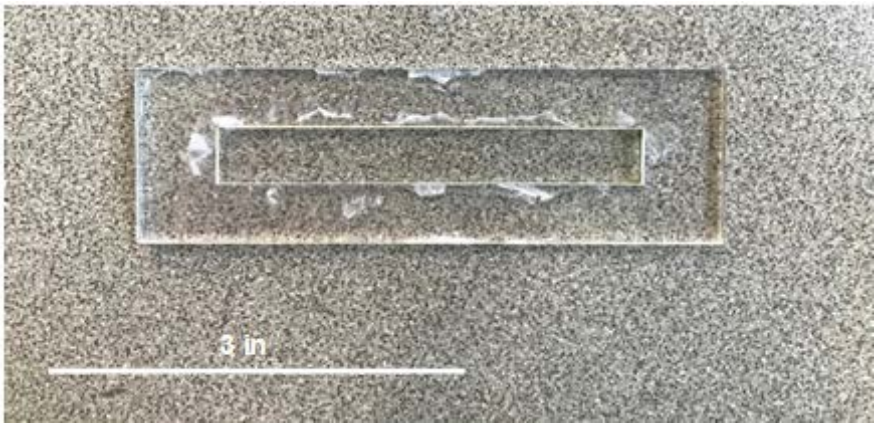

Figure 8. Bar mold utilized for control experiments.

This mold was then emptied on to a fresh Grafoil sheet with pinholes at regular intervals, and this was positioned over an alumina boat. The boat contained 1 g of urea pellets (Sigma-Aldrich, ~99% or LabPro) for the non-activated nickel precursor and 2 g of urea for the "activated" sample. The general setup is shown in Figure 9.

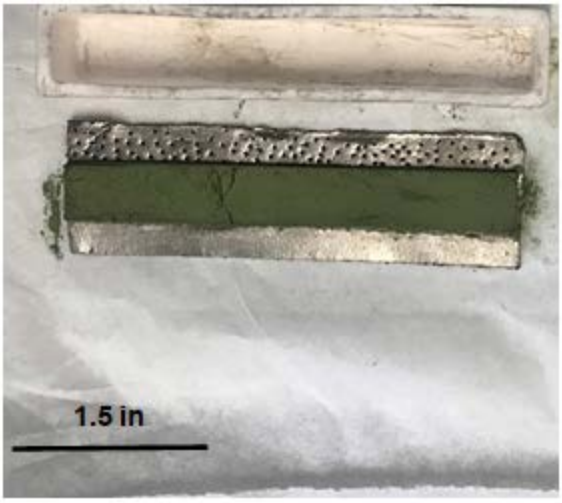

Figure 9. Emptied powder from the bar mold and alumina boat utilized.

3. Neutral Atmosphere

In order to avoid unwanted reactions, such as metal oxidation, all RES processes were conducted under an inert atmosphere of argon or nitrogen. Air, particularly oxygen, was “flushed” from the sealed quartz tube containing the particle-filled mold with a continuous flow of gas for a set period. The mold with the nickel precursors was placed into the quartz tube and the tube was placed under a flow of 99% purity nitrogen for 10 minutes (flow rate was approximately 19 ml/s). This time and flow rate was an estimation based on previous experiments. Generally, the flow should remove all the air or oxygen containing species from the volume where the experiment will take place. Usually, gas was allowed to flow for sufficient time to ensure that the volume of gas input was approximately three times the physical volume of the tube. The tube diameter was roughly 5.1 cm and the length was 150 cm. Therefore, the volume was around 3062 cm^3. The time it would take to fill three times this volume at 19 ml/s would be 484 seconds (8.1 minutes). Hence, the 10 minutes utilized in this experiment allowed room for potential error and ensured that a neutral atmosphere was obtained.

4. Furnace Treatment

As the air was removed and the tube was filled by only an inert atmosphere, a large clam-shell three-zone furnace (Carbolite, 72.5 cm) was set to 950 °C in each zone. When

the appropriate temperature was reached, the gas flow was lowered to almost zero and the tube was “slid” into the furnace so that the section of a tube containing the sample was directly in the center. It was kept in the furnace for 15 minutes at the same nitrogen flow rate and then removed and allowed to cool. This process was conducted for both the non-activated and “activated” samples.

This process was repeated a second time (two treatments) for the non-activated sample only. The entire process could theoretically be repeated many times, with variations, which is the basis for an “additive manufacturing” process. The amount of urea was changed to 2 g for the second bake. The experimental setup before furnace insertion is shown in Figure 10.

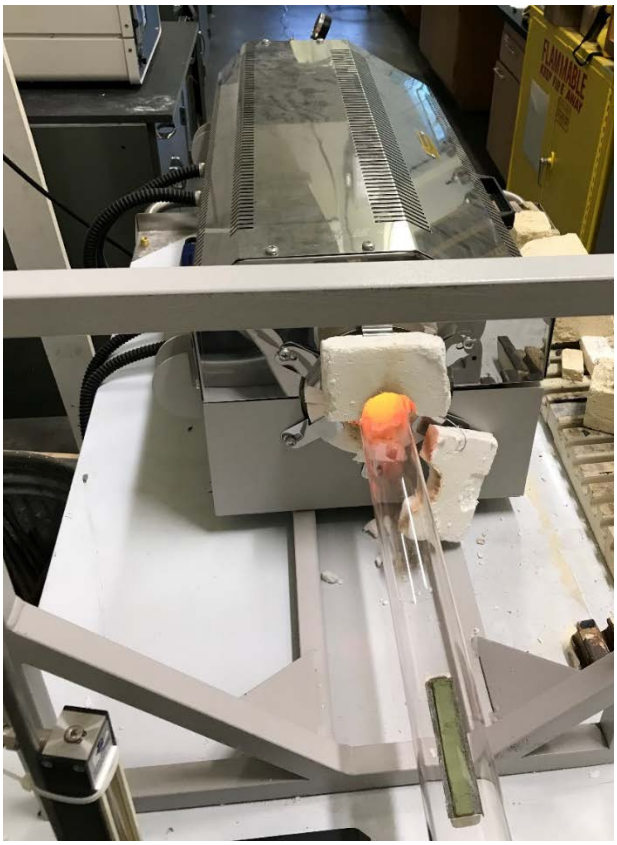

Figure 10. Clam-shell furnace with the molded nickel powder before insertion.

5. Post-processing Analysis

After firing, the samples were analyzed both through visual inspections and a series of hardness tests. The analysis methods are described below in detail.

a. Optical

The first characterization technique that was utilized in this research was a simple visual observation augmented by optical microscopy (Nikon Model Epophot 200). Visual observation was essential to determine if the created parts behaved as solids, or simply remained as a powder after treatment. This observation also allowed for a relativistic determination of the strength of the pieces made by how easily they broke or if the part remained as a solid. In addition, it was useful for noting cracks or deformations that may have occurred during treatment. The optical microscope allowed for visualization of smaller voids within the sample and helped to determine relative density of the parts created as compared to standard manufacturing methods for nickel. Utilizing the optical microscope also allowed for comparison after post-treatment such as polishing and cleaning.

b. Hardness Tests

The next method of characterization utilized for this study involved the hardness testing device based at the NPS shown in Figure 11. This was a Struers DuraScan device with the capability to perform a Vickers hardness test utilizing various loads. This test works by applying a load to the sample utilizing a small tipped press. The indent from the press is then measured optically utilizing a light microscope and the size of the indent allows for a determination of the hardness of the material. For this test to work, the material must typically be dense enough to retain its shape and must have at least a semi-reflective surface for the optical microscope to measure the indents. The amount of force applied to the indenter can be varied based on the material. It is typically best practice to choose the highest amount of force possible to allow for a larger indent, which increases the accuracy of measurement. This machine at NPS is capable of taking both single and series measurements of samples.

Figure 11. The Struers hardness testing machine at NPS.

C. RESULTS

The results from the two control experiments were especially interesting for both visual inspection and hardness tests. For example, the control proved that the powder mixtures could be placed in an acrylic mold and keep their shape after the mold was removed. In addition, it showed that significant shrinkage occurred after the RES treatment, as was expected. The control study utilizing the non-activated nickel powders produced the largest self-supporting solid piece created by RES to date. In addition, the hardness tests were promising, but the parts were extremely brittle.

1. Visual Observation Results

It was noted that large cracks appeared on the surface of the samples and that they seemed to originate where small cracks had been in the powder pack before heat treatment. This seems to suggest that sintering may not occur across large discontinuities between particles. However, these pieces seemed to be structurally sound and retained their shape very well. A very small amount of excess, or loose, powder fell from the part during routine handling after treatment. The treated non-activated part is shown in Figure 12, indicating structural integrity. This part shrank from approximately 7.62 cm to 7.5 cm after two treatments and is the largest self-supporting nickel part created utilizing RES to date.

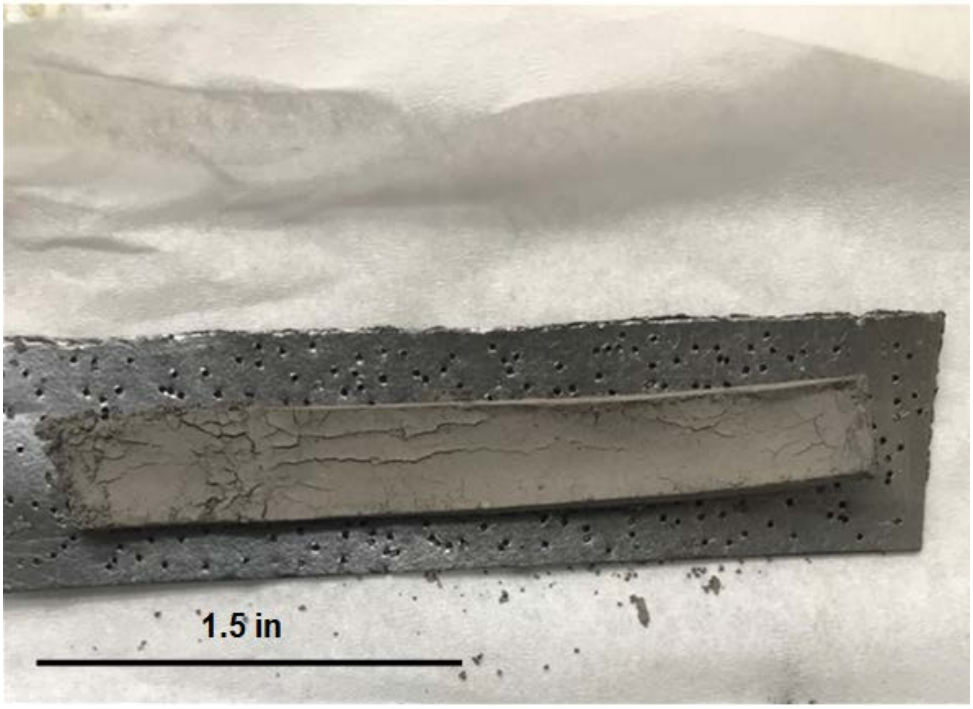

Figure 12. Pure nickel-metal part created utilizing the RES process.

In order to quantify the structure of these pure nickel pieces to a higher degree, hardness tests were also conducted. These particular samples had to be polished slightly before being tested because the hardness testing machine at NPS utilized an optical microscope to measure indents made during the particular test utilized (Vickers). The

pieces were polished utilizing a Buehler Variable Speed Grinder-Polisher for approximately ten minutes with progressively smoother polishing wheels. This allowed for a reflective surface conducive to the hardness tests. This polishing also indicated that these parts could be successfully surface-treated without wholly being destroyed or disintegrating.

2. Hardness Results

The hardness test utilized was a Vickers HV 0.025 method, and the results were relatively consistent. It was expected that, due to the relatively porous nature of the sample after the RES method, hardness tests would yield very little. The localized cracking that occurred seemed to validate that point and indicate that the hardness value may not be especially accurate. However, a hardness value average of 5.6 was obtained from measurements of the once-treated activated nickel sample. This is, of course, very low compared to the value of traditionally manufactured nickel but provides good insight into how brittle these samples seem to be. It also shows that these samples can be tested for hardness in the first place, indicating progress utilizing the RES method and allowing for comparison to other materials created in this way.

D. DISCUSSION

Comparing the activated nickel sample and non-activated sample after one treatment did not indicate any significant differences between the two parts, they were both self-supporting and appeared to have the same properties during routine handling. This indicates that activation of the precursor nickel powder to “clean” it may have almost no impact on the final structure. Both samples had large cracks appear where smaller cracks had originated in the powder pack before treatment, indicating that the sintering process through RES would likely not occur across large discontinuities.

Conducting a second RES treatment on the non-activated part seemed to provide some benefit to the structural integrity of the piece and seemed to remove some discolorations within the piece. The piece was noticeably more robust after two treatments, indicating that multiple RES treatments can improve the properties of a sintered metal part. The fact that multiple treatments can be applied and improve the part is the basis for this

process to be called “additive manufacturing”, and no material is ever removed. It is even feasible that more precursor could be added between treatments to modify the shape or size of the part.

Finally, the hardness tests conducted on the activated metal part seemed to indicate that these nickel pieces can be reliably surface treated by polishing, but have very low density. The hardness values were extremely low and localized cracking occurred, which shows that there may be pockets of un-bonded metal and uneven sintering. These results are consistent with previous work on RES to create fully sintered metal parts [10]. However, this study expanded the largest size part created utilizing RES to 7.5 cm, which paves the way for future work with progressively larger pieces and robust failure testing.

THIS PAGE INTENTIONALLY LEFT BLANK

V. SOLID CERMET PARTS

The first goal of this thesis was testing the applicability of the RES method to the production of solid cermet parts. Ideally, a part would meet these simple specifications: i) The formation of a solid part, that is one which can be handled without breaking, using the RES process, and ii) demonstration of successful densified to >90% ideal density, using Hot Isostatic Pressing or other sintering protocols

A. INTRODUCTION

Initial experiments were designed on the basis of a postulate that represents a direct extrapolation of the previous successfully demonstrated process for creating solid metal parts from mixtures of metal and metal oxide particles, RES-SM (see Ch. IV). It is summarized as follows: Application of the standard RES-SM process to a physical mixture of metal/metal oxide will yield solid cermet parts via a chemical/physical process. Metal particles will "neck" together due to a chemical process in which atoms or small clusters of metal created by the RES process diffuse within the bed, joining existing metal particles. This leads, as per standard theory, to sintering via an Ostwald Ripening process. In a concomitant process, ceramic particles would be surrounded by the growth of a continuous sintered metal matrix. Thus, the ceramic particles would be bound to the solid metal network not by a chemical process, but rather by physical containment.

It was discovered that the extrapolation of the RES-SM process to cermet formation did not work, indicating that the simple hypothesis outlined above is not correct. As discussed below, most of the solid parts generated on the basis of the RES-SM extrapolation were mechanically unstable and several did not bond at all and remained exclusively in the powder phase. Only a few cermet mixtures involving very low silica loading retained mold shape and these cermets were mechanically brittle. However, an understanding of the primary "failure" mechanisms was reached. It was clearly established that the RES process results in ceramic material "coating" the surfaces of metal particles, and this blocks the creation of metal necks connecting metal particles. That is, an unanticipated chemical process, ceramic oxide species coating metal, was discovered. This

was noted especially in parts created with both nickel and nickel oxide precursor powders. Thus, no stable part can form. This finding led to a new hypothesis: Ceramic will not coat metal oxide during the RES process, thus a bed of pure oxide will not be ceramic coated during the process, allowing a matrix of metal particles, surrounding included ceramic particles, to form. This concept was tested by performing the RES process on a bed of pure nickel oxide physically mixed with ceramic particles. In this case, the microstructure was much more promising and significant necking did occur. Thus, a promising protocol for creating "successful" solid cermet structures using RES was supported by preliminary analysis.

B. EXPERIMENTAL

The procedure for creating the cermet parts aligned closely with the procedure for the pure nickel control studies. Aside from the main change of adding ceramic particles to the metal precursor mixtures, a smaller furnace was primarily utilized for the heat treatment. In addition, rigorous neutral atmospheric calculations were conducted and procedures implemented to ensure that the atmosphere inside the sample tube was mostly inert gas.

1. Chemical Preparation

Several different precursors were prepared for testing the impact of initial composition on the final cermet properties. Five different types of ceramics were tired: 0.007 µm fumed silica (Sigma-Aldrich, ~99%), 80% 1-5 µm standard silica (Sigma Aldrich, 99%), 3 µm alumina (Alfa Aesar, 99.97%), 0.05 µm micropolish alumina (Buehler, 99%), and 0.01 µm silicon carbide (Sigma-Aldrich, ~99%). In addition, a single size <150 µm nickel particle was utilized (Sigma-Aldrich, 99.99%) as well as consistent nickel oxide particle size (<44 µm). The ceramics were mixed with both nickel and nickel oxide powders in most cases. In one case only nickel oxide was utilized, and no pure nickel powder. The impact of changing the ratio of total particle precursor to urea was also investigated.

These materials were placed in molds and heat-treated in a furnace under an inert atmosphere. It is interesting to note that, in previous work, the amount of ceramic present

was often reported as a percent by volume, likely because of the low density of ceramic particles compared to the metal. The percent volume was simply calculated utilizing the following formula for each phase in the sample utilizing the bulk density. It is important to note that bulk density varies widely with how the powder is handled, so approximate values were utilized from the specific products, if available [18]. The bulk density of fumed silica was 0.0368 g/ml [19], the bulk density of standard silica was 0.22 g/ml [18], the bulk density of the alumina was 0.24 g/ml [18], and the bulk density of silicon carbide was 0.069 g/ml [20].

$$\%v_{ceramic} = \left(\frac{\%m_{ceramic}}{\rho_{ceramic}} \right) \div \left(\frac{\%m_{ceramic}}{\rho_{ceramic}} + \frac{\%m_{nickel}}{\rho_{nickel}} + \frac{\%m_{nickel\ oxide}}{\rho_{nickel\ oxide}} \right) \quad (1)$$

where v is the volume of the particles in m^3, m is the mass in kg, and ρ is the density in kg/m^3. Table 1 indicates the percent mass and percent volume of ceramic particle mixtures utilized in the present study.

Table 1. Percent mass and percent volume of ceramic particles.

Sample Type (Percent Mass)	Ceramic Particle Size	Ceramic Percent Volume (Estimate)
30% Alumina	3 µm	52.3%
6.25% Alumina	3 µm	16.3%
1% Alumina	3 µm	2.9%
1 % Alumina (Micro)	0.05 µm	2.9%
1% Fumed Silica	0.007 µm	16.1%
1% Fumed Silica (NiO)*	0.007 µm	11%
1% Standard Silica	1-5 µm	3.45%
1% Silicon Carbide	0.1 µm	9.3%

*This mixture was utilized with only nickel oxide present and no pure nickel.

Percent volumes for metal matrix composites are typically around 15–20% volume fraction of ceramic, especially for powder processing techniques [1,8]. This value tends to provide a good baseline; however, much smaller and much larger percentages have been utilized depending on the applications. For example, cermets, which can be considered a special case of metal matrix composite, can have significantly higher volume percentages of ceramic, up to approximately 70% volume fraction (for use in films in particular) [5].

2. Mixture Preparation

Two distinct protocols were followed for mixing the precursors. Protocol I was based on the initial hypothesis that the RES-C process would be a direct extrapolation of the RES-SM process, and that the addition of ceramic would not produce any additional chemical process. This protocol involved utilizing pure nickel powder and nickel oxide powder in a 1:1 mass ratio and mixing with the required percent by mass ceramic particles.

Protocol II, however, was based on generally disappointing results from Protocol I. In this protocol, pure nickel powder was not included in the mixture, and only nickel oxide powder and the ceramic were physically mixed. This was based on the hypothesis the ceramic would not coat the metal oxide and allow for strong metal-metal bonds to form during the process. This protocol was attempted with 1% fumed silica by mass.

For both Protocol I and Protocol II, the powders were physically ground together with a pedestal for each experiment and placed in either a “cap” plastic mold or a bar shape acrylic mold. The “cap” mold was made by simply removing a cap from a sample tube holder. This “cap” mold corresponded to approximately 0.5 g of metal precursor mass and the bar mold to approximately 6.6 g when full. The molds are shown in Figure 13.

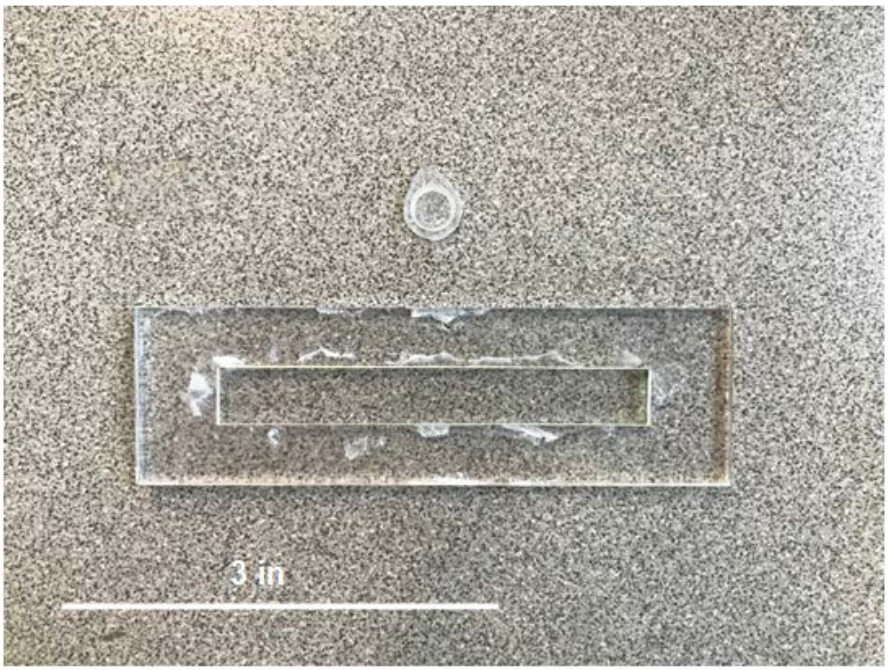

Figure 13. Types of molds used to form the powder mixtures before treatment.

The “cap” type of mold was useful to simply see if a solid part would form after treatment. This small mold has the advantages of compatibility with a small furnace, higher urea to nickel/ceramic precursor ratio, and minimal material requirement. The second type of mold was the bar mold which was made utilizing a laser cutter on acrylic. This mold was designed as a “first step” toward creating larger pieces, and to explore the feasibility of perhaps creating standardized “dog bones” for mechanical strain testing. This mold was only filled approximately a third of the way for use in the single zone clam-shell furnace due to size constraints and the need to maintain a relatively high ratio of urea to nickel/ceramic precursor.

The standard procedure for creating solid parts utilizing the RES process was the same for both the “cap” and bar molds. The nickel/ceramic powder mixture was poured into the mold and packed down as much as possible by hand utilizing a standard laboratory spatula. The mold was then placed on a fresh Grafoil sheet with holes punctured in it with a pin along regular intervals. The mold was often tapped with a spatula or moved back and forth to loosen the powder pack. After the powder was loose, the mold was removed

leaving the pack on the Grafoil, this was then packed down slightly with a spatula, and cracks were removed as appropriate. Finally, the Grafoil with the powder pack was placed over an alumina “boat” containing the urea pellets, as shown in Figure 14. This whole system was then placed in the quartz tube for heating in the furnace.

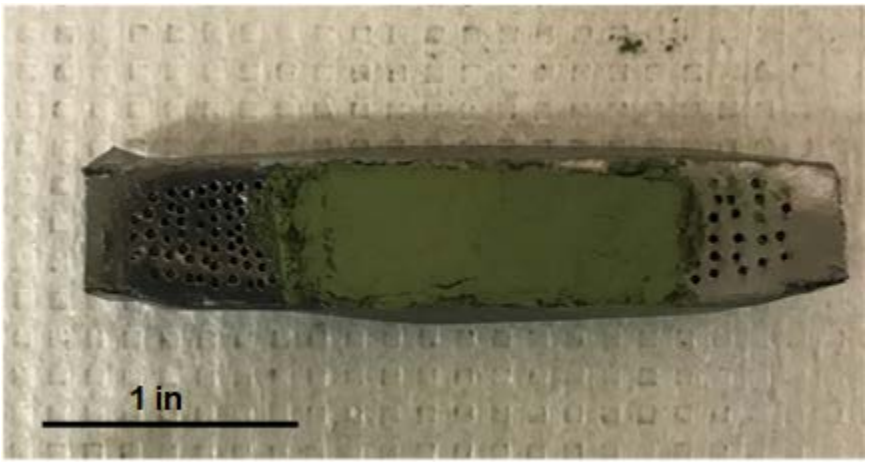

Figure 14. A powder pack on perforated Grafoil before heat treatment.

3. Neutral Atmosphere

As mentioned in the control studies section, in order to avoid unwanted reactions such as metal oxidation, all RES processes were conducted under an inert atmosphere of argon or nitrogen. Air, particularly oxygen, was “flushed” from the sealed quartz tube containing the particle-filled mold with a continuous flow of gas for a set time period. For the cermet part creation, a model was developed to accurately calculate the time it would take to flush the tube. The user had direct control over the flow rate and could ensure that the mixture of the natural gas to oxygen/atmospheric gas was within an acceptable tolerance (~95%). Generally, the time period and flow rate were set such that the tube was flushed with at least three volume equivalents of inert gas, and the model validated this control setting.

The gas flow process modeling was conducted with scaling in mind, as a rapid “flushing” of the tube with the least amount of gas would be useful if this process was ever

to be scaled up for industry or rapid production on orbit. A schematic of the process is shown in Figure 15.

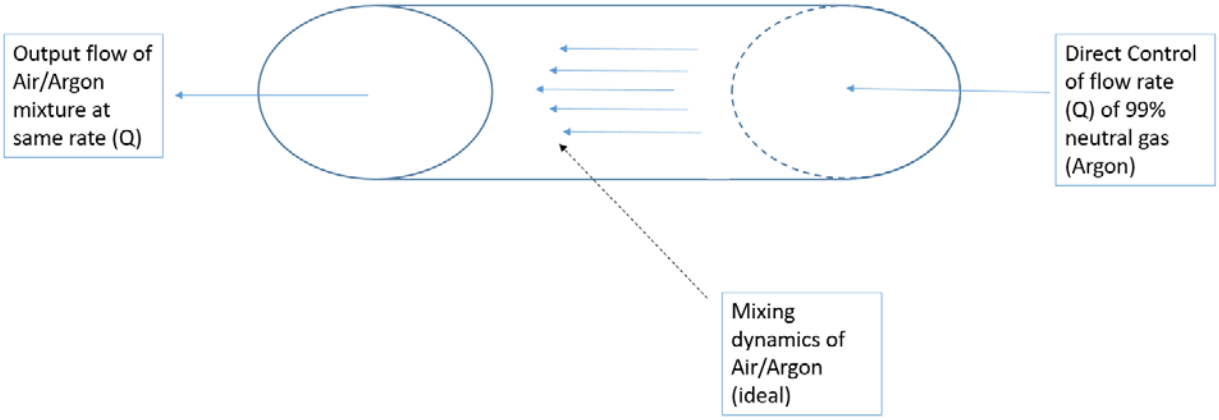

Figure 15. Model of the inert gas flow into the quartz sample tube.

The primary model for mixing was based on a common mixing model differential equation, which can be found in differential equations textbooks or courses [21]. The derivation is described where the state *x* is the volume of argon gas in milliliters. The volume flow rate in ml/s into the tube would be equal to the volume flow rate out as shown, which can be defined as a control variable:

$$Q_{in} = Q_{out} = u \tag{2}$$

The constant tube volume and percent argon input (99%) were also defined:

$$C = 268 \text{ cm}^3 \tag{3}$$

$$k = 0.99 \tag{4}$$

The change in volume of gas in the tube can be described in terms of the state variable *x* as a function of time:

$$\text{In}(t) - \text{Out}(t) = \dot{x} \tag{5}$$

The total amount of inert gas moving into the system can then be defined utilizing the concentration input percent:

$$k \bullet \text{In}(t) \tag{6}$$

In addition, the concentration of the substance in the tube at any point can be defined based on the state variable and the constant tube volume:

$$\frac{x(t)}{C} \tag{7}$$

This can be utilized to define the total amount of the substance leaving the tube:

$$\frac{x(t)}{C}\mathrm{Out}(t) \tag{8}$$

Subtracting the total amount of gas leaving the tube from the total amount of gas moving into the system leads to a net change of volume as defined below:

$$k \bullet \mathrm{In}(t) - \frac{x(t)}{C} \bullet \mathrm{Out}(t) = \dot{x} \tag{9}$$

Finally, substituting in the control variable for the input and output produces the necessary dynamic equation:

$$\mathrm{Out}(t) = \mathrm{In}(t) = Q = u \tag{10}$$

$$\dot{x} = \frac{-u}{C}x + ku \tag{11}$$

This equation can be solved utilizing standard differential equation techniques with the solution in the form below:

$$x = -265.32e^{-0.01131t} + B \tag{12}$$

where the constant B can be identified utilizing the initial conditions of zero argon gas at the initial time of zero:

$$0 = -265.32e^{-0.01131(0)} + B \tag{13}$$

$$B = 265.32 \tag{14}$$

Finally, the equation can be solved for the final time needed to obtain 95% purity of argon gas as shown:

$$0.95(268) = -265.32e^{-0.01131t} + 265.32 \tag{15}$$

$$t = \frac{\ln\left(-\frac{10.72}{-265.32}\right)}{-0.01131} = 283.7\,seconds = 4.7\,minutes \tag{16}$$

Therefore, the gas flow should be kept running for at least 4.7 minutes before the experiment can be run. However, approximately three times that time length was

implemented (15 minutes) in order to ensure high purity and follow the general rule of three volume equivalents of gas being utilized.

This model is a simplification of the flow dynamics actually occurring within the system and does not prove an optimal solution. It also does not take into account factors such as head loss of the flow, which is related to the energy in the flow. Head loss is essentially a friction factor, the less head loss should correspond to higher energy in the flow and, therefore, higher mixing. The Appendix shows an adaption of this system and an application of trajectory optimization theory. The specific equations utilized involve Pontryagin's Principle of Optimality as well as equations for head loss in a laminar flow. Utilizing this method, and propagating the system in a numerical solver, allowed for an optimal control solution to be found that both minimized time for mixing as well as head loss based on the capabilities of the specific experimental setup. The controller that was found dictated that the volume flow rate valve be opened to the maximum flow rate ($3.03\,\frac{ml}{s}$) for 860 seconds (14.3 minutes) to "flush" the 268 cm^3 tube. This produced a head loss of 1.6 $x10^{-4}$ m. Therefore, based on this optimal control study, as well as the simple differential equation modeling shown above, it made sense to flush the tube for approximately 15 minutes before starting heat treatment to ensure high purity of the inert gas atmosphere. Both the dynamic modeling and the optimal control solution are useful for scaling the process to be utilized either on an industrial level or on military deployments/on orbit.

4. Furnace Treatment

The primary furnace was a laboratory-style tube furnace with a clam-shell type opening (Linderg Blue, 45 cm). This was preheated to 950 °C for all the experiments conducted and is shown in Figure 16. Note, the quartz tube containing the powder from the molds (Figure 14) at the furnace center extends beyond the furnace. It is connected to the input gas supply (e.g., ultra-high purity argon, nitrogen, or argon/hydrogen) controlled by a rotameter directly connected to the tank with an Ultra-Torr fitting (right end) and to an exhaust line, also with an Ultra-Torr connector.

Figure 16. The primary tube furnace with quartz tube inserted.

The quartz tube sample holder containing the precursors in the alumina boat, under a neutral atmosphere, would be placed into the preheated furnace for 15 minutes for the treatment to occur. It would only be placed in the furnace after it had reached a temperature of 950 °C from pre-heating. This heat treatment was conducted at least once for all cermet mixtures. If a solid body was formed after one treatment, two more treatments were also applied.

In addition to this primary furnace, the larger clam-shell three-zone furnace was also utilized (Carbolite, 72.5 cm). This furnace allowed for individual control of each of the three zones and can accommodate much larger quartz tubes, hence far larger cermet molds, or multiple boats and precursor combinations. The furnace had a capability to maintain a temperature differential of roughly 200 °C between each zone. For example, if the first zone was at 500 °C, the second zone could be at a maximum 700 °C, and the third zone at 900 °C.

A unique experiment was performed with this furnace on the fumed silica cermet mixtures that relied on changes in the temperature across the three-zone furnace, which could allow for different types of sintering between the nickel particles to occur and form

a stronger bond. It was expected that “quick” sintering would occur in the highest temperature zone as the urea products were produced rapidly by decomposition. In addition, a gradual sintering was also expected from the slow decomposition and transport of urea products in the upstream, cooler, section of the furnace. This experiment was set up according to the schematic in Figure 17.

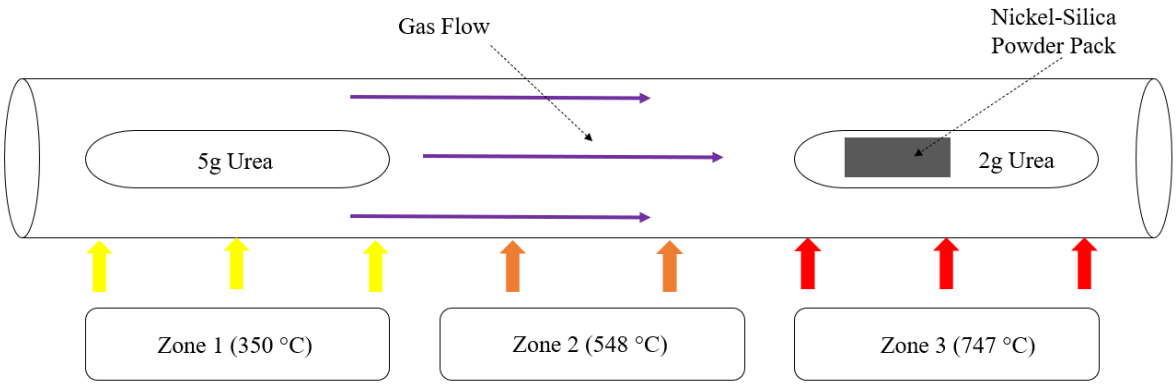

Figure 17. Placement of each of the alumina boats within the 3-zone furnace.

Table 2 summarizes a list of the powder mixtures and overall experimental conditions for all of the solid cermet part tests, as well as the amount of nickel oxide and urea utilized. It also distinguishes which part was created following Protocol II.

Table 2. Summary of test conditions.

Sample Type (Percent Mass)	Mold Type	Nickel Oxide Mass	Urea Mass	Gas Flow	Heat
30% Alumina	Cap	~0.24 g	0.70 g	Argon	950 °C/ 15 min
6.25% Alumina	Cap	~0.24 g	0.25 g	Argon	950 °C/ 15 min
1% Alumina	Bar	~1.1 g	0.5 g	Argon/Hydrogen	950 °C/15 min
1 % Alumina (Micropolish)	Bar	~1.1 g	0.75 g	Argon	950 °C/15 min
1% Fumed Silica	Cap	~0.24 g	0.5 g	Argon	950 °C/15 min
1% Fumed Silica	Bar	~1.1 g	0.5 g	Argon	950 °C/15 min
1 % Fumed Silica (2 treatments)	Bar	~0.55 g	0.5 g	Argon/Hydrogen	950 °C/15 min
1% Fumed Silica (3 treatments)	Bar	~0.275 g	0.5 g	Argon/Hydrogen	950 °C/15 min
1% Fumed Silica (3 Zone)	Bar	~3.45 g	7 g net	Nitrogen	350 °C/548 °C/747 °C (Zones)
1% Fumed Silica (Only NiO)*	Cap	~0.5 g	0.5g	Argon	950 °C/15 min
1% Standard Silica	Cap	~0.24 g	0.5g	Argon	950 °C/15 min
1% Silicon Carbide	Bar	~1.1 g	0.5 g	Argon/Hydrogen	950 °C/15 min

*This mixture was created following Protocol II (no pure nickel powder).

As a technical note, the whole length of the bar mold was never used except in the case of the three-zone furnace test. Typically, around a third of the bar mold was filled with the ceramic-nickel mixture before it was placed on the Grafoil. The mass of precursor mixture that this produced was approximately 2.2 g, which was placed in the furnace for treatment. This would allow for around 1.1 g of nickel oxide. Previous experiments have utilized a ratio of 2:1 urea to nickel oxide [11]. However, many of the tests in this thesis saw that number reversed in the form of a 1:2 ratio. This was due to the fact that higher amounts of urea could cause pressure bursts in the sample tube and cause the ends to be blown off. This pressure burst also causes the powder particles to “blow” apart even as the reaction or sintering is taking place. Therefore, a balance needed to be struck between effective and complete reactions occurring due to urea reduction, and the “blowing apart” caused by the rapid decomposition of the urea.

5. Post-Processing Analysis

Several different methods of characterization were utilized in this research to understand the mechanisms that occurred within each experimental run. These characterization techniques were used to improve the experimental methods and define the properties of the cermet parts and films that were created. This was accomplished based on the observation of the behavior of the various particles and phases as well as hardness qualities.

After firing, the products were analyzed utilizing a series of tools available at NPS. Visual observation and hardness testing were first conducted, and the techniques are described in detail in the control studies section. The additional analysis tools that were utilized for the solid cermet parts are described below.

a. Scanning Electron Microscope

The Scanning Electron Microscope (SEM), a Zeiss Neon 40 Field Emission Scanning Electron Microscope, was the primary characterization method utilized for this work and is shown in Figure 18. The basic operation of the SEM is similar to an optical microscope, except that it utilizes the diffraction of an electron beam through electromagnetic coils to magnify images as opposed to the diffraction of photons in an optical microscope. Because the wavelength of the electrons is so much smaller than that of photons, the SEM can take images at a much higher resolution due to the Rayleigh criterion. The SEM shoots a beam of electrons at high speed toward a sample and these electrons interact with the sample by producing either secondary electrons or backscatter electrons. Secondary electrons interact directly with the atoms in the sample and can provide insight into the different phase or elemental composition of a sample. Backscattered electrons, on the other hand, give information on the surface topography and can provide resolutions between 1–20 nm [22].

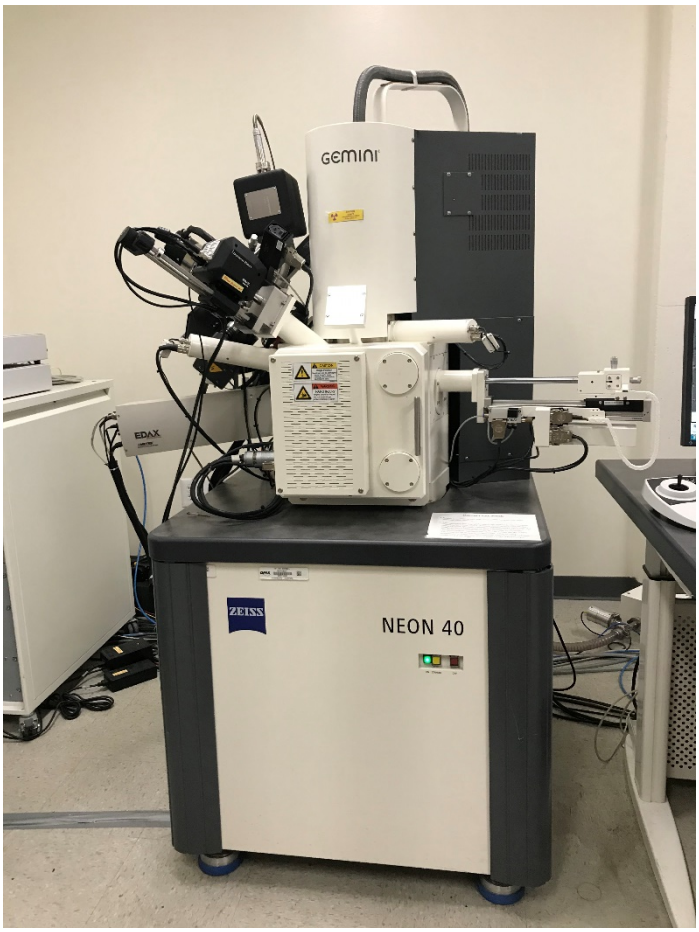

Figure 18. Scanning Electron Microscope at the Naval Postgraduate School.

The SEM was utilized to determine different phases within the samples and to determine if full sintering had occurred, for example. It was also utilized to detect the distribution of ceramic within the metal matrix and to determine how the metal and ceramic interacted both before and after heat treatment. The high resolution was key in this aspect to understanding the interplay between the various components of the metal matrix composites.

b. Energy Dispersive Spectroscopy

This technique, also known as EDS, relies on the interaction of electrons from the SEM with the elements in the sample being observed. The EDS utilized at NPS is attached to the SEM and is an EDAX Octane Elect Plus. When the SEM electrons hit the sample, they knock electrons in the sample atoms from one orbital shell to another. This transfer

between orbitals causes X-rays to be released from the sample that is characteristic of a particular element or atom. The X-rays can be detected and measured based on amount and energy. This allows for a qualitative analysis of the types of elements in the sample and which elements are present in which phases. It also allows for determination of particles in the sample that could be unknown or verification of full reduction, for example. Finally, the EDS has the capability to perform elemental mapping of samples and determine various elements present in an image from the SEM.

C. RESULTS

The results showed conclusively that, using Protocol I, it was only possible to create a self-supporting cermet body using the RES-C process in the case of low silica loadings (~1% by weight). Moreover, the bodies that did form at low loadings were very brittle, showing no evidence of metallic bonding, such as the ability to bend or compress without breaking under load. In addition, it was shown that using Protocol II with 1% fumed silica allowed for a distinctly different microstructure formation, and a notable lack of ceramic coating/higher metal necking.

At higher loadings and with different ceramics, solid bodies did not form. The material remained in particle form. The results for alumina and silicon carbide ceramics followed the trend observed for silica, in fact, were even less successful. Efforts to form self-supporting cermets with the RES-C process using alumina or silicon carbide, even at very low loadings, were disappointing. Only at very, very low loadings were extremely fragile bodies formed. These bodies could be “lightly” held and some “sticking” between particles did occur with the correct parameters.

1. Visual Observation Results

Simply observing the final state of the parts created allowed for a conclusion to be made about the success or failure of the particular cermet mixture utilized. For example, if only lightly sticking powder was the result of the experiment, then those conditions would indicate a failure to meet the objective. All cermet experiments conducted were compared visually and the results follow.

a. Alumina

RES-C of nickel/alumina mixtures to form cermet bodies using Protocol I failed the success criteria. Results obtained from the process are reviewed below and include findings that suggest a potential “parameter space” for future investigations.

For the 30% alumina iteration of the RES-C process, a significant amount of ceramic was utilized based on mass, which is an even greater percent by volume (52.3%). This caused the mixture of precursors to appear a much lighter “green” color (less nickel oxide) before treatment compared to the control precursor mixture. After treatment, there was almost no sintering, leaving a powder, hence no hardness test. The powder had changed color to a dark grey, indicating that nickel oxide reduction to nickel had taken place. It appeared that the relatively large amount of urea used in this case (0.70 g) had also served to “blow” the pack apart during reaction, as shown in Figure 19. This was most likely due to the pressure burst associated with rapid decomposition of the urea into the volatile gasses.

Figure 19. Alumina mixture after heat treatment (blown apart).

Based on the visual results from the previous experiment, it was determined that the amount of alumina in the sample would need to be drastically reduced in order to refine

the process. This led to the 6.25% alumina iteration. In theory, this would allow for stronger sintering between the metal particles and allow the ceramic particles to be “squeezed” between the metal as the metal bonded together.

The results, despite a 5 X reduction in ceramic content, were almost identical to those of the previous experiment. The powder was stuck together in the shape of the mold after the experiment, and it had all turned a dark grey color, indicating that the nickel oxide had been reduced. However, the “pack” broke into powder upon an attempt to lift it out of the mold. Conclusion: Little or no sintering or bonding occurred. Fortunately, there was no obvious “blowing apart” of the pack which can be attributed to a smaller amount of urea utilized (0.25 g), as shown in Figure 20.

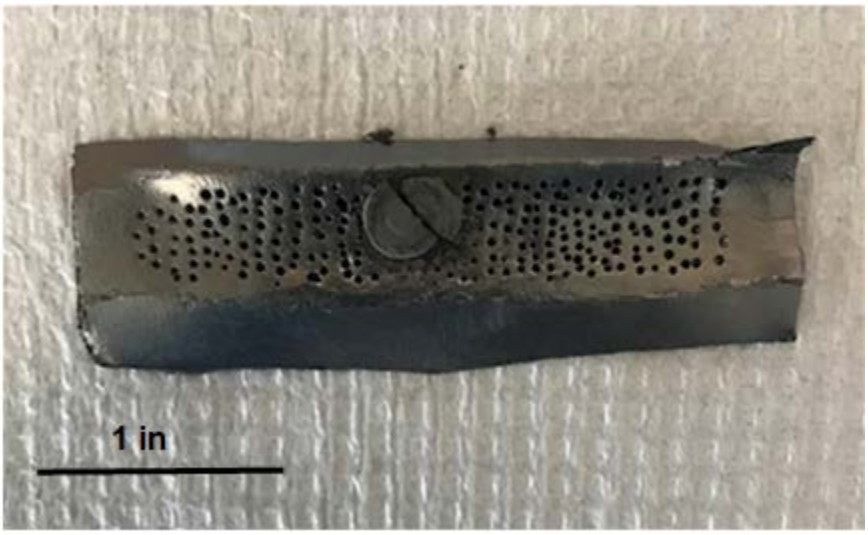

Dark gray color indicates full reduction and relative mold shape indicates no “blowing apart.”

Figure 20. The 6.25% alumina mixture after heat treatment.

Because of the lack of bonding between particles with higher percent weight ceramic mixtures, the ceramic content was drastically lowed to approximately 1% by weight, 2.9% by volume. Figure 21 indicates that the alumina (white particles), visually, took up a large volume of the mixture despite being 1% by mass.

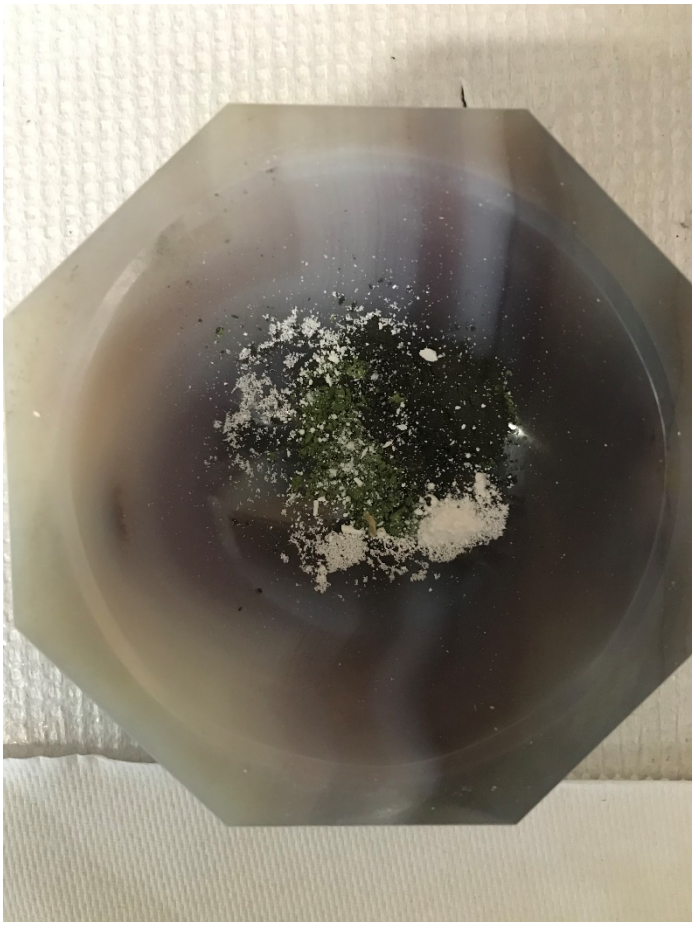

Figure 21. The 1% alumina (3 µm) precursors before being mixed.

The particles from this experiment stuck together fairly well after heat treatment, and a grey powder was formed that was almost “cakey,” but no solid part was actually maintained. All of the “solid” objects formed were broken easily, but there was noticeable sticking between particles at this lower concentration.

It was concluded that smaller ceramic particles could allow for bonding or sintering to occur between the nickel particles because there would be less “coating” by the ceramic and more free area for the reduction reactions to take place. This led to an iteration of the 1% micropolish alumina test. All factors were the same as for the earlier 1% alumina test, but for the size of the precursor alumina particles. That is, the multi-micron alumina was replaced with micropolish alumina with a 0.05 µm average particle size. The switch was made to test this hypothesis: Bonding/ neck formation between nickel particles is enhanced

if no large ceramic particles are between the metal particles. Large alumina particles interfere with the binding between nickel particles because they must be moved away in order for nickel particles to be joined by “necks”.

The results did not substantiate the above postulate. Substitution of the micropolish led only to a slight improvement in gross bonding. The part stuck together in extremely loose clumps, but there were easily broken apart by small disturbances with a spatula.

b. Silicon Carbide

A 1% silicon carbide mixture following Protocol I was tested utilizing the same procedures that were used to create the alumina mixtures. The particle size for this particular silicon carbide powder was 0.1 µm. The application of the RES-C process to this mixture produced extremely similar results to the outcome obtained from the alumina mixtures. The particles were lightly stuck together, and the pieces created were extremely low density and almost brittle in consistency. However, the silicon carbide held together in clumps slightly better than the part created with the 0.05 µm micropolish alumina. This suggests the specific type of ceramic, not just the ceramic particle size, impacts the strength of the pieces. SEM investigation, below, suggests this may be a product of the degree of ceramic coating of the metal particles.

c. Silica

Because of the failure of the alumina and silicon carbide mixtures to create a solid part that was bonded or sintered enough to be self-supporting, it was postulated that bonding between nickel particles might be enhanced if the ceramic particles were nano scale. This led to the utilization of fumed silica, with a particle size of approximately 0.007 µm.

Protocol I was first attempted and, after one RES-C treatment, a solid part was created from 1% by mass fumed silica that was self-supporting and looked similar visually to the control studies utilizing pure nickel. This experiment was conducted utilizing the “cap” mold with 0.5 g of urea, which allowed for a ~2:1 urea to nickel oxide ratio. However, the experiment was run again with the bar mold and 0.5 g of urea, which allowed

for a ~1:2 urea to nickel oxide ratio, and no significant difference was noted in the stability of the part produced. Significant shrinkage was noted, as was expected, for the bar mold test and is indicated in Figure 22. It was estimated to be between 15–20% shrinkage.

Figure 22. Comparison of a powder pack before and after heat treatment.

Utilizing smaller particles appeared to be beneficial in that it allowed more surface area for the reduction reaction to occur on the nickel particles. The ceramic particles did not have to be pushed out of the way or did not significantly block potential reaction sites on the nickel. The RES-C treatment was also applied two more times to the same piece shown in Figure 22. The successive iterations of the process caused the part to appear more visually stable, and fewer particulates detached after each treatment. These successive treatments were designed to ensure that all nickel oxide had been reduced in the sample and promote further bonding.

Protocol 1 with fumed silica was also run using the 3-zone furnace to test the hypothesis that net sintering would be improved by passing decomposition products of urea over the particle bed for longer periods (Figure 17). This experiment also failed to create a

body that met the success criteria. Specifically, the experiment was designed to test the hypothesis that volatilizing the urea at a low temperature, leading to slower volatilization and concomitantly increased time of passage for urea and its decomposition products over the particle bed, which was held at a higher temperature, would provide stronger bonding. As shown in Figure 17, urea was volatilized in the first zone at 350 °C, reached 548 °C in the second, and interacted with the particle bed at 747 °C in the third zone. A large puff of white smoke was noted at the furnace outlet 2 minutes and 15 seconds after inserting the sample into the oven, indicating some urea volatilization.

After the treatment, the density was noticeably less than previous silica cermet parts. The recovered piece was extremely brittle and barely self-supporting However, there was constant coloration throughout and no “green” colored nickel oxide. In addition, 2 g of urea byproduct were recovered from the upstream urea boat from the 5.0 g originally placed, indicating that a large portion had volatilized but never decomposed completely. This method could potentially be useful with a more capable furnace that could maintain a large temperature differential across various zones.

Protocol I with standard sized silica was also attempted in order to better understand the mechanisms occurring with this particular ceramic. Standard silica powder (80% 1-5 μm) was utilized to test if the specific type of ceramic had a meaningful impact, along with the size. The test was similar to the fumed silica iterations in the sense that a self-supporting piece was formed. This seemed to indicate that both the size and specific type of ceramic utilized both have significant impact on the outcome for this particular process. Moreover, this also showed that silica was clearly the most suitable ceramic variant for creating metal matrix composites with this process.

Finally, and most notably, Protocol II was attempted with 1% fumed silica to better understand the chemical mechanisms occurring. As mentioned, only nickel oxide and silica were mixed as precursor (no pure nickel powder). This iteration produced a part that was self-supporting on the outside, but had a powder core, with un-reduced nickel oxide in the center. This was most likely due to the higher relative concentration of nickel oxide to urea than in previous iterations. However, this experiment was conducted with the purpose of

understanding how the silica behaved, and the reduced, self-supporting, outer section of the part was observed more closely under the SEM.

2. SEM Observation Results

The SEM was the most useful tool in this study for understanding how the different phases of these cermets behaved and how they interacted with each other. It was also especially helpful in determining the relative amount of sintering or bonding that had occurred and how the ceramic particles behaved. Only the alumina and silica tests were observed under the SEM.

a. Alumina

Postulate: Alumina, if present in sufficient quantity, will form a complete coat of the nickel particles as a result of the RES-C process. The postulate of coating metal with ceramic is consistent with SEM images from alumina cermets of all loadings, and with alumina of different sizes. It is also consistent with EDS results. These samples were all formed utilizing Protocol I.

The first images to consider are from the 30% 3-μm alumina loading sample (Figure 23). These suggest complete coverage of metal by alumina. That is, the images show a material texturally different, “fluffier,” than metal, and a material “whiter” in the SEM than metal particles.

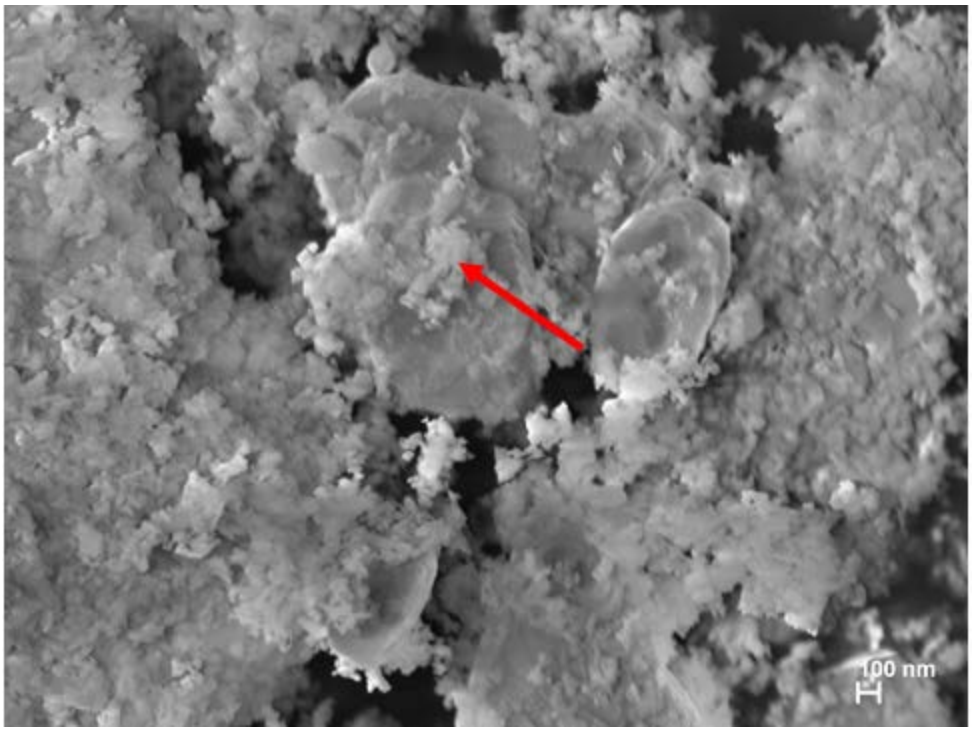

Figure 23. 25,000 X magnification SEM image showing a coating on larger nickel particles (30% alumina).

In addition, as indicated by Figure 24, there appeared to be very little difference between the baked and unbaked samples at high magnification, even with the 1% alumina test. Theorized flecking by the alumina was noted in the baked sample.

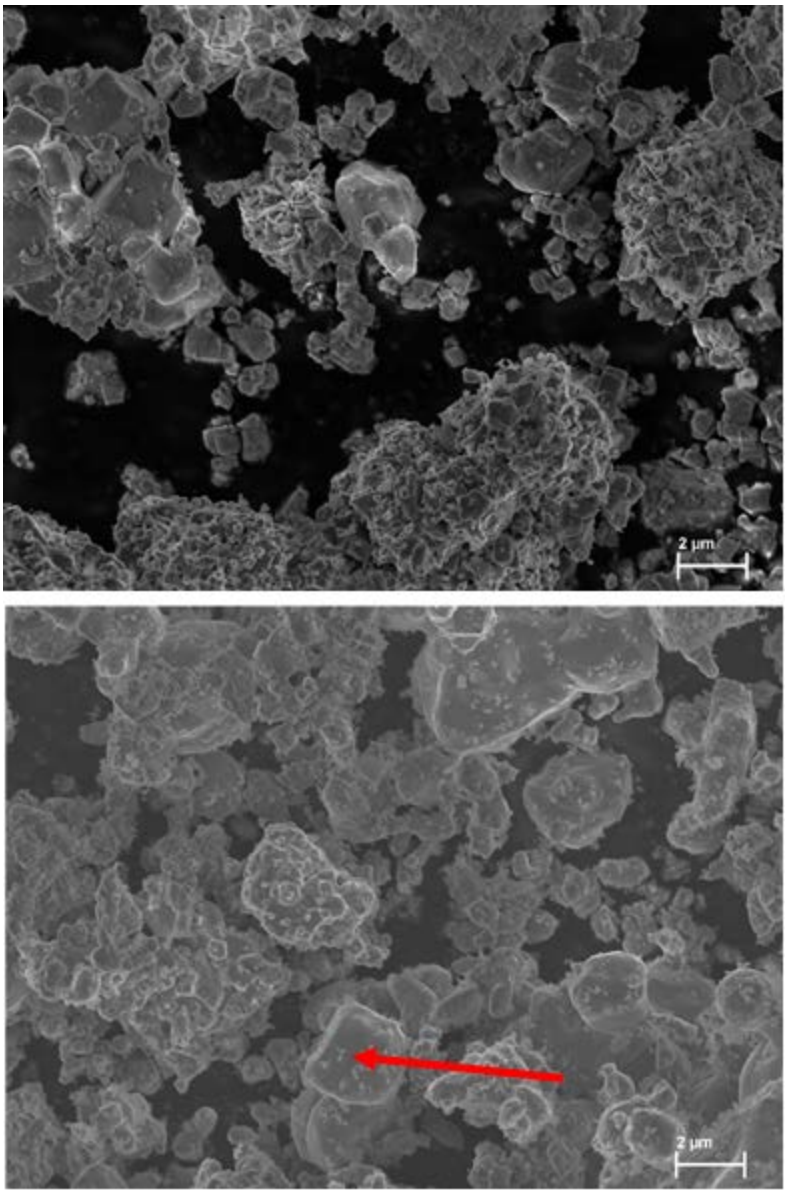

Top: No treatment.
Bottom: Heat treated.

Figure 24. 5,000 X SEM images of the 1% alumina (3 µm) mixture (flecks indicated).

Next under consideration are additional SEM images of RES-C samples made with only 1% 3-µm alumina. With lower alumina, some “smoothing” of the primary particles was noted. In addition, there is also “fluffy” and “whiter” material on the surface of what is clearly nickel (Figure 25). However, there is not enough alumina present to make a full coating. Thus, rather than a coating, there appeared to be “flecks” of a substance sticking

to the larger primary particles. Figure 25 shows a more detailed view of the nickel particles with the hypothesized alumina flecks.

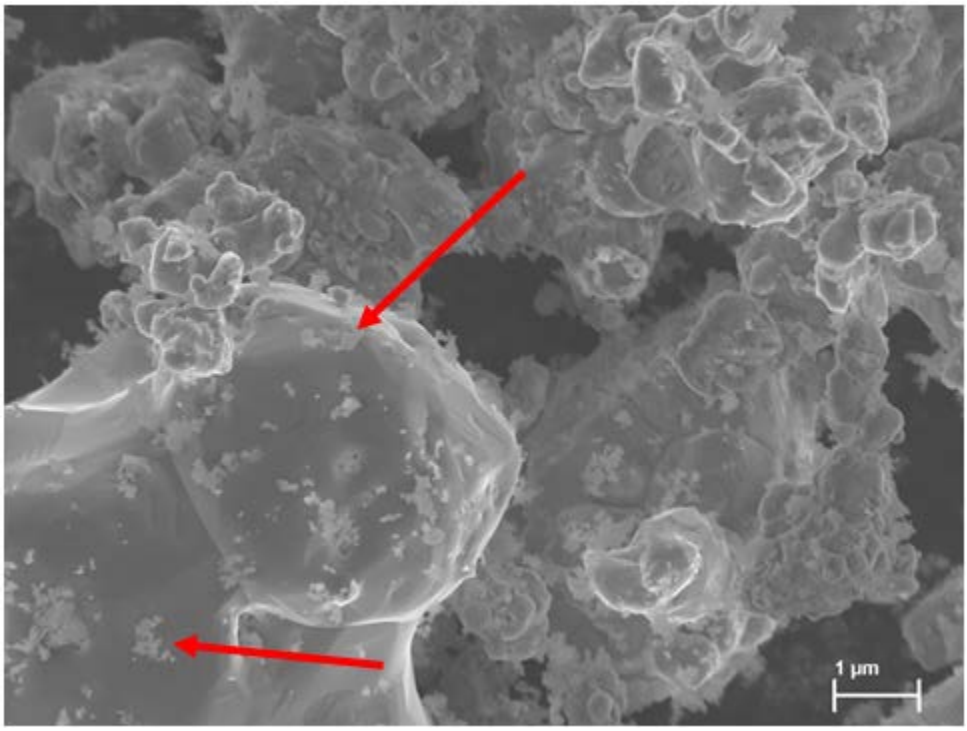

Several small particles coating the larger nickel primary particles are indicated.

Figure 25. A 10,000 X SEM view of the 1% alumina (3 µm) mixture.

The next image is from RES-C nickel/alumina made with the 1% micropolish alumina. The particles were bonded to a higher degree than the previous iterations with alumina, as shown in Figure 26.

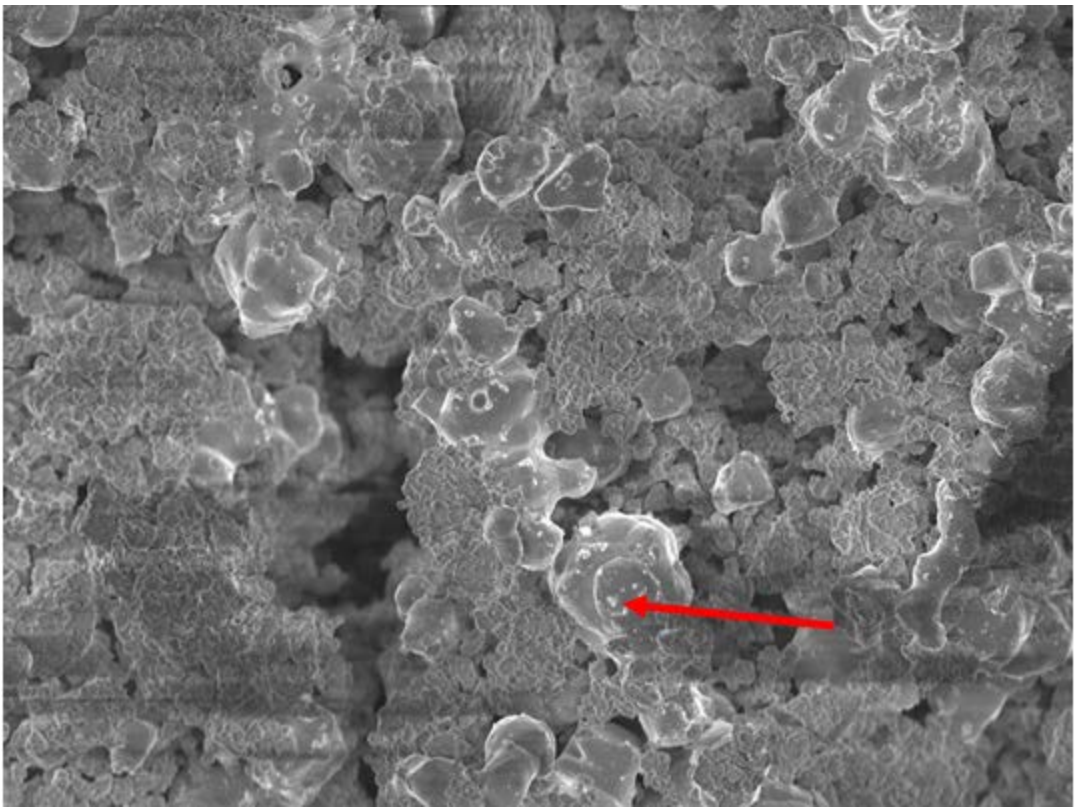

SEM image shows that the particles are packed relatively close and some slight charging is occurring. Light flecking is noted on primary nickel particles.

Figure 26. 2,000 X magnification of the 1% alumina (0.05 µm) mixture.

It was also interesting to note that this particular mixture, utilizing the micropolish alumina, experienced charging under the SEM beam at most voltages. This indicated that the micropolish alumina decreased the conductivity of the sample more than the other ceramic particle additions. This was notable because different levels of electrical conductivity could be desirable for cermet or metal matrix parts, depending on the application. Mixing in small quantities of micropolish alumina could potentially serve to alter the conductive qualities of these materials in a significant way.

b. Silica

The SEM images taken of the silica mixtures were the most revealing in terms of the creation of the cermet solids. The silica particles were not “squeezed” between the nickel as initially hypothesized. They appeared to be simply resting on top in a light

coating. This is demonstrated with the fumed silica part created via Protocol I in Figure 27.

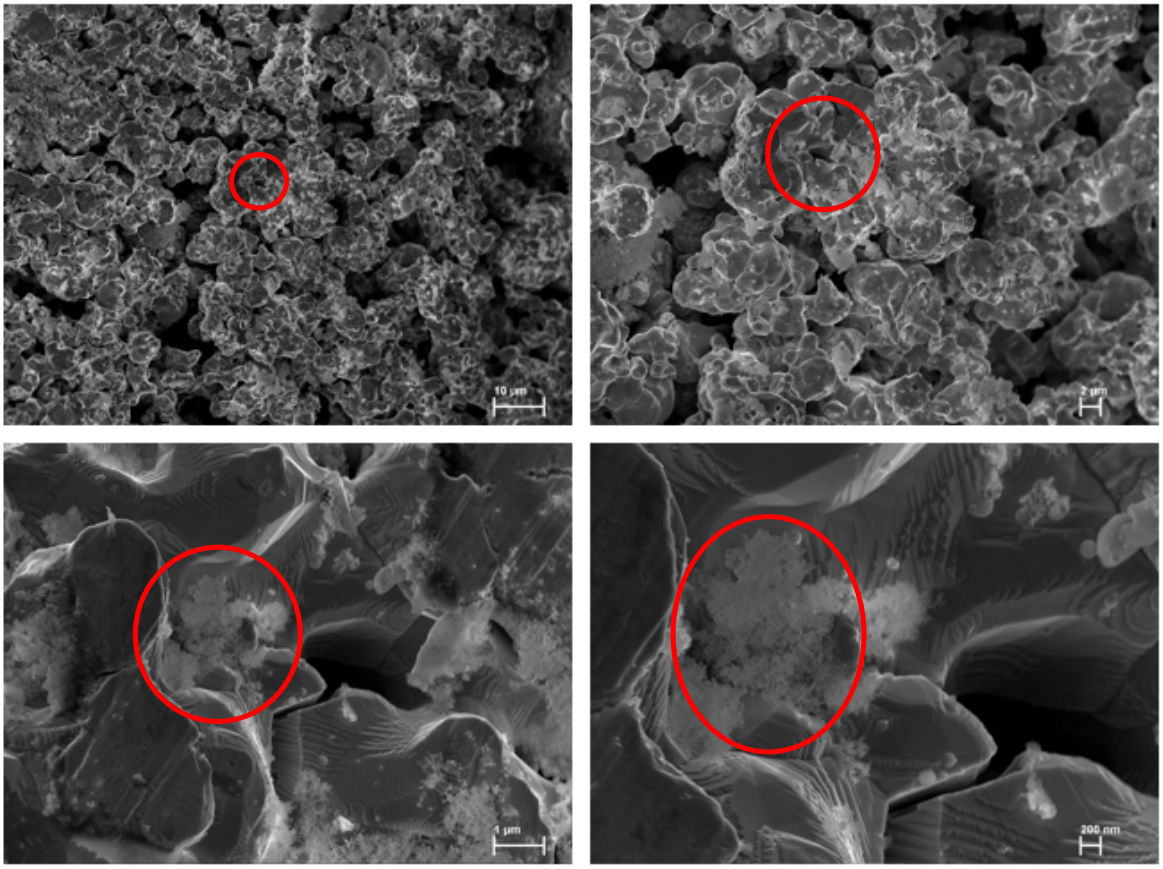

From left to right: a 1,000 X, a 2,000 X, a 10,000 X, and a 20,000 X magnification of a nickel-silica part under the SEM.

Figure 27. Fumed silica particles coating larger, necked nickel particles.

It was theorized that conducting multiple RES-C treatments on one piece of the nickel and fumed silica mixture would improve the overall density of the part and allow the particles to bond more closely. A portion of the same nickel and fumed silica piece was heat-treated three times with urea. After the third RES-C treatment, it appeared that the particles were much more closely packed and more “necking” between particles had occurred, indicated in Figure 28. This corroborated the visual observation results.

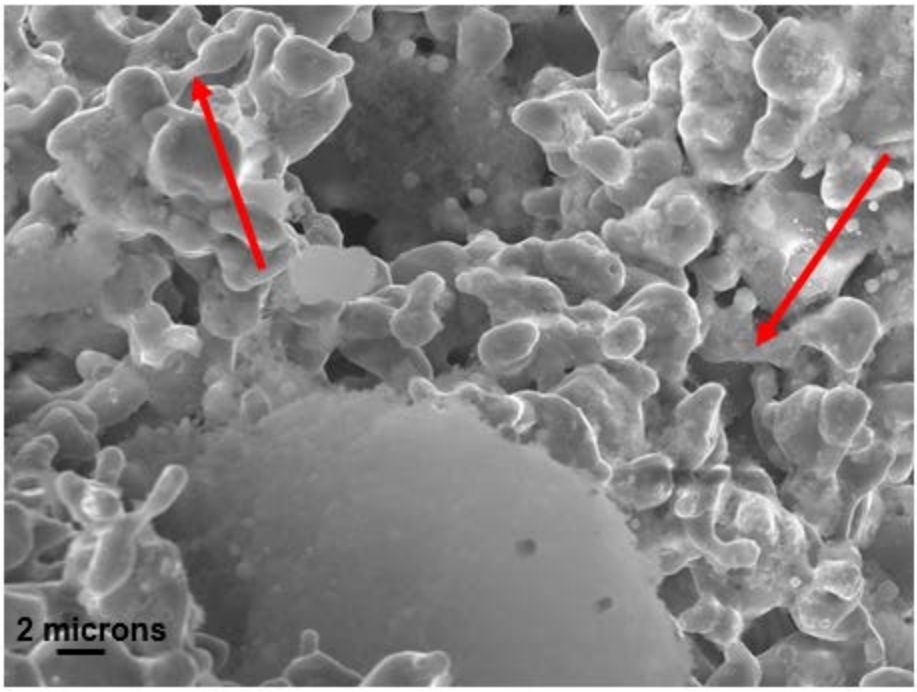

Arrows indicate necking between primary particles with silica embedded in between.

Figure 28. Nickel-fumed silica part, treated three times, showing neck formation between particles.

The piece created with standard silica also seemed to show similar behavior, and a "spreading" of particles, but to a somewhat lesser degree, as shown in Figure 29.

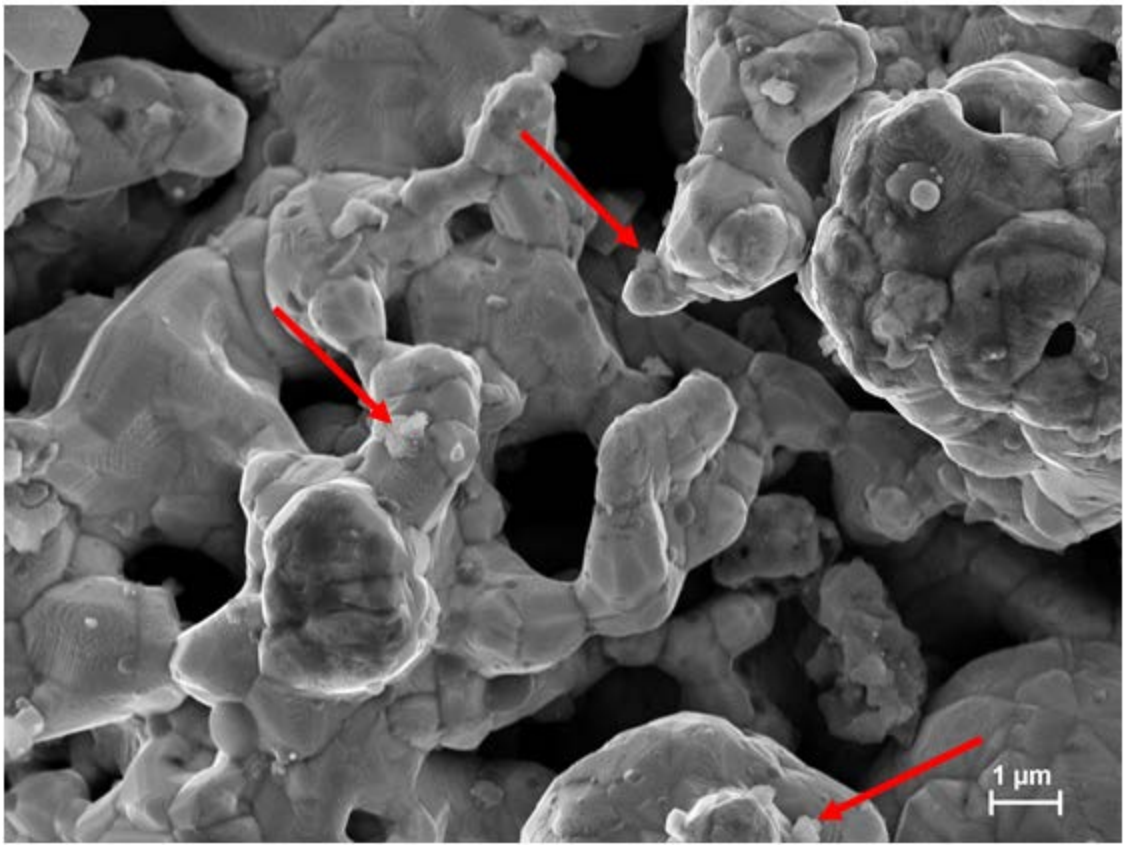

Postulated silica particles are marked as “flecking” the larger nickel particles.

Figure 29. Arrows indicate positions of silica particles on nickel-standard silica part, treated once.

Observing the part created following Protocol II (only nickel oxide and fumed silica) was also revealing in terms of the behavior of the fumed silica. There was an obvious difference in the microstructure and the positioning of the fumed silica on the pure nickel oxide precursor surfaces, as shown in Figure 30.

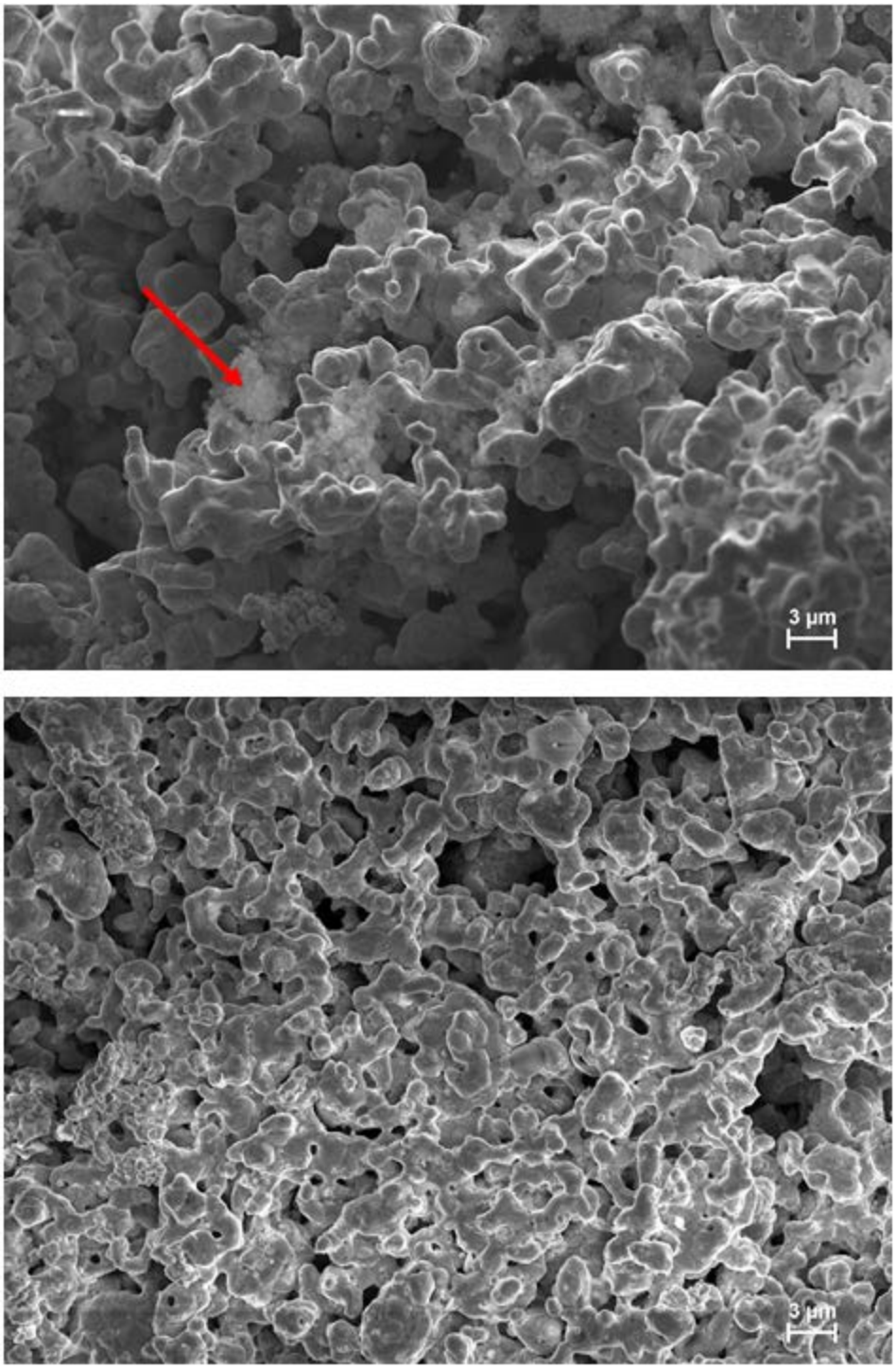

The obvious fumed silica “coating” is shown on the part with the pure nickel included. In addition, the microstructure is much more jagged with large voids. Omitting the pure nickel seems to cause stronger bonding and necking as indicated by the bottom image.

Figure 30. Comparison of parts made with Protocol I (top) and Protocol II (bottom).

This demonstrates that the fumed silica seems to “move” more freely when pure nickel is present (Protocol I). Protocol I (Ni and NiO) leaves fumed silica resting on top of the particles. In contrast, in Protocol II (NiO only) the fumed silica tends to congregate around grain boundaries and is interspersed between particles, as shown in Figure 31.

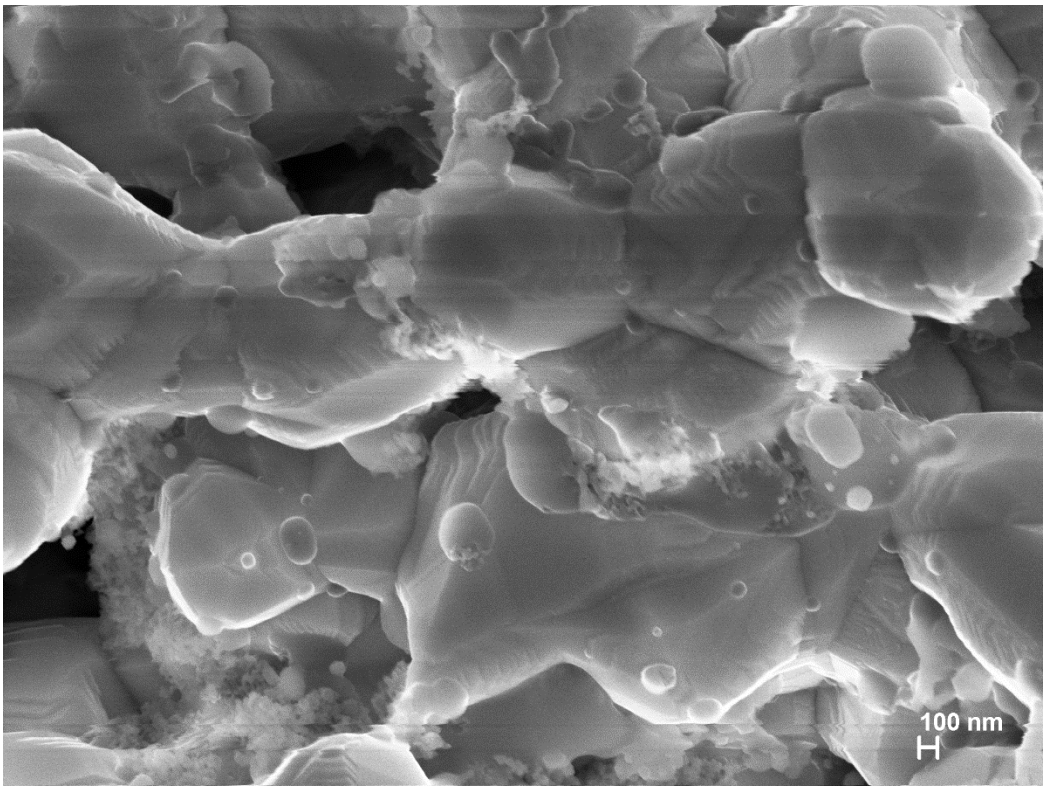

The fumed silica seems to be more interspersed and closer to grain boundaries.

Figure 31. Protocol II leaves fumed silica at boundaries between particles.

3. Hardness Results

The 1% silica composites were the only mixture that produced self-supporting pieces of sufficient strength to attempt hardness tests. Protocol I samples were tested and compared with the once-fired pure nickel (control) piece.

The hardness testing apparatus at NPS requires a polished reflective surface to obtain an accurate measurement. After polishing for approximately twice the amount of time as the pure nickel control study, a fully reflective surface could not be obtained. This

could be due to the fact that polishing of cermets is typically conducted with a form of diamond polishing that was not attempted; the inclusion of fumed silica particles may have prevented full polishing from occurring. In addition, the resin that was used to mount the parts for polishing and hardness testing may have seeped into the parts due to low density, preventing a fully polished surface. Despite these issues, a small level of reflectivity was obtained utilizing the polishing capabilities at NPS, and Vickers hardness tests were conducted utilizing the HV0.025 method (the lightest amount of force possible).

The hardness values that were obtained spanned a large range, with an average value of around 15, consistent with an inhomogeneous material. This value is much larger than the hardness values obtained for the pure nickel control tests. Hypothesis: Inclusion of fumed silica particles, even at very low loadings, increases overall hardness. Additional tests were also conducted on the twice-fired nickel/fumed silica piece as well as a piece that was fired three times. These tests also had a large range between values, with the twice treated piece having an average hardness value of 46.4 and the 3X treated piece having an average hardness value of 33.9.

4. EDS Observation Results

Observation under the EDS was essential to fully understand the distribution of the cermet particles within the samples, it allowed for a more accurate analysis of which particles corresponded to a particular phase. EDS was only conducted on the alumina and silica samples.

a. Alumina

Analysis utilizing the EDS confirmed the hypothesis that the “fluffy” particle coating was alumina and it was coating almost all of the nickel particles in the 30% alumina samples. This most likely prevented them from bonding. Some nickel was also detected in addition to various contaminants on all alumina cermet mixtures, as indicated in Figure 32.

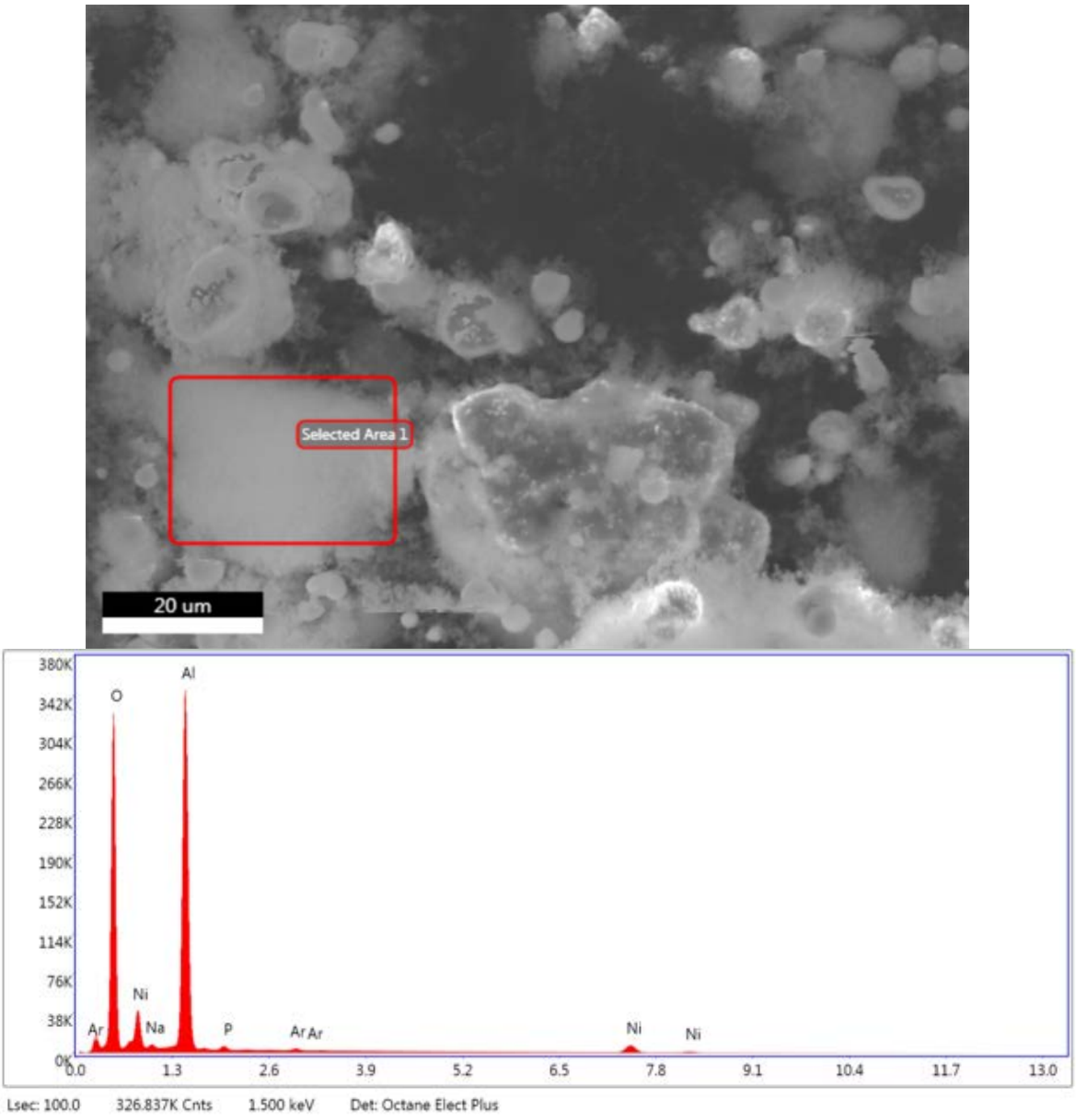

The aluminum and oxygen are the largest peaks in the spectra, which indicate a large presence of alumina in the target area.

Figure 32. EDS area analysis on the 30% alumina sample indicating alumina peaks.

b. Silica

The results were similar to the alumina samples, it appeared that the lighter, "fluffier" particles corresponded to the ceramics. It was interesting to note that there appeared to be roughly spherical particles embedded in large zones or clumps of fumed

silica particles within the sintered piece. These particles appeared to be either nickel oxide or nickel. This was supported by an EDS scan map of one of these areas, shown in Figure 33. These roughly spherical particles have also been observed in other nickel-based bodies that utilize RES.

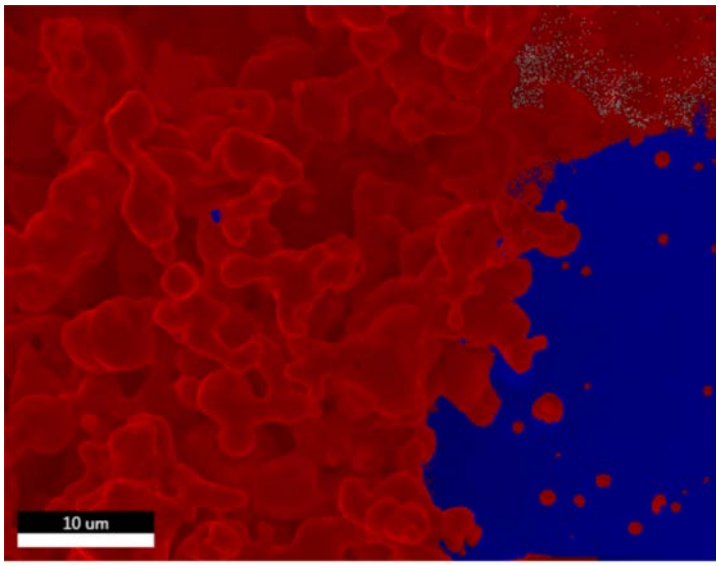

The blue areas represent silica elements and the red areas represent nickel or nickel oxide. There is a large concentration of the spherical particles embedded in the silica.

Figure 33. EDS map of an area of nickel-silica (three treatments).

This EDS scan could indicate that the addition of fumed silica attracted the nickel oxide or nickel particles and acted as a heat sink, which prevented the particles from heating and a complete reduction/bonding from occurring.

D. DISCUSSION

It was clear from these results that the RES-C process failed to form self-supporting bodies from Ni/NiO particle-alumina and Ni/NiO particle-silicon carbide mixtures at all loadings. The visual results indicated that all of the samples created with these ceramics remained as a powder, although there was some “sticking” at lower ceramic concentrations. In earlier studies of RES generation of brown bodies from pure metal/metal oxide mixtures, the “glue” between particles were metallic necks. Bodies that were composed of metal

particles connected by metallic necks displayed mechanical metallic behavior. Specifically, they deformed plastically under compression [10]. In the absence of this type of interparticle neck growth, bodies formed were clearly brittle and readily fractured under even low loads. The cermets formed in the present study utilizing Protocol I showed an almost complete absence of interparticle metal neck formation. This is consistent with the finding that either there was no binding at all, or bodies formed were very brittle. This was likely due to two factors. First, large ceramic particles tend to physically impede necking between nickel particles. Indeed, the number/fraction of "adjacent" nickel particles capable of inter-particle neck growth is reduced inverse to the concentration of large ceramic particles. Second, and perhaps more deleterious to metal-metal bonding: the ceramics, alumina and silica in particular, appear to coat the nickel surface. This is evident from both the direct SEM images and from EDS studies, at both low loadings and at high loadings. A ceramic coating on virtually all metal surfaces will certainly act to block metal neck formation.

The finding that ceramic coats the metal in Protocol I requires some explanation. One possible mechanism would be melted ceramic leading to the creation of a liquid film on the metal. After cooling, this film would form a solid. This appears an unlikely explanation as the temperatures employed were far below the melting temperature of the ceramics. However, it is well known that the addition of impurities to ceramics will dramatically reduce the softening and spreading temperature. For example, although silica melts at around 1700 ℃, the addition of a few percent of impurities to silica leads to softening at lower temperatures, corroborated by the Alkemade theorem [23]. In addition, it has been determined that nanoparticles with insoluble impurities experience a depression in melting point, even when compared to bulk materials of the same element [24]. It is possible that, at the metal/ceramic interface, a compound forms that permits enough atomic movement for "wetting" to occur. In fact, wetting of silica by aluminum has occurred as low as 799 ℃ [25]. In addition, wetting has been noted at 850 ℃ on silica substrates by silver-copper based alloys [26]. There also appears to be a beneficial correlation between the "dissolved oxygen in a liquid metal on the wetting and adhesion of the metal on an oxide surface," beginning at temperatures of around 950 ℃ [27], which is the temperature

RES-C is conducted at. These observations are also consistent with the physical/thermodynamic expectation that ceramic-metal bonding will lower the net energy of the system [27].

Another source of relevant information regarding metal/ceramic interactions is from the catalysis literature. Indeed, the catalysts employed in vehicle exhausts ("catalytic converter"), in petroleum refining operations, in fine chemicals production, and in many other uses often consists of nanometer-scale metal particles strongly bonded to high surface area ceramics such as alumina, silica, and magnesia [28,29]. The nature of this bonding is a function of many factors such as the degree of hydroxylation of the ceramic surface, the identity of the ceramic and the details of the fabrication process; however, there are some excellent examples of atomically thin, very strong, metal-ceramic interface structures forming. For example, it is known for some catalyst fabrication techniques that, until base metals, like iron and nickel, form a complete atomic monolayer on alumina, no "metallic" structures can be produced [30]. The initial one or two atomic layers of metal form a "compound," like a metal-aluminate, with the underlying ceramic. The metal in this "compound interface" is in an oxide state, hence catalytically inactive. Only metal layers formed on top of this "intermediate" metal/ceramic can be reduced to the metallic state.

It is reasonable to postulate that the RES-C process utilizing Protocol I leads to the formation of such a thin layer compound interface on the metal surfaces. Indeed, all the elements required for this are present: metal, ceramic, and temperatures even higher than those employed to create heterogeneous catalyst. Moreover, the postulate is consistent with all observations made in this study.

E. SUMMARY

The weak bonding/particle nature of the cermet parts created following Protocol I was likely due to a coherent, strongly bonded film of ceramic covering all the metal surfaces. This occurred even at very low loadings indicating that a ceramic film on the order of a few atomic layers might be sufficient to prevent "metal-metal" bridge formation between adjacent metal particles. In the absence of these bridges, the structures observed to create the interconnected metal particle networks in RES-SM studies cannot form.

The original hypothesis that cermet formation using RES-C would be a simple extrapolation of RES formation of solids was proven wrong. Unanticipated chemical interactions between metal and ceramic particles during treatment prevented success. There is a silver lining, however. The omission of pure nickel, following Protocol II, seems to improve the bonding and microstructure of the parts created. The fumed silica did not appear to coat or congregate to the extent it formed on the samples with pure nickel present. This method assumes the ceramic coating cannot form on metal oxides. Thus, stronger and more stable structures could potentially be created with no metallic particles, only oxide particles. An additional method is also suggested for creating a cermet using a two-step RES process. This method would allow metal bonding to take place and strong bonding to occur between metal and an interstitial, fully connected ceramic matrix. The process: i) Create a pure nickel piece utilizing RES as conduced in the control studies. ii) Treat the part a second time after applying a "gel" of ceramic particles. This gel would be made from a mixture of fumed silica and deionized water, which would be painted on to the pure nickel part. This would be allowed to dry in a fume hood for several days and then baked at 90 °C to remove any excess water, as the fumed silica filled the small voids in the metal part. The part would then be treated in the furnace at 750 °C for three hours to allow the ceramic particles to bond to the metal. It is theorized that this process will utilize the chemical reactions occurring between the metal and the ceramic in an advantageous manner to create additional bonds.

THIS PAGE INTENTIONALLY LEFT BLANK

VI. CERMET FILMS

The creation of a nickel-silica film was attempted using a new protocol. It is a "new" protocol in the sense it was modified, on the basis of "lessons learned", from that employed in the previous chapter to make solids. Specifically, the cermet metal films protocol was to "paint" a metal substrate surface with a homogeneous mixture of metal oxide particles, urea, and ceramic particles, then heat in an inert gas. Note, this aligns with Protocol II from the creation of solid cermet parts. This reflects a simple hypothesis supported by preliminary studies with the bulk cermet part samples: a strongly bonded ceramic coating will not form, blocking bridge formation between particles, if the original mixture only contains metal oxide particles (metal particles are excluded). A notable additional change was that urea was directly mixed with the metal oxide and ceramic, hence Protocol III. This third protocol reflects an earlier successful employed protocol for creating pure chrome metal films on substrates. In that effort, urea was directly mixed into the precursor "paint" [14,15].

These changes improved outcome as coherent cermet films were formed on several metal substrates. The success of this effort yields "lessons learned" that could be applied to making solid cermets and films with higher loadings of ceramic.

A. INTRODUCTION

The focus of this chapter is on the potential use of the modified RES-C process to make cermet films on various solid substrates. Success of a protocol was defined as one that creates films adhered to the part that do not detach easily with normal handling. In addition, consistency of the film thickness and ability to be surface treated without damage after the RES-C process were indicates of higher levels of "success".

The primary parameter that was varied was the metal substrate that was utilized, all cermet films were conducted with 1% by mass fumed silica precursor. In addition, no pure nickel particles were utilized in the precursor mixture. The results for the films were encouraging, as they could be created successfully on iron, copper, and titanium substrates. The films on iron, in particular, were able to be surface treated, and multiple treatments

could potentially allow for a very uniform thickness. Notably, the creation of films on titanium allowed for these films to be “peeled” from the substrate and remain self-supporting, which could have several useful applications. Finally, these films were also tested by spectral absorption and it was found that they could be potential candidates for selective solar absorbers.

B. EXPERIMENTAL

The application of RES-C to create cermet films was based on previous work utilizing RES to create micron-scale chrome coating on iron wire. The procedure was followed almost exactly with the nickel-oxide/ceramic mixture, with some slight modifications to substrate surface preparation and mixture ratios [14,15].

1. Chemical Preparation

First, thin metal pieces were polished utilizing P1000 sandpaper then were wiped off with bleach, rinsed with deionized water, and air dried. The metal pieces that were utilized included iron foil strips (Alfa Aesar, 0.25 mm), titanium foil discs (Gallium Source, 0.1 mm), iron foil discs, and copper sheet metal discs (K&S, 0.41 mm).

After this, the powder precursors were prepared utilizing 2 g of urea, 1 g of the same type of nickel oxide utilized in the experiments with solid parts (<44 μm), and 0.01 g of fumed silica (0.007 μm). The goal was to have the urea and nickel oxide in a 2:1 weight ratio and to have the fumed silica at 1% by mass compared to the nickel oxide. No pure nickel particles were utilized in the precursor mixture, this closely aligns with Protocol II for creating bulk solids from the previous chapter.

2. Mixture Preparation

The urea, nickel oxide, and ceramic powders were physically mixed for 5 minutes and deionized water was added until a paste was formed. This was mixed for 2 additional minutes and is shown in Figure 34.

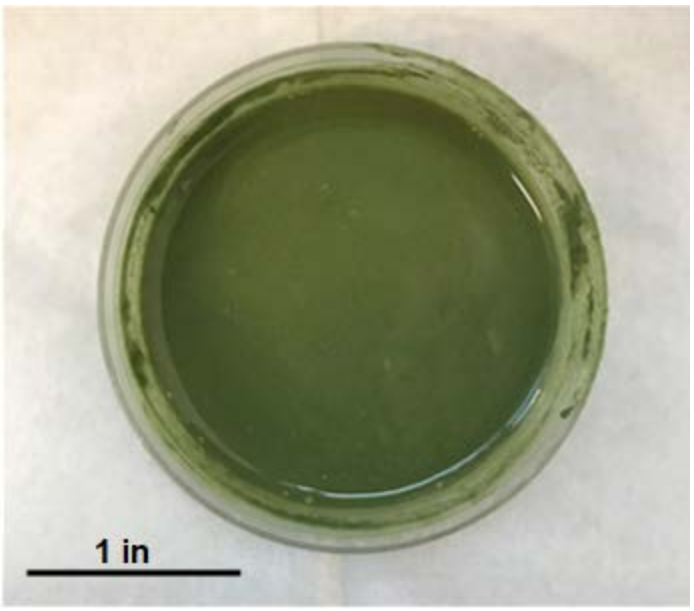

Figure 34. Mix of the nickel oxide, fumed silica, urea, and water formed into a paste.

The prepared metal was then dipped in the paste for 3 minutes and left to dry for approximately 2 hours, as shown in Figure 35.

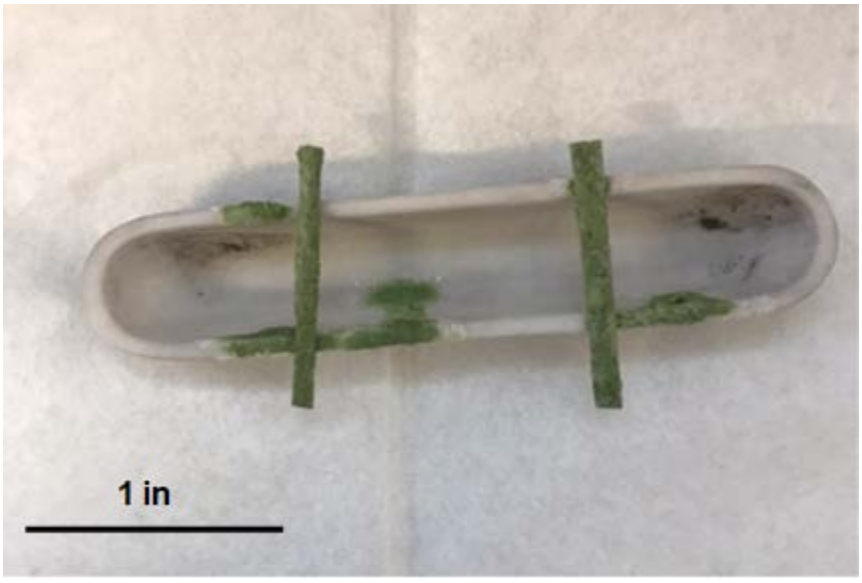

Figure 35. Iron foil strips coated with the precursor mix after drying.

3. Neutral Atmosphere

The metals with the dried coating were then placed into the quartz sample tube. For the thin iron strips, a smaller quartz tube was utilized which was flushed at 3.03 ml/s for 25 minutes with argon. Due to the larger diameter of the metal discs (~2.54 cm), a slightly larger quartz tube was utilized. In these cases, it was flushed at 3.63 ml/s for 30 minutes with argon. The flushing of the tube with gas met or exceeded the prescribed time that was calculated from the flow model used for the solid cermet parts.

4. Furnace Treatment

The same small furnace that was utilized for the solid cermet part experiments was utilized for the film tests (Linderg Blue, 45 cm). This was preheated to 950 °C for all the experiments conducted. For the iron foil tests, the flow was reduced to 0.25 ml/s and the samples were then placed in the furnace for 15 minutes at 950 °C. However, because the tube utilized for the metal disc experiments had a larger volume, the flow was reduced to 0.631 ml/s for treatment for 15 minutes. All films were removed and allowed to cool after treatment.

Table 3 summarizes the conditions for each experiment for cermet films.

Table 3. Test conditions for cermet film creation.

Substrate	Cermet Mixture	Treatment Flow Rate
Iron Strips	1% Silica	0.25 ml/s
Iron Discs	1% Silica	0.631 ml/s
Copper Discs	1% Silica	0.631 ml/s
Titanium Discs	1% Silica	0.631 ml/s

5. Post-processing Analysis

Several different methods of characterization were utilized in this research to understand the mechanisms that occurred within each experimental run. After firing, the products were analyzed utilizing a series of tools available at NPS. Visual observation was first conducted followed by SEM/EDS observation in the case of the iron foil strips and

titanium disc substrate. These techniques are described in detail in previous sections. Additional tests that were conducted on the films included spectral analysis (on iron strip substrate films) and a form of simple failure testing (on titanium substrate films). Notably, hardness tests were not conducted for any of the film experiment results.

a. Spectral Analysis

An additional observation method of visible light reflection analysis was utilized to define the absorbance capabilities of the films in the visible spectrum. This was the first step to defining how these materials might work as spectrally selective coatings for spacecraft applications, as a high solar absorbance is desirable for these materials. The test was conducted utilizing a Filmetrics Film Thickness Measurement Tool which could detect the reflectance of a material over a set wavelength. This reflectance could simply be subtracted from unity in order to determine the absorption. The concept was based on the conservation of energy equation and the fact that it was assumed that no light would be transmitted through the opaque samples [31]. The conservation of energy equation is shown.

$$\alpha + \tau + \rho = 1 \tag{17}$$

where α is the absorption, τ is the transmission (set to zero in this case), and ρ is the reflectance. This testing was conducted on both the films that were produced on iron, the controls of pure iron (substrate) as well as pure nickel to determine how the cermet materials would behave. If more than one measurement was available, the simple average over all the samples was taken in order to calculate the absorption values.

b. Failure Testing Titanium Substrate Films

The films made on Ti, and only on Ti, could be removed, or “peeled” off in relatively large sheets. These films can be evaluated, without the complication of having a metal substrate. One sample “qualitative” test was employed, “bend to failure”. Removed film was bent at successively larger angles and allowed to return to original shape. At some

angle of bend, elastic behavior gave way to plastic behavior. Once past “elastic”, the film was bent further for “yield” angle.

C. RESULTS

In sum, below it will be shown that it was possible to create cermet films on various metal substrates successfully. The ceramic particles behaved in a manner similar to the cermet parts from the previous section created via Protocol II (omission of the pure nickel particles). The films appeared to adhere well in all cases except for the titanium substrate, which produced large sections of film that could be “peeled” off the substrate. In addition, the films demonstrated the capability to be surface treated and showed promise in spectral testing for use as selective solar absorbers

1. Visual Observation Results

Simply observing the final state of the films created allowed for a conclusion to be made about the success or failure of the particular experimental conditions. All cermet experiments conducted were compared visually and the results are organized below.

a. Iron Strips and Discs

After one RES-C treatment, a film was successfully created on an iron foil strip that was ashy and gray in color, as shown in Figure 36.

Figure 36. Nickel-silica film after one RES treatment on iron foil.

Clearly, this film is rough and uneven without post-processing treatment such as polishing. However, it was bonded well to the iron substrate, as shown in Figure 37 with the iron discs. A pure iron disc was also placed in the furnace with the treated iron discs as a comparison.

Figure 37. Iron discs with cermet coating (left) and no coating (right).

b. Copper Discs

In order to compare the behavior of the nickel-silica films more thoroughly, the films were also tested on copper substrates. Figure 38 shows a copper disc with the film coating next to a pure copper disc that had been placed in the furnace with the treated samples. The film deposition on the copper may not be as thick as the deposition on the iron substrate, as sections of the copper can be seen through the film coating. However, the coating did appear to be bonded slightly better to the copper, and not as “ashy” and rough.

Figure 38. Treated copper disc (left) next to an untreated sample (right).

c. Titanium Discs

The final metal substrate that was chosen for comparison of performance with the nickel-fumed silica films was titanium. This was chosen due to its relative stability and high melting point. For this metal substrate, it was especially interesting to note that after treatment, the nickel-fumed silica film seemed to “peel” easily off the titanium substrate. There was almost no bonding to the titanium, as shown in Figure 39. The film was able to be peeled off in large sections about the same thickness as paper, and was self-supporting. The cause was theorized to be a reaction of the titanium to the heating and urea decomposition that allowed the films to be removed easily. These films could have potential use in electrical coatings and have a strong ability to be shaped and formed to meet specific requirements.

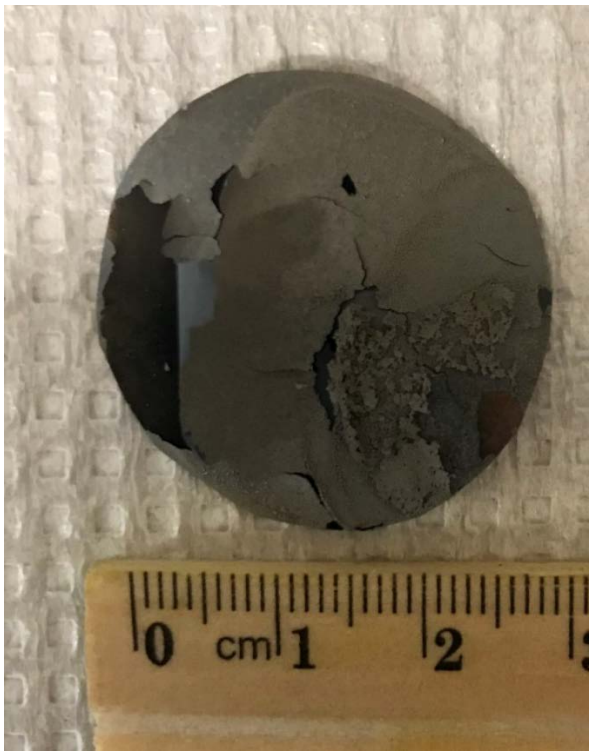

Figure 39. Treated titanium disc showing the peeling of the nickel-fumed silica film.

2. SEM Observation Results

The nickel and fumed silica coating on the iron strip substrate, and the nickel and fumed silica film that was peeled off the titanium substrate were observed under the SEM to determine composition and primary properties.

a. Iron Foils

The coated iron foils were cut in order to show edge properties and provide contrast. As shown in Figure 40, there is an obvious film surface on the iron foil that extends from the cut edge toward the back of the image.

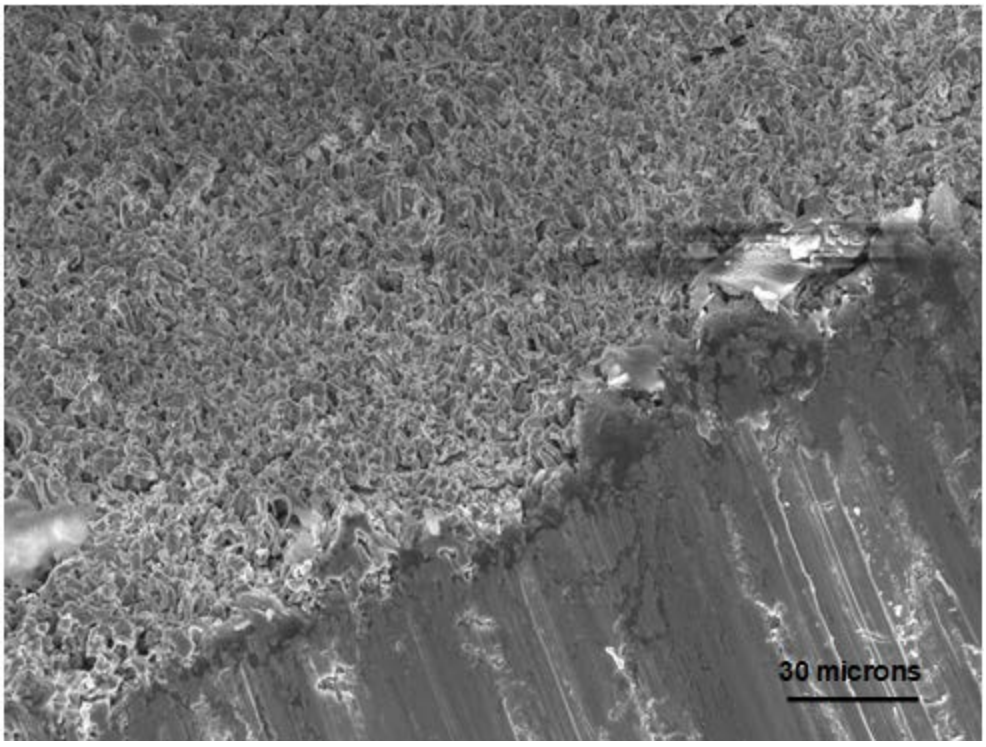

SEM image taken at an angle to exaggerate the film/substrate contrast at a cut edge.

Figure 40. SEM image of nickel-silica film on iron magnified 500 X.

This coating was estimated at approximately 5–10 microns thick. In addition, the film appeared to be somewhat rough on the surface. This may be potentially removed through multiple treatments or polishing. Notably, it was more difficult to identify the different components of the coating (such as which particles in particular corresponded to silica) as compared to the solid parts that were created. There were no obvious “fluffy” ceramic particles resting on, or coating, the larger nickel pieces.

An interesting comparison can be drawn between the films created utilizing this process and the solid parts created in the previous chapter with Protocol I (pure nickel included), as shown in Figure 41.

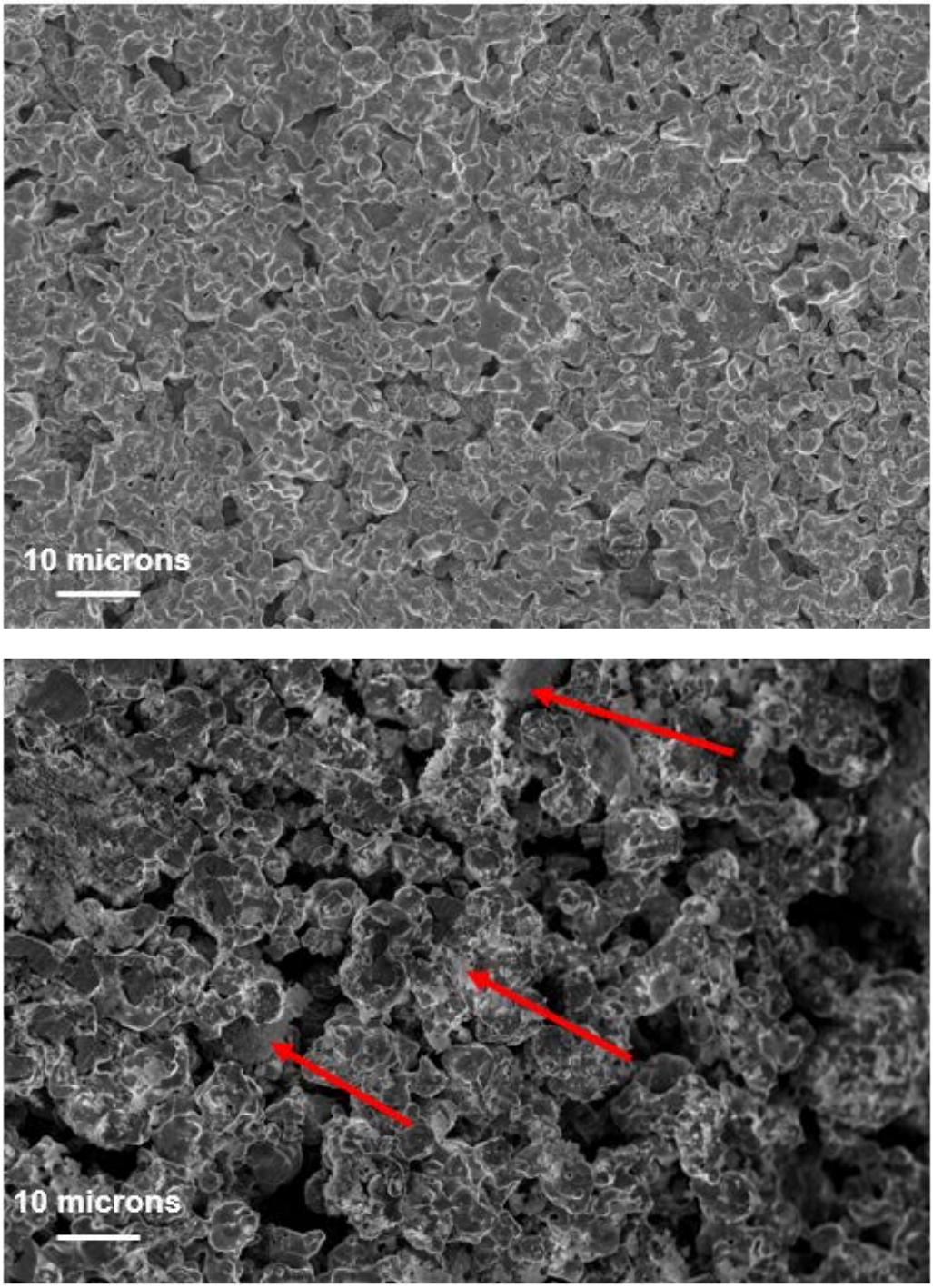

Top: Nickel-silica film on iron substrate created with Protocol III.
Bottom: Nickel-silica solid cermet part created with Protocol I.
Significant silica flecking is noted on the solid part surface. There are also much larger voids, and this is consistent with the direct bulk sample comparison from the previous chapter.

Figure 41. SEM comparison of the nickel-silica film and nickel-silica solid piece.

This comparison demonstrates that there was no obvious flecking or coating of the primary particles with the fumed silica in the case of the films. In addition, the particles on the films seemed to be bonded together to a much higher degree based on the number of large necks and relatively few number of voids. This is likely due to the omission of pure nickel particles in the creation of the films. The films behave in a similar manner to the solids created utilizing Protocol II, as shown in Figure 42.

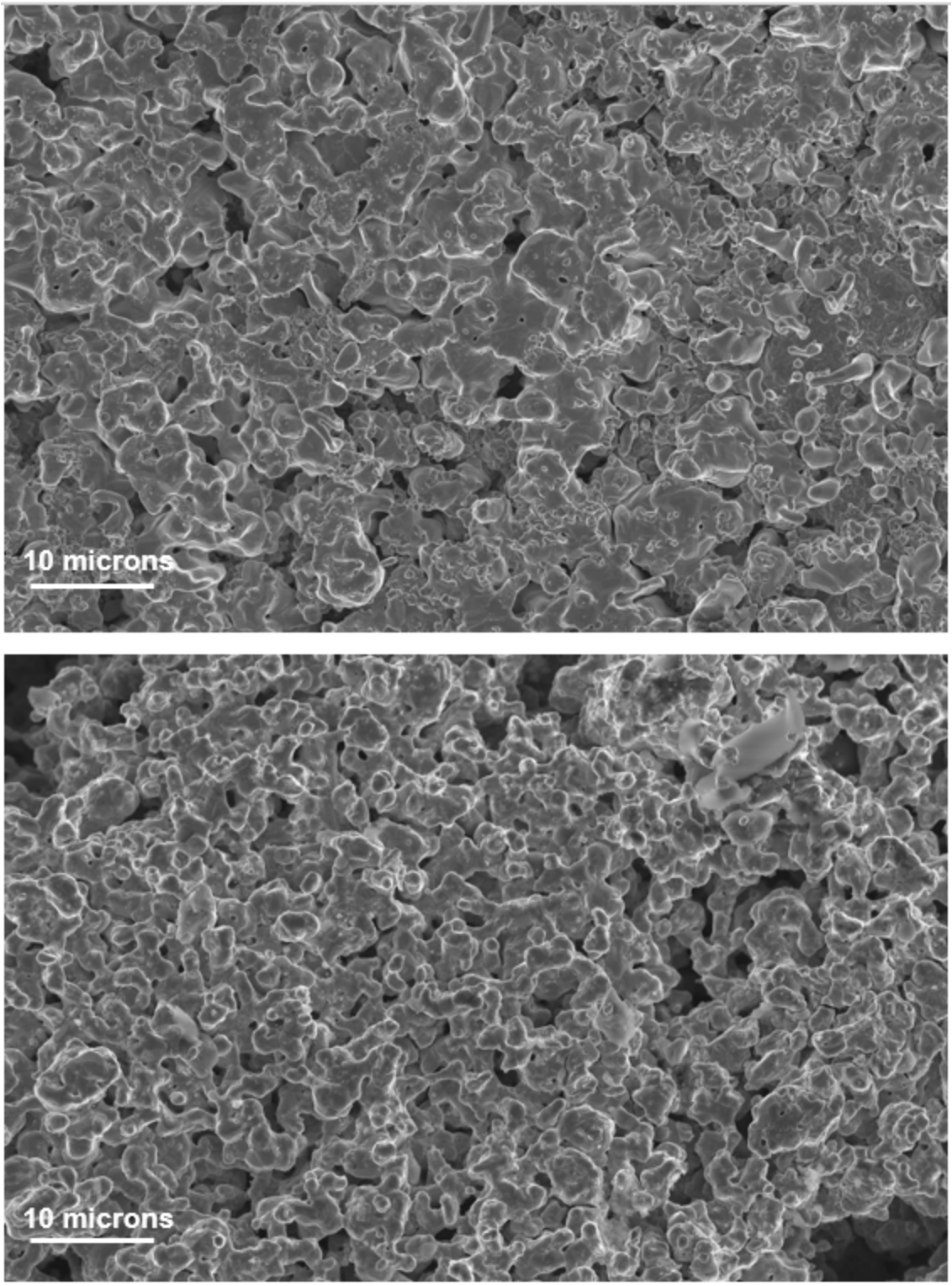

Top: Nickel-silica film on iron substrate created with Protocol III.
Bottom: Nickel silica solid cermet part created with Protocol II.

Figure 42. SEM comparison of film (Protocol III) and solid cermet part (Protocol II) with similar microstructure.

The films on the iron foils were also polished lightly in order to understand how they would behave after post-treatment and if polishing was even feasible. One sample was first wiped down with bleach and a paper towel, rinsed with ethanol, and then polished utilizing the automatic polisher at NPS with P2500 roughness polishing wheels. The sample was polished utilizing light pressure until the first grey “ashy” surface had been removed. This took roughly 30 seconds. It was originally thought that all of the film has been removed. However, as shown in Figure 43, it appeared the polishing had begun to smooth the surface considerably. There were patches of unpolished film and large spots of polished surface. This polishing also helped create a uniform film surface from the rough patches.

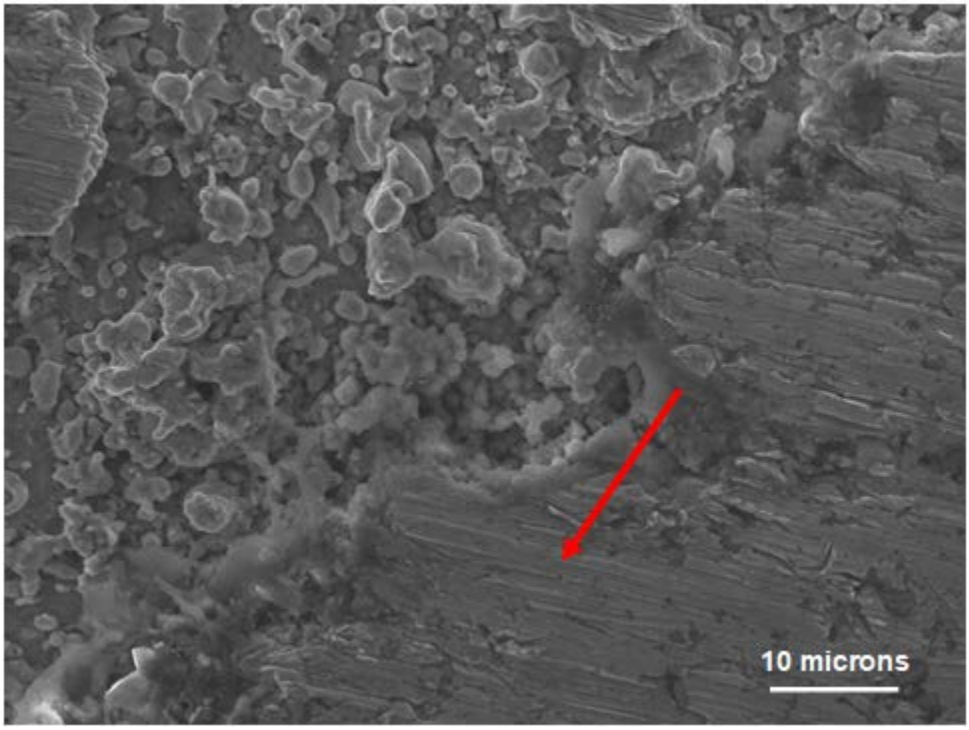

Smooth patches on the surface are marked.

Figure 43. Polished nickel-silica film at 1,500 X magnification from above.

In addition, inconsistent light and dark areas, shown in Figure 44, suggested that the polishing had smoothed the film surface extremely well in this particular section (near an edge) and appeared to indicate that the iron below had not yet been reached.

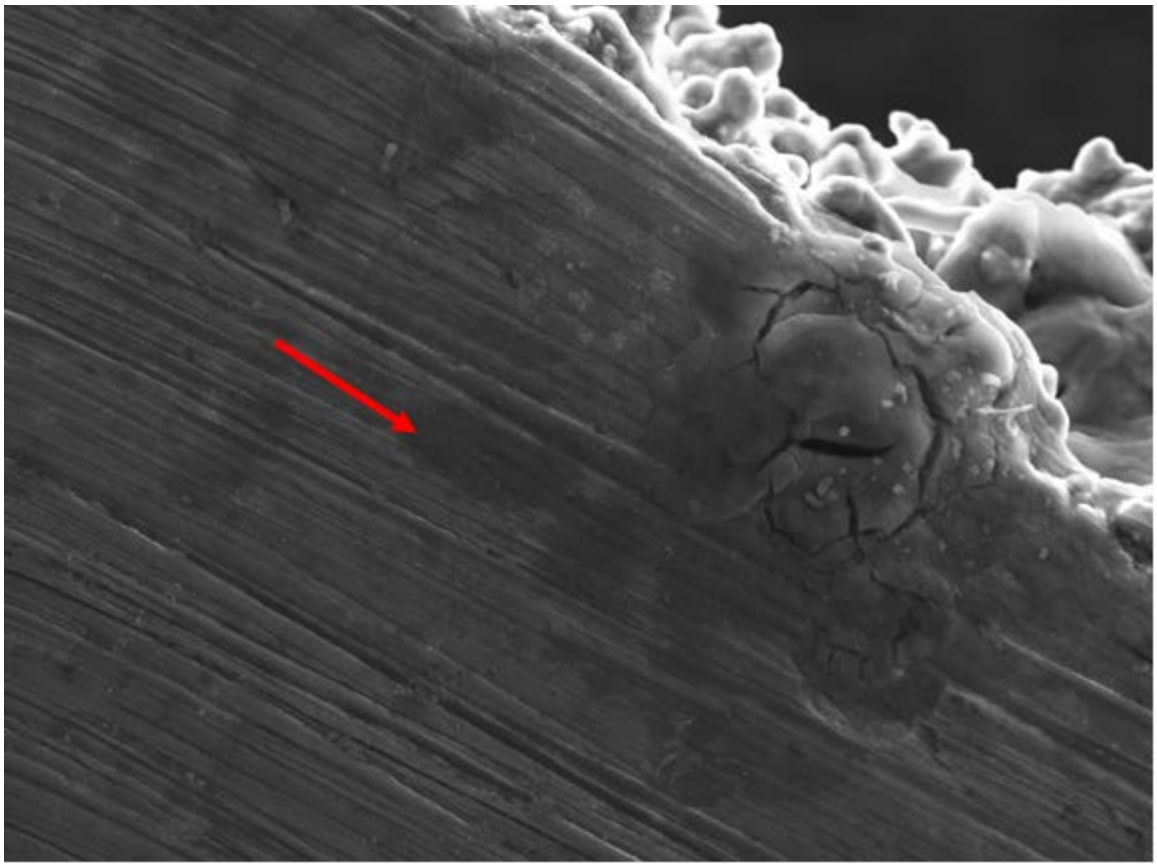

Figure 44. Polished section of nickel-silica film on iron showing dark colorations at 3,000 X magnification.

b. Films Formed on Titanium

After peeling the films off the titanium substrate, they were examined in the SEM and both the top face and bottom face (the side that was originally facing the titanium) were analyzed. The image in Figure 45 demonstrates that a thin "secondary" film had formed underneath the nickel and fumed silica mixture. This could have been a by-product of titanium, and preliminary EDS analysis corroborated this. This provided additional stability to the film that was created and allowed it to be removed from the bulk titanium substrate. The unique growth structure, resembling small needles, seems to suggest that the RES-C process caused a reaction on the surface of the titanium allowing these structures to grow simultaneously with the formation of the nickel and fumed silica film. This is an interesting property that was not observed on the other substrates, and could potentially be leveraged to create unique film structures and morphologies.

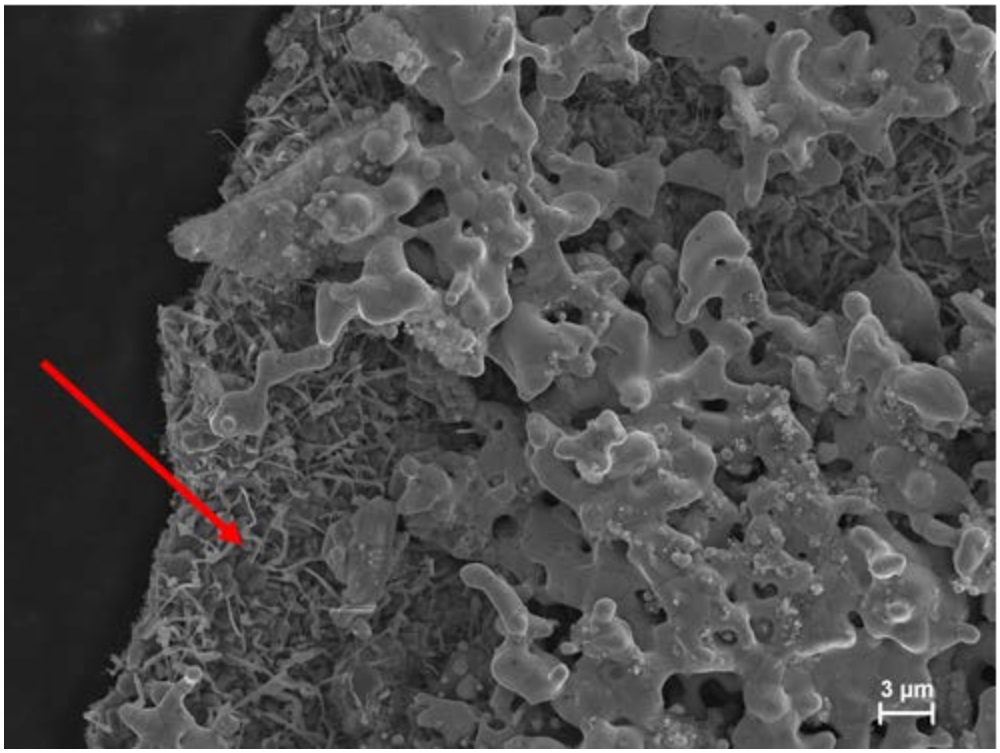

A thin growth surface with needle-like structures is obvious underneath the large nickel conglomerates.

Figure 45. A top view of nickel and fumed silica film formed on titanium.

3. EDS Observation Results

Because there was no obvious fumed silica particles resting on the nickel primary particles in the iron film samples, EDS analysis was attempted. Fumed silica was detected utilizing the EDS mapping feature on the SEM, as indicated in Figure 46. This showed that silica appeared to have clumped together, as opposed to a light coating on top of the large nickel primary particles which was observed in the solid cermet parts created via Protocol I.

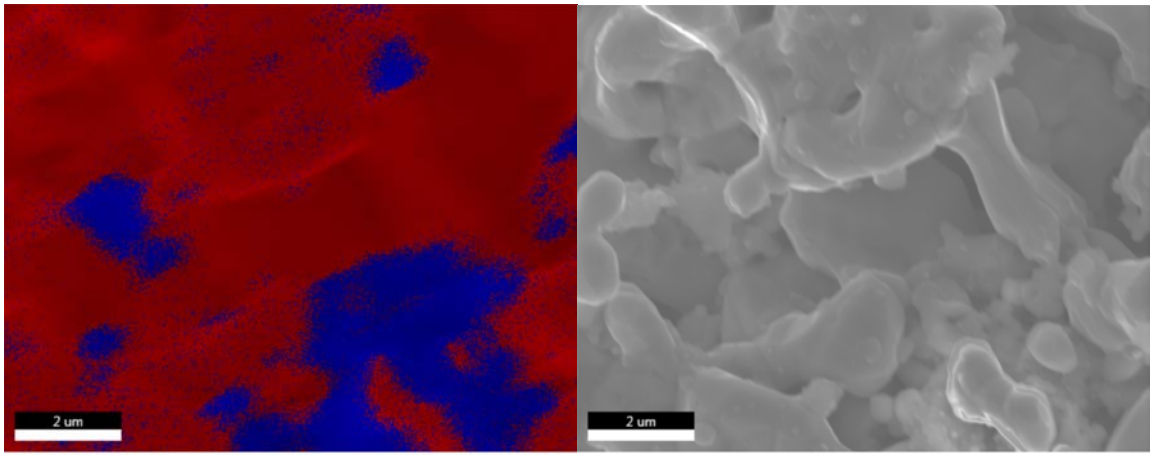

Blue corresponds to fumed silica and red corresponds to nickel detection.

Figure 46. EDS map and corresponding image.

The primary particles seemed to have bonded together relatively well on the film, despite the rough surface. This surface finish could potentially be adjusted by polishing of the film or by multiple coating treatments. Overall, it appeared that this method of preparation allowed for the fumed silica particles to become more "integrated" as individual particles into the microstructure as opposed to simply creating a thin ceramic coating all metal surfaces. This is similar to what was observed in the creation of the solid parts using Protocol II. In addition, it was interesting to note that there appeared to be small voids on the coating where nickel and fumed silica did not form a film and only iron substrate was detected in the EDS.

4. Spectral Analysis Results

The results from the spectral absorbance analysis on the cermet film with iron substrate were plotted over the wavelength in the visible spectrum, based on the capabilities of the measurement equipment. The absorbance of both polished and unpolished film samples are shown in Figure 47, along with both pure nickel and pure iron spectra.

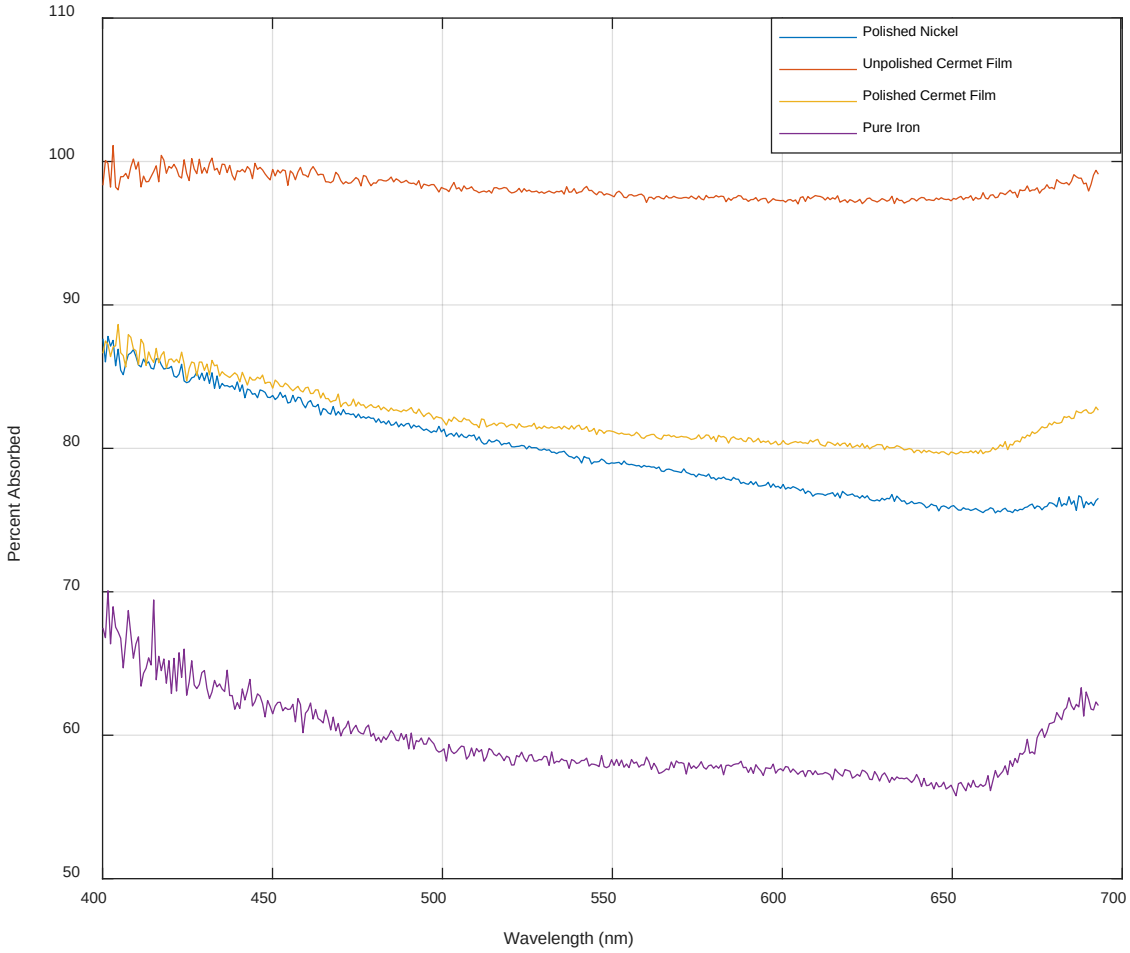

Figure 47. Percent of the visible wavelength absorbed by the various samples.

Interestingly, there is a slight bend in the absorbance curve for the polished cermet film that occurs at the same wavelength that the bend in the curve appears for the pure iron substrate. This property is desirable because the cermet seems to cause the substrate to behave in the same manner but proportionally higher, and a higher solar absorbance is desirable for these coatings. It appears from this plot that the unpolished cermet film outperforms the polished variants and the controls. This makes sense because a smooth surface will tend to reflect more incident light.

It is noted that polishing the sample seems to drop the reflectively by around 15%. However, the polished film still outperforms both the polished nickel and pure iron

substrate, indicating that these films may be positive candidates for higher absorption. These results are important because this is the first step in qualifying whether or not these cermets could be used as spectrally selective films.

Based on the relatively high absorbance of both the polished and unpolished cermet films over the visible wavelength (approximately 0.85 and 0.98 respectively), these could be potentially explored as a viable option for a spectrally selective coating. More data would obviously be needed to cover the full spectrum from 0.25 – 2.5 μm (which is a typical data set for absorbance in the solar spectrum) and this would be weighted with the air mass zero solar spectrum to produce a single absorbance value [6]. This data would also need to be compared to the thermal emittance values of the cermet coatings to order to produce a ratio of absorbance in the solar spectrum to emittance in the IR spectrum, which could be used as a direct comparison to other cermet coatings and methods of preparation.

5. Failure Testing Results

The failure analysis test on the films created from the titanium substrate demonstrated that the films were self-supporting and relatively malleable. Figures 48–50 demonstrate a series of failure tests, where a sample of film was bent at successively higher angles until ultimate failure.

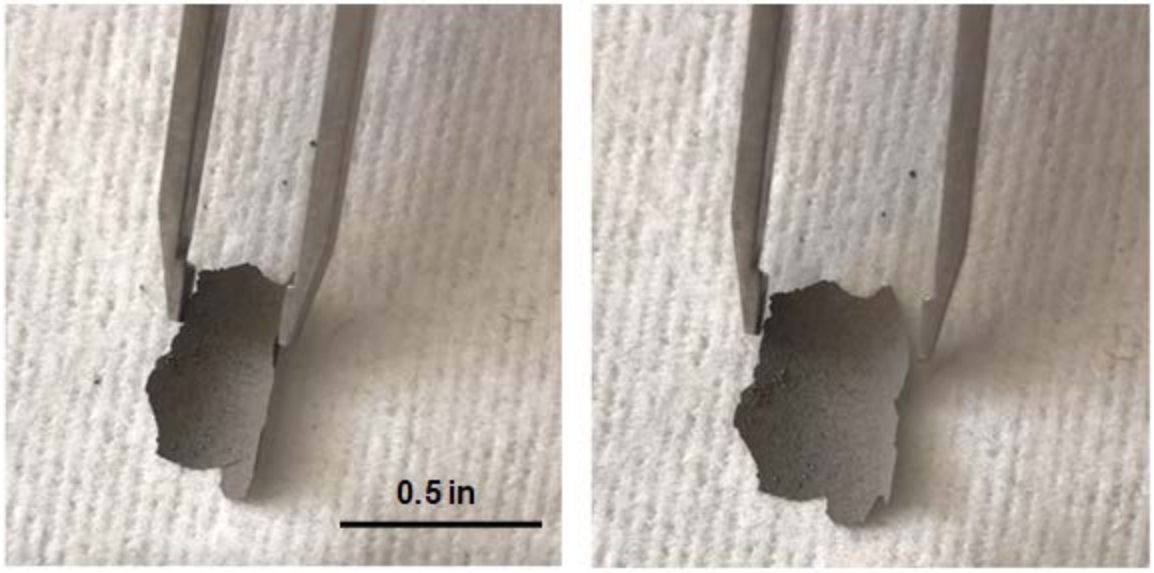

Left: Initial slight bend with tweezers.
Right: No deformation after load is removed.

Figure 48. Initial “bend test” on film removed from the Ti substrate showing no plastic deformation.

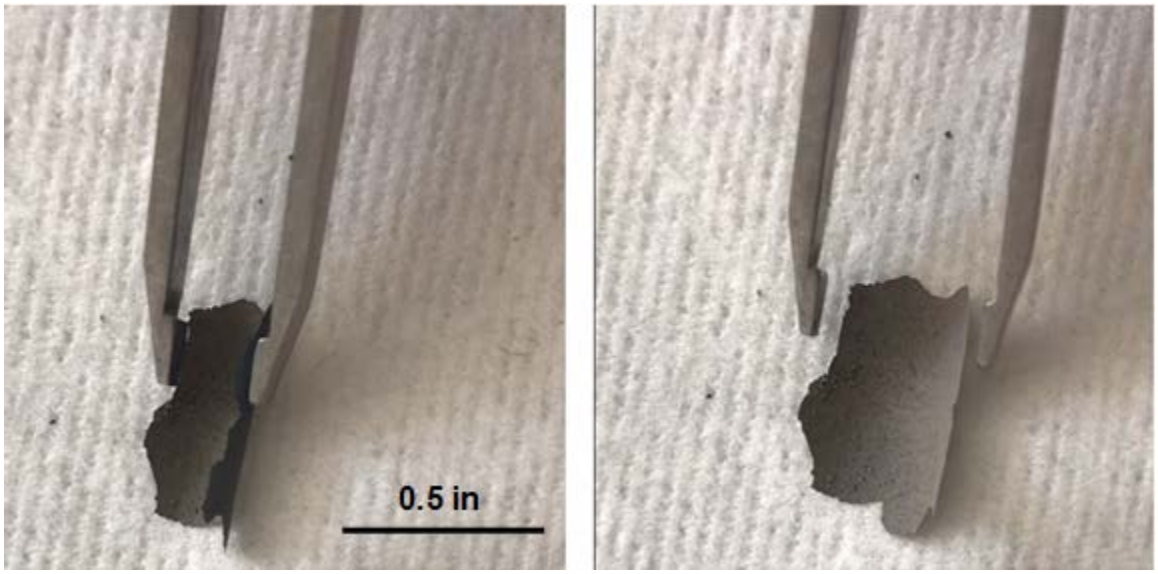

Left: Higher load applied to film with tweezers.
Right: Slight plastic deformation after load is removed.

Figure 49. Secondary “bend test” on film removed from Ti substrate showing slight plastic deformation.

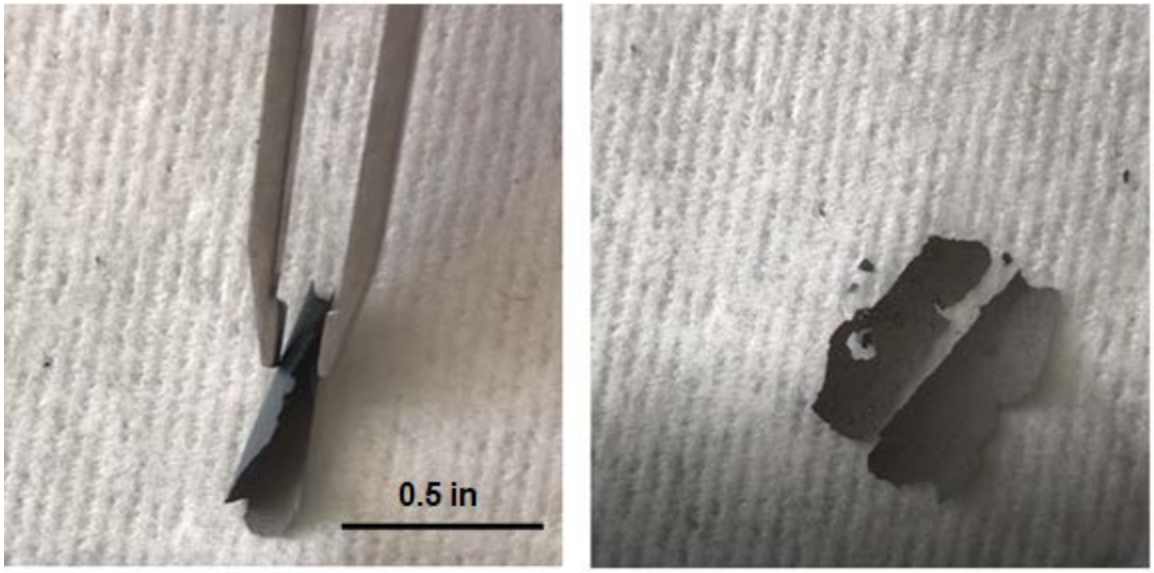

Right: Load applied to fold film in half.
Left: Failure of the film structure after load is removed.

Figure 50. Final "bend test" on film removed from Ti substrate showing ultimate structural yield.

These tests demonstrate that the films produced from the nickel/fumed silica on titanium substrates were relatively malleable after being removed from the titanium surface. After bending slightly, there was some slight deformation, but the films did not break until after being folded almost in half. This is promising for future applications of these films such shaped electrical components or insulation.

D. DISCUSSION

It was clear from these results that nickel/fumed silica cermet films can be created using the RES process on a variety of metal substrates. These films appeared to have better stability as compared to the solid cermet parts that were created in previous chapters; the microstructure closely resembled the bulk parts created utilizing Protocol II (no pure nickel particle in the precursor mixture).

The film properties were a function of the identity of the metal substrate. The iron substrate produced a rough and cakey film. The copper substrate produced a thin and relatively uniform film. The titanium substrate produced a film that could be easily removed from the substrate.

The fact that on all substrates films were coherent and “tough” rather than “particulate” and broken, suggests a similarity with bulk samples created with Protocol II using NiO and fumed silica. In both cases this “success” is attributed to the fact that only nickel oxide, urea, and fumed silica were utilized before being “painted” on to the metal substrates. In contrast, reduced metal particle precursors appeared to interact with the ceramic and become coated. It is postulated that the inclusion of the pure nickel causes wetting, or an atomic layer “film”, with the ceramic particles. This causes a movement of the ceramics to the surface of the particles and a bonded coating to be formed, which blocks bond formation between adjacent metal particles. As a result, neither a solid part nor coherent film can form.

In addition, it is a common phenomenon for materials created as thin films to behave differently than their corresponding bulk components. For example, the mechanical properties of films are dependent on the substrate, especially for stress (since the films may contract or expand at different rates compared to the substrate). This tends to cause stress discontinuities at the interface between the film and substrate. Obviously, this is not the case for bulk solids because stresses are continuous throughout [32]. Other notable impacts that change the behavior of a film from that of a bulk material include the large surface-to-volume ratio and the obvious constraint imposed by the substrate properties [33].

For the nickel-silica films on iron, it appeared that they could be polished and surface treated relatively well, and that this treatment seemed to even the surface out and remove several rough patches. However, the film appears to be delicate, and multiple treatments could potentially help improve its strength. The fumed silica particles do not rest on top of the primary particles as either flecks or as a coating, most likely due to the absence of pure nickel particles in the film creation process. In addition, the spectral results for these films are promising in that they tend to absorb high amounts of visible radiation, most likely due to their relatively dark color. These are promising results for future work defining these films for use as spectrally selective absorbers.

An especially unique discovery was the fact that the nickel-fumed silica films on titanium substrates could be peeled off easily and remain as thin metal film sheets that were self-supporting and almost as thick as paper. It was shown that these films could also be

bent almost in half before experiencing failure. The mechanism responsible for this appeared to be a thin titanium growth surface, composed of needle-like structures, that was caused by the RES-C process interacting with the titanium. Large conglomerates of nickel and silica were able to grow on this surface and it provided added stability, even with removal from the bulk titanium disk. These types of films could be potentially very useful as molded electrical parts or insulation. Significant future work in this area is merited.

VII. CONCLUSIONS

The results of this study indicate that, generally, utilization of alumina and silicon carbide to create solid cermets utilizing the RES-C process was not successful. Utilizing smaller percentages and particle sizes, such as in the 1% by mass with micropolish alumina, saw limited success as compared to large percent by mass tests (the powder seemed to "stick" very loosely after treatment). Moderately successful cermets were the ones created utilizing the 1% by mass silica as the ceramic following both Protocol I and Protocol II. However, the microstructure was noticeably improved by following Protocol II and omitting pure nickel particles from the precursor mixture. It also appeared that treating the fumed silica cermets multiple times with the RES-C process promoted stronger bonding between the materials. The hypothesis that the ceramic particles would be "squeezed" between the bonding nickel particles did not appear to be correct, as unanticipated chemical reactions occurred between the ceramics and the nickel particles.

Creating films with the silica cermets on a metal substrates was more successful, and saw a change in how the ceramic particles interacted with the overall matrix, as they were not "fluffy" and simply resting on top of the nickel particles in a coating. This was most likely due to the absence of pure nickel particles in the creation of the precursors for the cermet films. Only nickel oxide, urea, and the ceramic particles were utilized. Removing the pure nickel, and closely aligning the process with Protocol II from the creation of the bulk samples, may have prevented the wetting of the nickel by the ceramic particles and prevented the ceramics from forming a coating, or flecking, the surface of the nickel during the reaction. With the absence of this ceramic coating, the nickel oxide particles were able to bond together to a higher degree.

As far as testing of the mechanical and spectral properties of the materials, the hardness tests were helpful in that they indicated that the fumed silica cermet parts were somewhat harder than the pure nickel control studies. However, issues did occur with the polishing of these samples that could be attributed to either the lack of a cermet-specific polishing method or the fact that, when the parts were embedded in a resin matrix for polishing, they may have absorbed the resin. Finally, the absorbance values of the cermet

films were relatively high (between 0.85-0.98) which indicate that they could potentially act as effective solar absorbers.

A. OVERALL SUCCESS

Overall, it was clear that the RES-C process can potentially be applied to create cermet or metal matrix composite solid parts and films. However, the standard RES-C process cannot be applied universally and is only successful for certain mixtures and percent compositions. For example, larger percent (>1% by mass) do not appear that they will work at all. In addition, larger sized particles such as those in alumina do not seem to be conducive to this process due to size and possible heat absorption preventing sintering and bonding between the nickel particles. Generally, smaller size ceramic particles seem to work more effectively. The best case scenario appeared to be the utilization of particles on the order of scale of fumed silica (0.007 μm) and pure nickel oxide as precursors.

The RES-C method worked well for the creation of metal-matrix or cermet films on iron, copper, and titanium. An especially interesting and notable result was the fact that the films created on titanium substrates could be easily “peeled” off from the metal base. These self-supporting, thin films of metal could have many potential electrical or spectral applications if they can be formed or shaped.

It appears that the creation of films utilizing this method is the most likely application for the RES-C process. The initial spectral testing also seems to indicate a high absorbance values for these films, at least compared to the control studies of the pure nickel. This would be the first step in classifying these films for use as spectrally selective solar absorbers and calculating an absorbance to emittance ratio for direct comparison. This creation method could have a significant impact on the field of space-based solar absorbers and present a new way for these films to be created, and even a method for creation on-orbit or on station. The bulk cermet parts that were created were generally very brittle and, although the hardness values of these parts were greater than that of pure nickel, there were still issues with voids and low density that was also noted in the pure nickel components. However, the application of the RES process to cermets and metal matrix composites is feasible and could perhaps even be extended to different types of inclusions besides particle

ceramics such as plastics or fibers. The objectives of this thesis were met and the hypothesis that variations of the RES process could potentially be utilized to create cermets was proven

B. POTENTIAL FUTURE WORK

One avenue for future work in this area would be to test the feasibility of utilizing the RES-C process to create "brown" bodies that are not fully dense, but are self-supporting. These cermet bodies would have the general shape of a specific part or tool to be created, and could be transported easily to either a military deployment site or on a space mission. After they have reached their desired use location, these materials could potentially be Hot Isostatic Pressed (HIP) in order to create a dense part. Studying this capability and process would be useful for fully classifying the viability of the RES-C method to create useful parts. However, the primary focus for future work should be on fully optimizing the process for creating films and a full characterization of these materials. For example, lower percent by mass of the ceramic particles such as alumina and silicon carbide could be tested to see if they would create more robust films on the metal substrates. In addition, more layers of the fumed silica films could be created, one on top of the other, to see if this would prevent gaps from occurring during the RES-C process and allow for a more uniform film creation. Additionally, optimization of this film creation process, especially in regards to furnace heating variables and gas flow, could be studied in order to facilitate scaling the process for industrial applications. This could also be helpful in fitting the process into a space-based setting such as on the ISS. Finally, further characterization of the films (and solid parts) could be done in order to better understand their spectral properties, especially under different thermal conditions and in vacuum.

THIS PAGE INTENTIONALLY LEFT BLANK

APPENDIX. FLOW OPTIMIZATION

In order to facilitate scaling up of the RES-C process, and its potential for use as a valid manufacturing method on military deployments or on orbit, a time minimization problem was studied in the context of optimality for obtaining the proper conditions for the process. The main problem was to minimize both the time for the atmosphere in the quartz tube sample holder to have a concentration of >95% argon purity as well as minimize the head loss of the flow through the tube. It was assumed that the gas and air were perfectly mixed throughout the process. Minimizing the head loss, or energy of the flow lost to friction on the walls of the tube, would logically cause mixing closer to a perfect system due to the increase in net energy of the flow. The goal was to generate an optimal control input for gas input flow rate that would minimize both the time and the head loss. In order to do this, Pontryagin's Principle was utilized as well as the numerical optimal control solver developed by Dr. Isaac Ross, titled DIDO [34].

A. MODELING

The model and various needed equations for head loss of flow in a pipe are shown below [35]. It was assumed that the flow was laminar for all cases. The following equations represent the needed constants for the problem where D is the constant tube diameter, A is the tube cross sectional area, and L is the tube length.

$$D = 0.022\,m \tag{18}$$

$$A = \pi(\frac{D}{2})^2 = 0.00038\,m^2 \tag{19}$$

$$L = 0.705\,m \tag{20}$$

The kinematic viscosity, v, of the gas was calculated utilizing the Microelectronics Heat Transfer Lab Fluid Properties Calculator [36] and the gravitational constant was defined as g.

$$v = 1.342 \bullet 10^{-5}\,\frac{m^2}{s} \tag{21}$$

$$g = 9.8\,m/s^2 \tag{22}$$

The velocity of the flow in m/s was defined in terms of the control variable *u*, which is the input rate of the gas in m^3/s and could be directly controlled by the user.

$$V = \frac{u}{A} \tag{23}$$

The Reynolds number could then be defined based on the kinematic viscosity, the flow velocity, and the pipe diameter.

$$Re = \frac{DV}{v} \tag{24}$$

This could be used to define the frictional factor for laminar flow [35].

$$f = \frac{16}{Re} \tag{25}$$

Finally, the combination of the previous parameters could be used to define the head loss of the flow in terms of the control variable.

$$h = 2f\left(\frac{L}{D}\right)\left(\frac{V^2}{g}\right) = 2\left(\frac{16v}{DV}\right)\left(\frac{L}{D}\right)\left(\frac{V^2}{g}\right) = \left(\frac{32vL}{AgD^2}\right)(u) \tag{26}$$

The boundary conditions and bounds on the control are also shown below based on the derivation of the dynamics of the system and the initial and final desired concentration of argon.

$$x_0 = 0\,ml \tag{27}$$

$$x_f = 0.95 \bullet C\,ml \tag{28}$$

The bounds on the control were based on the capabilities of the flow meter that was utilized and the desire to have at least some flow during experimentation.

$$0.25\frac{ml}{s} \le u \le 3.03\frac{ml}{s} \tag{29}$$

Finally, the cost function is shown below. It is a standard minimum time problem so the cost function simply incorporates the final time for the system to reach as the endpoint cost with no running costs.

$$J = t_f \tag{30}$$

A unique aspect to this problem was the minimization of the head loss. In order to do this, a trade space must be established. The minimum time problem for the mixing dynamics

would first be solved, followed by the problem indicated by the equation solving for the net head loss over all time.

$$h_{net} = \int_0^{tf} h\,dt \tag{31}$$

In order to find the final time, t_f, a graph of head loss versus time would be established, with one bound of the graph being the minimum time of the mixing dynamics and another bound being the time of mixing that corresponds to the lowest possible head loss. The final time for this problem would most likely be the "knee" in this curve of head loss versus time. This will give a balance of the shortest time for mixing and minimum head loss. A summary of the initial value problem is shown below.

$$\begin{gathered} \boldsymbol{x} = [x], \\ u = [u] = \{0.25 \le u \le 3.03\} \end{gathered} \tag{32}$$

Minimize:

$$\begin{gathered} J(x, u, tf) = tf \\ h_{net} = \int_0^{tf} h\,dt, \;\; tf \; is \; free \end{gathered} \tag{33}$$

Subject to:

$$\begin{gathered} \dot{x} = \frac{-u}{C}x + ku \\ t_0 = 0 \\ x_0 = 0 \\ x_f = 0.95 \bullet C \\ h = \left(\frac{32vL}{AgD^2} \right)(u) \end{gathered} \tag{34}$$

B. SCALING

A scaled version of the initial value problem is needed to ensure good numerical results, this is shown below (this will allow the states, control, and costates to within the same numerical range). The basic method was adapted from a process developed by Dr. Isaac Ross and Dr. Mark Karpenko at the Naval Postgraduate School and taught in a series

of class lectures in Fall of 2019 and Spring of 2020. These lectures were based on Pontryagin's Principle and explained in detail in Dr. Ross' book [37].

$$\tilde{x}=\frac{x}{S},\tilde{t}=\frac{t}{T},\tilde{u}=\frac{\frac{u}{S}}{T},\tilde{C}=\frac{C}{S} \tag{35}$$

$$\dot{x}=\frac{-u}{C}x+ku \tag{36}$$

$$\frac{d\tilde{x}}{d\tilde{t}}=\frac{d\left(\frac{x}{S}\right)}{d\left(\frac{t}{T}\right)}=\frac{dx}{dt}\left(\frac{T}{S}\right)=\left(\frac{T}{S}\right)\left(\frac{-u}{C}x+ku\right)=\left(\frac{T}{S}\right)\left(-\frac{S}{TS\tilde{C}}\tilde{u}\bullet\tilde{x}S+\frac{kS\tilde{u}}{T}\right)=-\frac{\tilde{u}}{\tilde{C}}\tilde{x}+k\tilde{u}$$

$Define: S=3 and\ \tilde{x}\left(t_f\right)=0.95\bullet\frac{C}{3}$

$T=1$

$$\left[\tilde{u}\right]=\left\{0.25\left(\frac{S}{T}\right)\frac{ml}{s}\le u\left(\frac{S}{T}\right)\le 3.03\left(\frac{S}{T}\right)\frac{ml}{s}\right\} \tag{37}$$

Utilizing these scalars, the properly scaled initial value problem can be defined, where the head loss is calculated in engineering units outside the numerical solver.

$$\begin{gathered}\left[\tilde{u}\right]=\left\{0.75\le\tilde{u}\le 9.09\right\}\\ \frac{d\tilde{x}}{d\tilde{t}}=-\frac{\tilde{u}}{\tilde{C}}\tilde{x}+k\tilde{u}\\ t_0=0\\ \left(\widetilde{x_0}\right)=\left(0\right)\\ \left(\widetilde{x_f}\right)=\left(\frac{C}{3}\bullet 0.95\right)\end{gathered} \tag{38}$$

The following table summarizes the constants for this problem as well as the scaling parameters (chosen as designer units). Several constants are needed for the flow calculations as defined previously.

Table 4. Summary of relevant constants and parameters.

Name	Value	Units	Use
Tube Volume (C)	268	ml	State Eqn.
Input Concentration (k)	0.99	N/A	State Eqn.
Dynamic Viscosity (v)	$1.342 \cdot 10^{-5}$	m^2/s	Head Loss Eqn.
Tube Length (L)	0.705	m	Head Loss Eqn.
Cross-Sectional Area (A)	0.00038	m^2	Head Loss Eqn.
Gravity (g)	9.8	m/s^2	Head Loss Eqn.
Tube Diameter (D)	0.022	m	Head Loss Eqn.
State Scaling (S)	3	N/A	Scaling
Time Scaling (T)	1	N/A	Scaling

C. PONTRYAGIN'S PRINCIPLE

After the scaled initial value problem was defined, the next step was to apply Pontryagin's Principle to form a scaled boundary value problem, as well as identify the equations that can be used to verify optimality and feasibility. The general process and equation forms were provided by Dr. Isaac Ross and Dr. Mark Karpenko at the Naval Postgraduate School during a series of classes in Fall 2019/Spring 2020. These lectures were based off of Pontryagin's Principle outlined in Dr. Ross' book [37].

The first step is to form the Hamiltonian.

$$\boldsymbol{\lambda} = [\lambda_x]$$
$$\boldsymbol{f} = \left[-\frac{\tilde{u}}{\tilde{C}}\tilde{x} + k\tilde{u} \right]$$
$$H = F + \lambda^T f = 0 + \lambda_x \left(-\frac{\tilde{u}}{\tilde{C}}\tilde{x} + k\tilde{u} \right) \tag{39}$$

The Adjoint Equations can then be formed; they are useful for validation to observe behavior of the costate. It should be a curve based on equation form.

$$-\dot{\lambda}_x = \frac{dH}{d\tilde{x}} = \lambda_x \left(-\frac{\tilde{u}}{\tilde{C}} \right) \tag{40}$$

The next step is to minimize the Hamiltonian with respect to *u.*

$$\frac{dH}{d\tilde{u}} = 0 = -\frac{\lambda_x}{\tilde{C}}\tilde{x} + \lambda_x k$$
$$2.5 \le \tilde{u} \le 30.3 \tag{41}$$

The Hamiltonian Value Condition can then be derived. The result is useful for validation because the Hamiltonian needs to be equal to -1 at the final time.

$$\check{E} = E + w^T e = t_f + w_1\left(\tilde{x}_f - x^f\right) \tag{42}$$

$$H\left(t_f\right) = \frac{d\check{E}}{dt_f} = -1 = \lambda_x\left(-\frac{\tilde{u}}{\tilde{C}}\tilde{x} + k\tilde{u}\right) \tag{43}$$

Next, the Hamiltonian Evolution Equation can be found. It is useful for validation because the Hamiltonian will need to, necessarily, be a constant value.

$$\frac{\mathrm{d}\check{H}}{\mathrm{d}t} = \frac{dH}{dt} = 0 \tag{44}$$

Finally, the transversality conditions can be applied, which provide no real information in this case.

$$\lambda_x\left(t_f\right) = \frac{dE}{\tilde{x}_f} = w_{1,} \tag{45}$$

The fully scaled boundary problem can then be summarized.

$$\begin{gathered} 0.75 \le \tilde{u} \le 9.09 \\ \frac{d\tilde{x}}{d\tilde{t}} = -\frac{\tilde{u}}{\tilde{C}}\tilde{x} + k\tilde{u} \\ \dot{\lambda}_x = \lambda_x\left(\frac{\tilde{u}}{\tilde{C}}\right) \\ t_0 = 0 \\ \widetilde{x_0} = 0 \\ \widetilde{x_f} = \frac{C}{3}\bullet 0.95 \end{gathered} \tag{46}$$

The minimum time optimization problem above can be solved iteratively by increasing the upper bound on the control by a constant *A* until it reaches the final value of ~9.09.

$$0.75 \le \tilde{u} \le 0.75 + A \tag{47}$$

All values of the control and final time will be output, descaled, and converted into compatible units for head loss (from ml/sec to m^3/sec).

$$h = \left(\frac{32vL}{AgD^2}\right)(u) \tag{48}$$

Since the head loss equation (a form of friction) is directly related to the control, it will be plotted versus the final time in order to identify the solution to the original equation for minimization as stated.

$$h_{net} = \int_0^{tf} h\,dt \tag{49}$$

Finding the "knee" in this curve will give the minimum time optimization solution and minimum head loss (minimization of both parameters). After the application of Pontryagin's Principle, it was decided to use the numerical tool DIDO in order to solve this problem. This tool was developed by Dr. Isaac Ross [34]. This choice was made because of the switching function ("bang-bang") control anticipated by the application of Pontryagin's Principle due to the limits set on the controller. DIDO is able to numerically handle this type of controller better than either the shooting method or collocation method for solving these boundary value problems. The relevant plots and explanations are shown below.

D. NUMERICAL RESULTS

Figure 51 indicates a decision within the trade space to balance the minimum time with the minimum head loss and choose the corresponding control values. The data tip indicates the "knee" in the curve with the time as approximately 860 seconds and a head loss of 1.7×10^{-4} m. This time provides a balance between minimum time for mixing and minimum head loss.

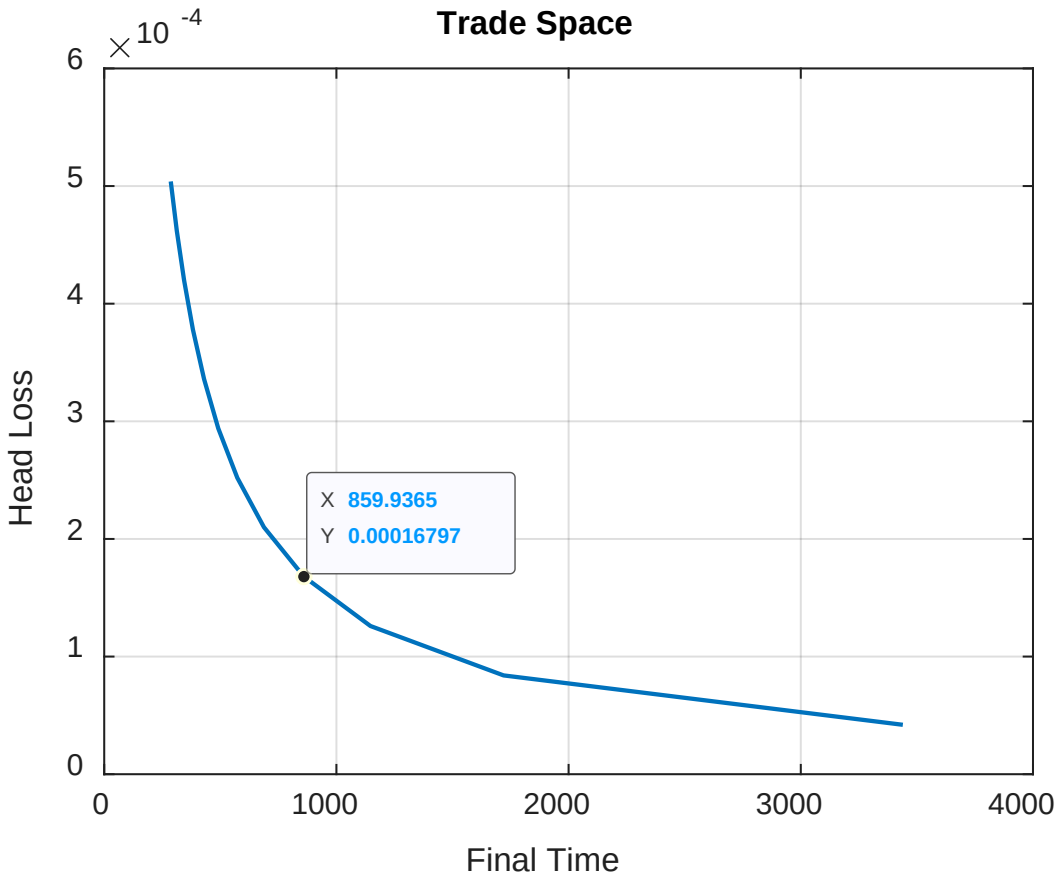

Figure 51. Head loss versus final time to complete the mixing problem.

In Figure 52, the various control optimal trajectories are plotted versus the final time they produce in the system. The data tip indicates choosing a control of 1 allows for the same time as predicted by the trade space.

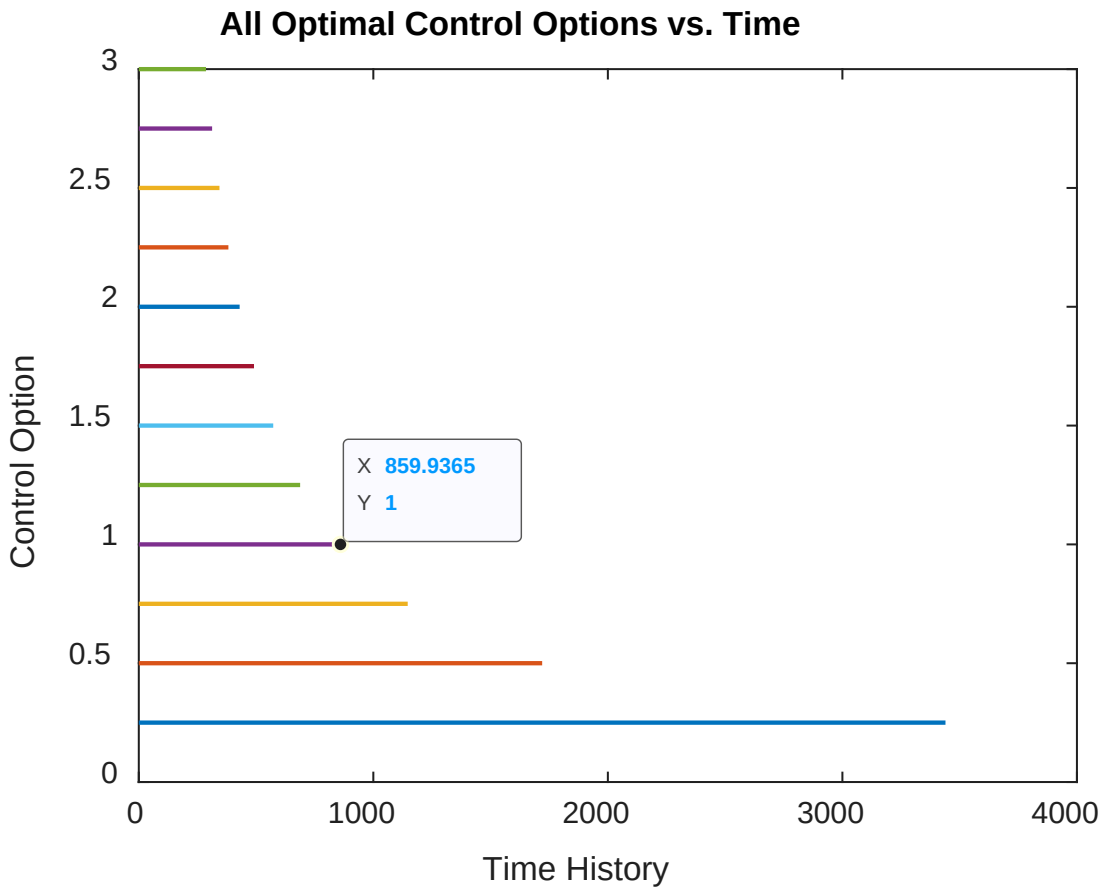

Figure 52. Optimal control trajectories versus the final time they produce.

The following plots show a comparison of the states, control, and costates that correspond to the control that produces the balance between minimum time and minimum head loss, and the control that produces a true minimum time. As expected, both iterations utilize a control value that resembles a “bang-bang” type controller. It is at a flat maximum value for the whole period of the dynamics. In Figure 53, the blue curve shows a true minimum time problem which corresponds to utilizing the maximum available control value. The red curve corresponds to utilizing the control value of 1 that allows for minimum head loss and time balancing. Both start at zero and end at 95% of the tube volume as expected.

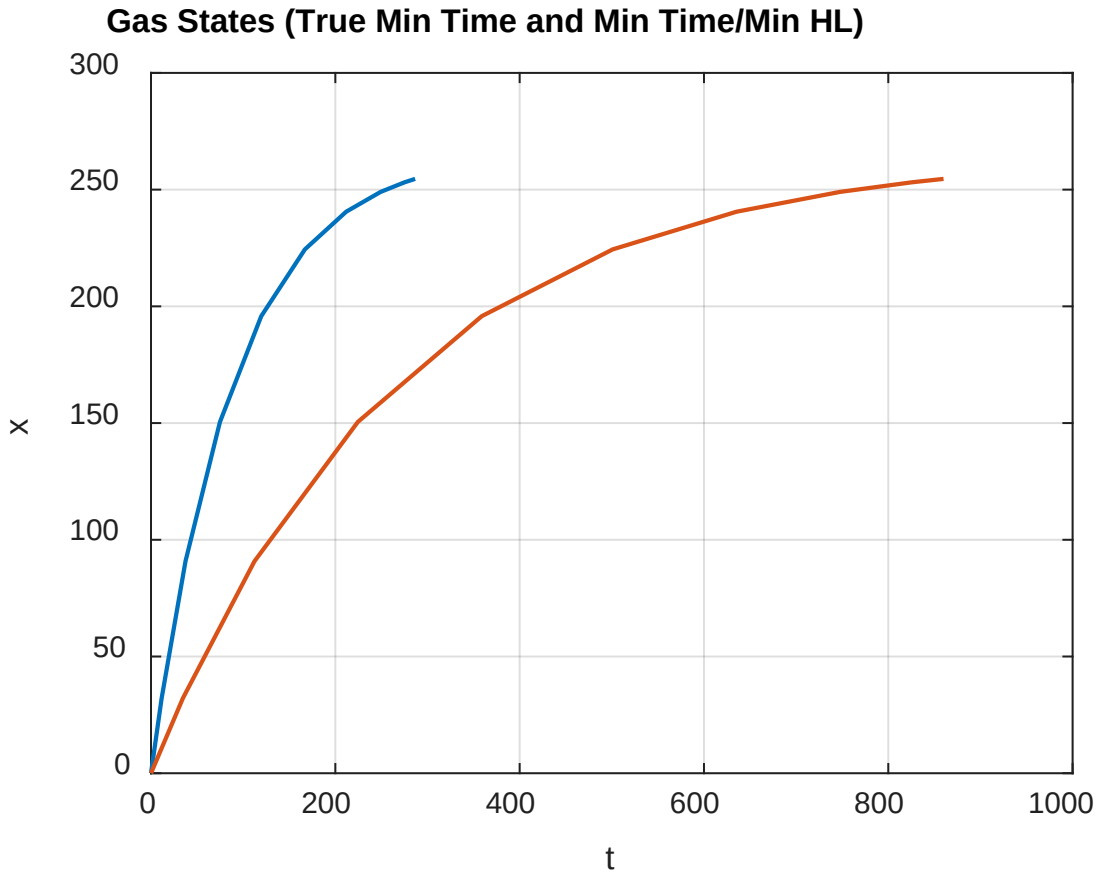

Figure 53. Unscaled state *x* (volume of argon gas) as a function of time.

In Figure 54, the blue curve shows a true minimum time problem which corresponds to utilizing the maximum available control value for the costates. The red curve corresponds to utilizing the control value of 1 that allows for minimum head loss and time balancing for the costates.

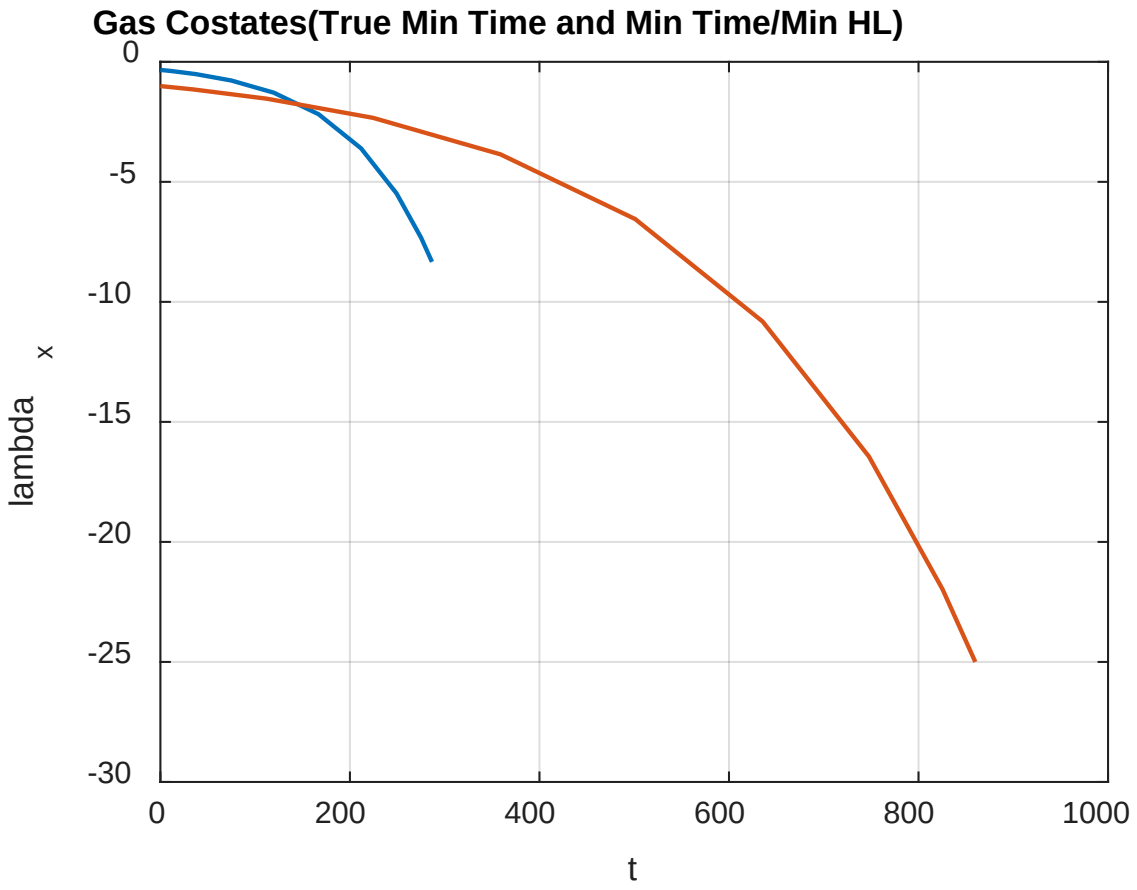

Figure 54. Indication of the unscaled costates as a function of time.

The following plots show how the dynamics were scaled to fit this problem and produce good numerical results in addition to demonstrating the satisfaction of Pontryagin's Principle and validation tests. In Figure 55, the state (blue curve) and control variable (red curve) are within the same numerical range. In addition, the state starts at zero and ends at 95% of the scaled tube volume as expected and the control is a consistent value of 3 throughout.

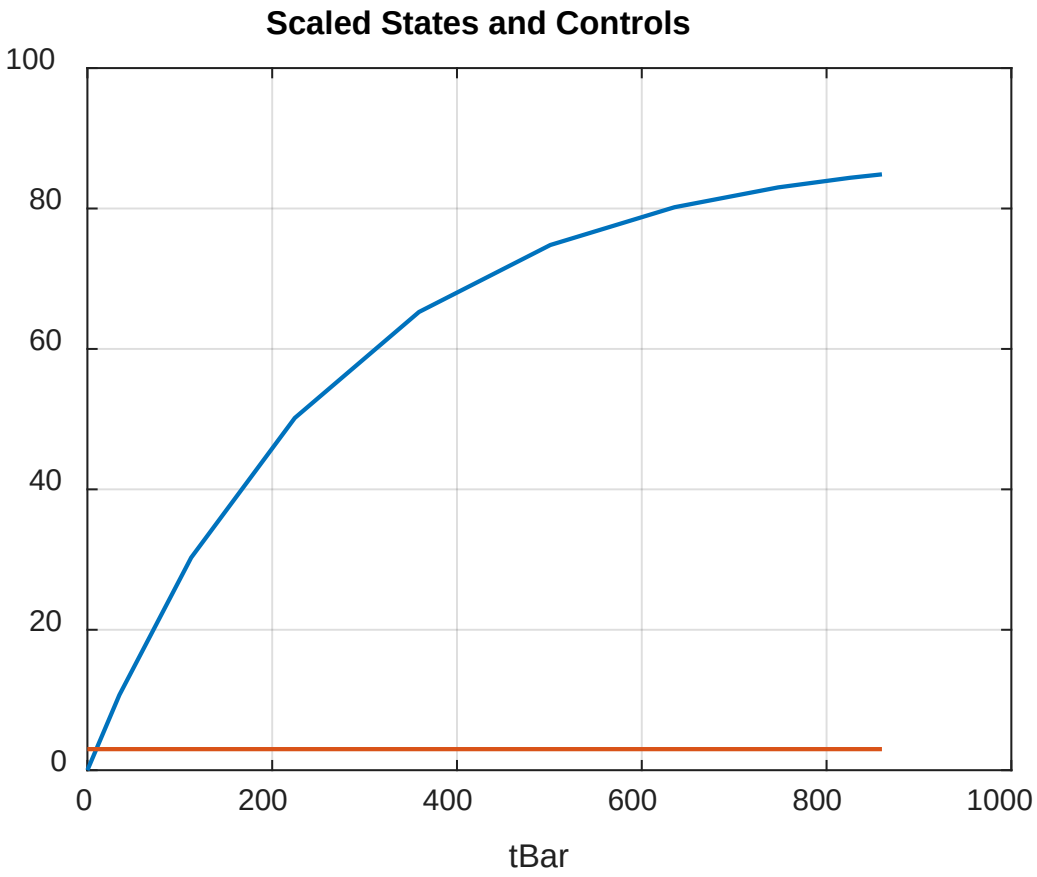

Figure 55. Scaled state and control variable for the minimum time/head loss problem.

In Figure 56, it is demonstrated that the scaled costates are within the same numerical range as both the scaled states and control. It also follows a curve as expected from the necessary conditions (not a constant or zero).

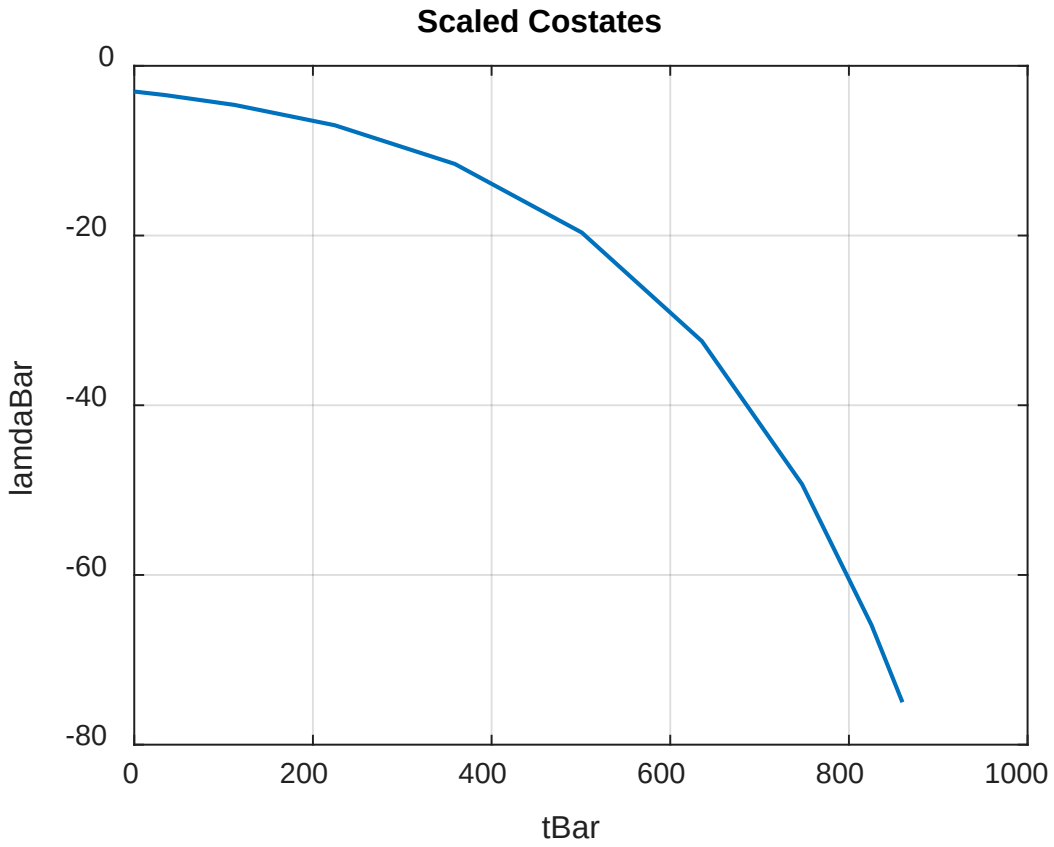

Figure 56. Scaled costate for the minimum time/head loss problem.

In order to verify the Hamiltonian conditions, the unscaled and scaled versions were plotted next to each other in Figure 57. They are both roughly constant and at -1 as expected by the BVP equations and Pontryagin's Principle. The numerical range on the y-axis is, notably, extremely small.

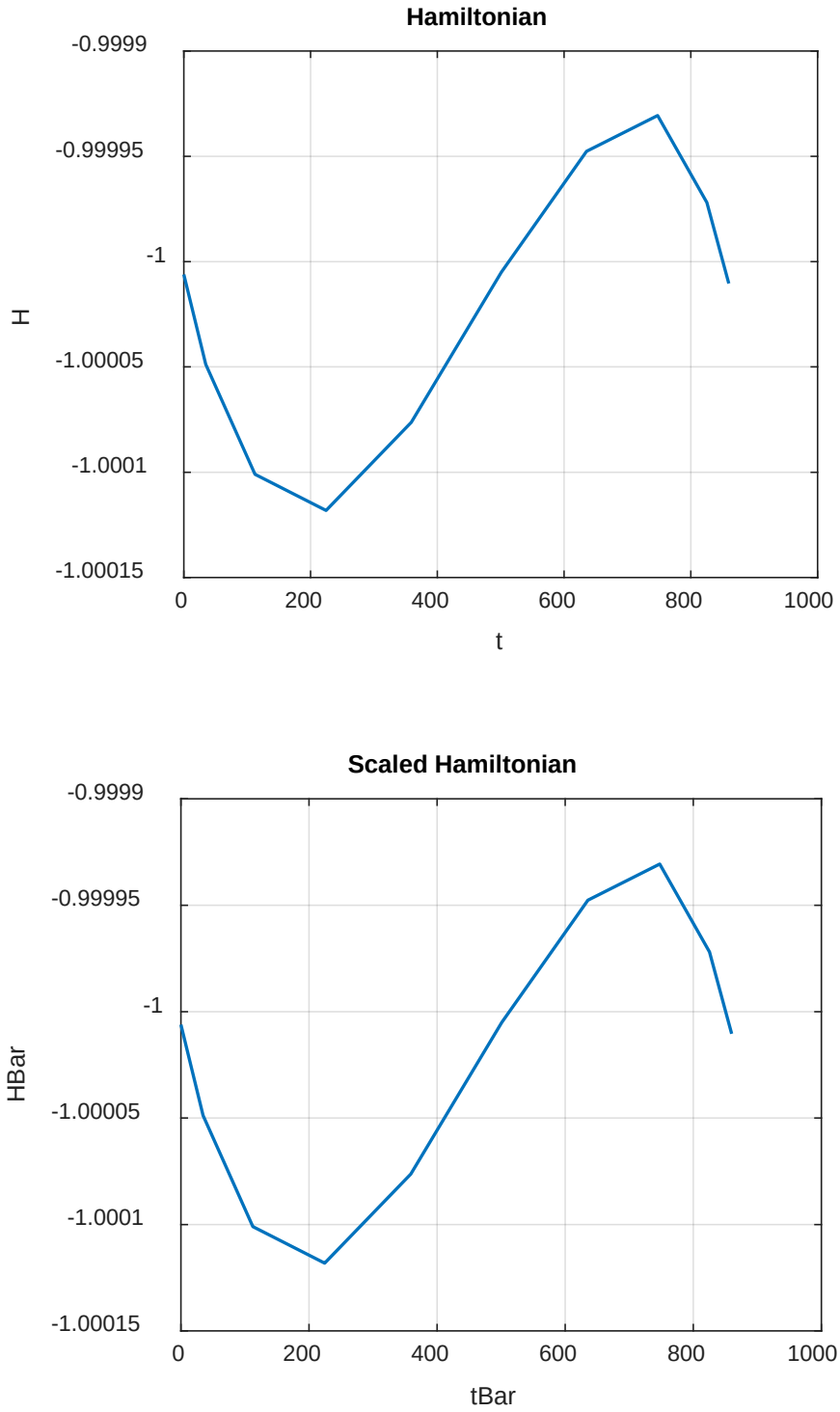

Figure 57. Hamiltonian and scaled Hamiltonian for the minimum time/head loss problem.

Finally, Figure 58 demonstrates that the state history from the derived equations for the boundary value match the propagation of the plant using the solved values of the control history relatively well (error depends on nodes used). This was produced by propagating the control produced from DIDO through the dynamics of the problem utilizing ODE45 in MATLAB.

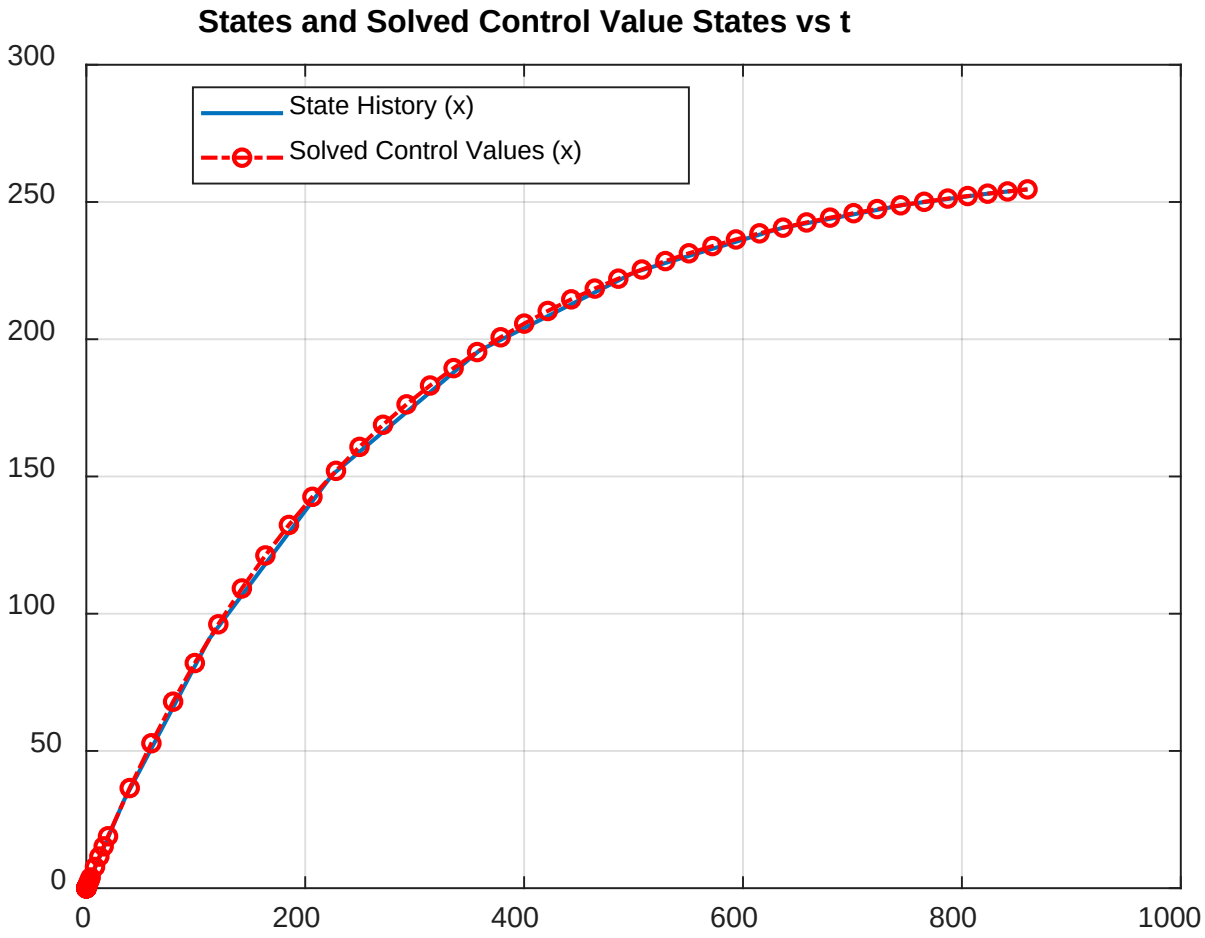

Figure 58. Propagation of the dynamics with the solved control value from DIDO.

E. CONCLUSIONS

Some issues that were encountered during the solving of this problem included finding a way to incorporate head loss into the overall architecture of the problem, since it

is not directly related to the dynamics but it utilized the control values. The way this was overcome was by generating a trade space outside of the numerical solver and iterating the time optimal problem through several values of maximum available control and plotting these values. The problem would, of course, become much more complicated if the mixing equations directly incorporated head loss. More complicated mixing would most likely incorporate head loss directly into the dynamics equations (it was assumed that lower head loss would mean better mixing due to less energy loss), but to keep this problem manageable the mixing did not directly incorporate the head loss. In addition, finding an appropriate scaling factor and utilizing it within DIDO was difficult. However, looking at the scaled Hamiltonian allowed issues to be found and corrected within the code until the Hamiltonian was a constant value as predicted. Finally, the last main issue was storing the full vectors of time, control, state, scaled state, etc., after each iteration of the DIDO time-optimal solver. DIDO had to be called and run for each new step increase of the maximum control, so a *for* loop was utilized. Indexing the variables to store each vector set was difficult, but utilizing standard MATLAB Documentation, MathWorks examples, and trial and error allowed for a solution.

Overall, utilizing DIDO, it was possible to find a solution to this problem utilizing only ten nodes due to the simplicity of the dynamics with an error of -1.2×10^{-3} (difference between the desired value for the final state and the actual solved value). More nodes would exponentially increase the time of operation due to the fact that DIDO would need to be run completely for each iteration of the optimal control maximum value as it increased in the main script. It was determined, by utilizing the trade space, that the tube could be filled with 95% argon in around 860 seconds (14.33 minutes) with a head loss of 1.6×10^{-4} m. This is the optimal balance of minimizing time to mix with minimal head loss as shown by the trade space. The time optimality of this solution was shown by the propagation of the states as well as the consistency of the Hamiltonian, and it was validated through the original dynamics. Future validation of this method could be done through actual physical testing of the model in the materials lab at NPS.

LIST OF REFERENCES

[1] Chawla, K. K., 2012, “Metal Matrix Composites,” Composite Materials: Science and Engineering, K.K. Chawla, ed., Springer, New York, NY, pp. 197–248.

[2] Schrand, Amanda “Additive Manufacturing in the DoD,” DSIAC, accessed April 27, 2020, https://www.dsiac.org/?journals=additive-manufacturing-in-the-dod.

[3] Rawal, S. P., 2001, “Metal-Matrix Composites for Space Applications,” JOM, 53(4), pp. 14–17.

[4] Cao, F., McEnaney, K., Chen, G., and Ren, Z., 2014, “A Review of Cermet-Based Spectrally Selective Solar Absorbers,” Energy Environ. Sci., 7(5), pp. 1615-1627.

[5] Woods, B., Thompson, D. W., and Woollam, J. A., 2006, “Cermet Thermal Conversion Coatings for Space Applications,” Protection of Materials and Structures from the Space Environment, J.I. Kleiman, ed., Springer, Netherlands, pp. 265–276.

[6] Jaworske, D., 2011, “Space Durable Solar Selective Cermet Coating,” Journal of Thermophysics and Heat Transfer, 25(3), pp. 462-463.

[7] Boyd, I., Buenconsejo, R., Piskorz, D., Lal, B., Crane, K., and Blanco, E., 2017, “On-Orbit Manufacturing and Assembly of Spacecraft,” IDA Paper No. P-8335.

[8] Miracle, D., 2005, “Metal Matrix Composites—From Science to Technological Significance,” Composites Science and Technology, 65, pp. 2526-2540.

[9] Sekino, T., Nakajima, T., Ueda, S., and Niihara, K., 1997, “Reduction and Sintering of a Nickel–Dispersed-Alumina Composite and Its Properties,” Journal of the American Ceramic Society, 80(5), pp. 1139–1148.

[10] Daniels, Z. A., Rydalch, W., Ansell, T. Y., Luhrs, C. C., and Phillips, J., 2019, “Reduction Expansion Synthesis of Sintered Metal,” Materials, 12(18), pp. 1-13.

[11] Lowell, S., Luhrs, C. C., and Phillips, J., 2015, “Reduction Expansion Synthesis for Magnetic Alloy Powders,” M.S. thesis, Naval Postgraduate School, Monterey, CA.

[12] Canty, R., Gonzalez, E., MacDonald, C., Osswald, S., Zea, H., and Luhrs, C. C., 2015, “Reduction Expansion Synthesis as Strategy to Control Nitrogen Doping Level and Surface Area in Graphene,” Materials, 8(10), pp. 7048–7058.

[13] Zea, H., Luhrs, C. C., and Phillips, J., 2011, “Reductive/Expansion Synthesis of Zero Valent Submicron and Nanometal Particles,” Journal of Materials Research, 26(5), pp. 672–681.

[14] Pelar, C., Greenaway, K., Zea, H., Wu, C.-H., Luhrs, C. C., and Phillips, J., 2018, "Novel Chemical Process for Producing Chrome Coated Metal," Materials, 11(1), pp. 1-9.

[15] Pelar, C. J., 2017, "Reduction Expansion Synthesis of Chromium and Nickel Metal Coatings," M.S. thesis, Naval Postgraduate School, Monterey, CA.

[16] Gow, A., and Phillips, J., 1992, "Microcalorimetric Study of Oxygen Adsorption on Catalytically Promoted Gasification Chars: Mechanistic Evidence for Alkali– and Alkaline-Earth-Metal Carbonate Catalyzed Reactions," Energy and Fuels, 6(4), pp. 526–532.

[17] Gow, A., and Phillips, J., 1991, "Microcalorimetric Study of Oxygen Adsorption on Catalytically Promoted Gasification Chars," Journal of Catalysis, 132(2), pp. 388–401.

[18] "Bulk Material Density Guide," Hapman, accessed April 27, https://www.hapman.com/education-support/bulk-material-density-guide/.

[19] "Silica, Fumed S5130," Sigma Aldrich Product Catalog, accessed April 27, 2020, https://www.sigmaaldrich.com/catalog/product/aldrich/s5130.

[20] "Silicon Carbide 594911," Sigma Aldrich Product Catalog, accessed April 27, 2020, https://www.sigmaaldrich.com/catalog/product/aldrich/594911.

[21] Dummit, E., 2016, "Differential Equations (Part 1) : First-Order Differential Equations," Arizona State University Department of Mathematics, accessed April 27, 2020, https://math.la.asu.edu/~dummit/docs/lindiff_1_first_order_differential_equations.pdf.

[22] "Scanning Electron Microscopy," Nanoscience Instruments, accessed 27 April, 2020, https://www.nanoscience.com/techniques/scanning-electron-microscopy/.

[23] Nordnes, E., 2019, "Softening and Melting Properties of Quartz," M.S. thesis, Norwegian University of Science and Technology, Trondheim, Norway.

[24] Hock, C., Straßburg, S., Haberland, H., v. Issendorff, B., Aguado, A., and Schmidt, M., 2008, "Melting-Point Depression by Insoluble Impurities: A Finite Size Effect," Phys. Rev. Lett., 101(2), pp. 1-4.

[25] Eustathopoulos, N., Chatain, D., and Coudurier, L., 1991, "Wetting and Interfacial Chemistry in Liquid Metal-Ceramic Systems," Materials Science and Engineering, (135), pp. 83–88.

[26] López-Cuevas, J., Jones, H., and Atkinson, H. V., 2000, “Wettability of Silica Substrates by Silver–Copper Based Brazing Alloys InVacuo,” Journal of the American Ceramic Society, 83(12), pp. 2913–2918.

[27] Li, J. G., 1993, “Wetting and Interfacial Bonding in Liquid Metal/Solid Ceramic Systems,” Composite Interfaces, 1(1), pp. 37–53.

[28] Ross, J., 2011, Heterogenous Catalysis: Fundamentals and Applications, Elsevier, New York.

[29] Topsoe, H., Clausen, B.S., and Massoth, F.E., 1996, Hydrotreating Catalysis Science and Technology, Springer Verlag, New York.

[30] Phillips, J., and Dumestic, J. A., 1984, “Production of Supported Metal Catalysts by the Decomposition of Metal Carbonyls,” Applied Catalysis, 9(1), pp. 1–30.

[31] Palmer, J. M., 1995, “The Measurement of Transmission, Absorption, Emission, and Reflection,” Handbook of Optics (Volume II: Fundamentals, Techniques, and Design). M. Bass et al., eds., McGraw-Hill, New York, pp. 25.1-25.25.

[32] Ohring, M., 1993, “Why Are Thin Films Different from the Bulk?,” Proceedings of SPIE 2114, Boulder, CO, July 28, 1994, doi: 10.1117/12.180875, pp. 624–639.

[33] Alexopoulos, P. S., and O’Sullivan, T. C., 1990, “Mechanical Properties of Thin Films,” Annual Review of Materials Science, 20(1), pp. 391–420.

[34] Ross, I., 2020, “DIDO,” Programing language, Elissar Global, Carmel, CA.

[35] Subramanian, R.S., “Pipe Flow Calculations,” Clarkson University, accessed April 27, 2020, https://web2.clarkson.edu/projects/subramanian/ch330/notes/Pipe%20Flow%20Calculations.pdf.

[36] “Fluid Properties Calculator,” University of Waterloo Microelectronics Heat Transfer Laboratory, accessed December 3, 2019, http://www.mhtl.uwaterloo.ca/old/onlinetools/airprop/airprop.html.

[37] Ross, I., 2009, A Primer on Pontryagin’s Principle in Optimal Control, Collegiate Publishers, Carmel, CA.

THIS PAGE INTENTIONALLY LEFT BLANK

INITIAL DISTRIBUTION LIST

1. Defense Technical Information Center
   Ft. Belvoir, Virginia

2. Dudley Knox Library
   Naval Postgraduate School
   Monterey, California